Western Graduate&PostdoctoralStudies

Western University
Scholarship@Western

Electronic Thesis and Dissertation Repository

6-3-2015 12:00 AM

# Novel Video Imaging to Examine Cardiac Function in Xenopus Embryos

Judith Sull
*The University of Western Ontario*

Supervisor
Thomas Drysdale
*The University of Western Ontario*

Graduate Program in Physiology and Pharmacology
A thesis submitted in partial fulfillment of the requirements for the degree in Master of Science
© Judith Sull 2015

Follow this and additional works at: https://ir.lib.uwo.ca/etd

Part of the Other Physiology Commons

## Recommended Citation

Sull, Judith, "Novel Video Imaging to Examine Cardiac Function in Xenopus Embryos" (2015). *Electronic Thesis and Dissertation Repository*. 2880.
https://ir.lib.uwo.ca/etd/2880

This Dissertation/Thesis is brought to you for free and open access by Scholarship@Western. It has been accepted for inclusion in Electronic Thesis and Dissertation Repository by an authorized administrator of Scholarship@Western. For more information, please contact wlswadmin@uwo.ca.

# NOVEL VIDEO IMAGING TO EXAMINE CARDIAC FUNCTION IN *XENOPUS* EMBRYOS

(Thesis Format: Monograph)

by

Judith I. Sull

Graduate Program in Physiology & Pharmacology - Collaborative program in Developmental Biology

A thesis submitted in partial fulfillment
of the requirements for the degree of
Masters of Science

The School of Graduate and Postdoctoral Studies
The University of Western Ontario
London, Ontario, Canada

© Judith I. Sull 2015

# Abstract

Congenital heart defects (CHDs) occur in approximately 1% of live births and the etiology has been associated with disturbances in cardiogenesis. However, the majority of research examining CHDs relies on static morphological data, which does not elucidate how defects alter cardiac function. I used *Xenopus laevis* embryos to examine the association between CHDs and functional alterations using a novel imaging system that can obtain high-resolution images through a non-invasive procedure. A high-speed video camera and software were used to assess cardiac function, permitting functional characterization of late *Xenopus* cardiogenesis. Verification of the imaging system's ability to detect changes in function was confirmed by exposing embryos to well-established agents that alter heart rate. Additionally, significant functional changes were detected following exposure of embryos to small molecules known to disrupt morphogenesis. The imaging system will be a useful alternative to current imaging modalities for elucidating mechanisms underlying CHDs in optically transparent embryos.

Keywords *Xenopus*, imaging, cardiogenesis, congenital heart defects, cardiac function, morphogenesis

# Co-Authorship Statement

I personally performed the experiments and writing contained within this thesis. Co-authorship belongs to Dr. Thomas Drysdale, my supervisor, who is responsible for supervision, suggestions for experiments and data analysis, and writing edits. As well, Dr. Kambiz Norozi also deserves co-authorship as he introduced me to the imaging system and guided my initial training with this system.

# Acknowledgements

I would like to thank my supervisor, Dr. Thomas Drysdale, for his invaluable guidance and mentorship during my Master's degree. To my colleagues at the CHRI and fellow lab members (both past and present), I would like to thank each of you for your help and for making the past two years very memorable. Lastly, thank you to my friends and family that have supported me throughout the years.

# Table of Contents

**Abstract** ........ **ii**

**Co-Authorship Statement** ........ **iii**

**Acknowledgements** ........ **iv**

**Table of Contents** ........ **v**

**List of Figures** ........ **ix**

**List of Appendices** ........ **xii**

**List of Abbreviations** ........ **xiii**

**Chapter 1** ........ **1**

**1 Introduction** ........ **1**

- **1.1 *Xenopus* as a Model Organism** ........ **1**
- **1.2 Cardiogenesis in *Xenopus laevis*** ........ **3**
  - 1.2.1 Myocardial Specification ........ 3
  - 1.2.2 Cardiac Morphogenesis ........ 5
  - 1.2.3 Secondary Heart Field ........ 10
  - 1.2.4 Circulation and Cardiac Structure ........ 12
- **1.3 Congenital Heart Defects** ........ **15**
- **1.4 Disruption of Cardiogenesis** ........ **16**
  - 1.4.1 Blebbistatin ........ 16
  - 1.4.2 Rockout ........ 17
  - 1.4.3 Retinoic Acid and Retinoic Acid Receptor Antagonist ........ 17
- **1.5 Assessing Cardiac Function** ........ **18**
  - 1.5.1 Rationale ........ 18
  - 1.5.2 Relationship Between Cardiac Morphology and Function ........ 18
  - 1.5.3 Cardiac Function Terminology ........ 19
  - 1.5.4 Previous Literature Examining Cardiac Function ........ 20
  - 1.5.5 History of the Novel Imaging System ........ 21
- **1.6 Rationale & Hypothesis** ........ **21**

1.6.1 Rationale ........ 21
1.6.2 Hypothesis ........ 22

**Chapter 2 ........ 23**

**2 Materials and Methods ........ 23**

**2.1 Embryo Collection ........ 23**
**2.2 Mounting and Live Imaging of Embryos ........ 24**
**2.3 IO Imaging System & HeartMetrics Program ........ 26**
2.3.1 Equipment ........ 26
2.3.2 Program Procedure ........ 26
2.3.3 Overview of the Imaging System ........ 27
**2.4 Computing Cardiac Function ........ 33**
2.4.1 Heart Rate ........ 33
2.4.2 Ventricular Wall Thickness ........ 34
2.4.3 Stroke Volume & Volume of Blood in the Ventricular Cavity at End-Diastole ........ 35
2.4.4 Cross-sectional Area of the Ventricular Cavity ........ 36
2.4.5 Cardiac Output ........ 36
2.4.6 Flow Velocity ........ 37
**2.5 *Xenopus* Treatments ........ 38**
2.5.1 Known Modulators of Heart Rate ........ 38
2.5.2 Small Molecule Treatments on Embryos ........ 39
**2.6 Whole Mount *In Situ* Hybridization ........ 40**
**2.7 Cardiac Morphology Measurements ........ 41**
**2.8 Origin of Cardiac Response ........ 41**
**2.9 Statistical Analyses ........ 42**
2.9.1 Normative Sample ........ 42
2.9.2 Classical Modulators of Heart Rate ........ 42
2.9.3 Comparison of Cardiac Function & Morphology Following Disruption of Cardiogenesis 42
2.9.4 Origin of Cardiac Response ........ 43

**Chapter 3 ........ 44**

**3 Results ........ 44**

**3.1 Establishing Normal Cardiac Function Parameters for *Xenopus* embryos ........ 44**

3.1.1 Ejection Fraction ........ 45

3.1.2 Heart Rate ........ 45

3.1.3 Ventricular Wall Thickness ........ 47

3.1.4 Stroke Volume and Cardiac Output ........ 50

3.1.5 Flow Velocity ........ 53

3.1.6 Conclusions ........ 53

**3.2 Classical Modulators of Heart Rate ........ 55**

3.2.1 Rationale ........ 55

3.2.2 Atropine, Epinephrine, and Isoproterenol ........ 55

3.2.3 Metoprolol and Drug Combinations ........ 59

3.2.4 Conclusions ........ 59

**3.3 Functional Changes Due to Morphological Alterations ........ 62**

3.3.1 Blebbistatin and Rockout ........ 62

3.3.2 Retinoic Acid and Retinoic Acid Receptor Antagonist ........ 77

3.3.3 Ethanol ........ 90

**3.4 Origin of Cardiac Response ........ 102**

**Chapter 4 ........ 104**

**4 Discussion ........ 104**

**4.1 Measurements of Normal Cardiac Function ........ 104**

4.1.1 Comparison of our Data to the Previous Measures of Cardiac Function ........ 104

4.1.2 Classical Modulators of Heart Rate ........ 106

**4.2 Novel Assessments of Changes in Function ........ 107**

4.2.1 Rationale for Blebbistatin and Rockout ........ 107

4.2.2 Blebbistatin ........ 110

4.2.3 Rockout ........ 111

4.2.4 Retinoic Acid and Retinoic Acid Receptor Antagonist ........ 112

4.2.5 Ethanol ........ 113

**4.3 Origin of Cardiac Response ........ 115**

**4.4 Advantages ........ 116**

**4.5 Limitations ........ 117**

**4.6 Significance ........ 118**

References ..... 120

Appendix ..... 136

Curriculum Vitae ..... 137

# List of Figures

Figure 1. The three layers of the heart. 6

Figure 2. Cardiac development in *Xenopus* embryos. 9

Figure 3. A confocal microscopy image of a morphologically mature embryonic *Xenopus laevis* heart. 14

Figure 4. Mounting of *Xenopus* embryos for live cardiac imaging. 25

Figure 5. Functions available for the HeartMetrics program. 28

Figure 6. Depictions of end-diastole using HeartMetrics. 30

Figure 7. Depictions of end-systole using HeartMetrics. 32

Figure 8. Heart rate increases in *Xenopus laevis* embryos from stages 45 to 48. 46

Figure 9. Average ventricular wall thickness of *Xenopus laevis* embryos increases from stages 45 to 48. 49

Figure 10. Average stroke volume and cardiac output increases between stages 45 and 48 in *Xenopus laevis* embryos. 52

Figure 11. Flow velocity in the left aortic arch of stage 48 *Xenopus* embryos. 54

Figure 12. Atropine, epinephrine, and isoproterenol exposure result in increases in heart rate for *Xenopus* embryos. 58

Figure 13. *Xenopus* embryos exposed to metoprolol and atropine demonstrated the expected changes in heart rate. 61

Figure 14. Abnormal cardiac morphogenesis in *Xenopus laevis* embryos following exposure to blebbistatin and Rockout. 64

Figure 15. Increase in heart rate of *Xenopus* embryos following exposure to blebbistatin, but not following exposure to Rockout. 66

Figure 16. Reductions in cardiac function following exposure of *Xenopus laevis* embryos to blebbistatin and Rockout at stage 26. 69

Figure 17. Reductions in ventricular size in *Xenopus* embryos exposed to blebbistatin and Rockout at stage 26. 71

Figure 18. Cardiac function was not significantly altered in *Xenopus* embryos exposed to blebbistatin and Rockout at stage 33/34. 74

Figure 19. Exposure of *Xenopus* embryos to blebbistatin at stage 33/34 did not significantly alter ventricular morphology, although Rockout exposure resulted in an increase in ventricular dimension. 76

Figure 20. *Xenopus laevis* embryos had reductions in heart rate and ventricular dimensions following exposure to retinoic acid and retinoic acid receptor antagonist. 80

Figure 21. Exposure of *Xenopus laevis* embryos to retinoic acid and retinoic acid receptor antagonist at stage 14 resulted in decreased cardiac function and altered morphology. 83

Figure 22. Retinoic acid and retinoic acid receptor antagonist exposure initiating at stage 26 resulted in reductions in ventricular morphology and function. 86

Figure 23. Disruption of retinoic acid signaling resulted in significant reductions in cardiac function, but did not result in statistically significant changes in ventricular morphology. 89

Figure 24. *Xenopus laevis* embryos exposed to ethanol displayed altered cardiac morphology and no significant differences in heart rate. 92

Figure 25. Ethanol exposure at stage 8.5 caused reductions in ventricular morphology and cardiac function. 95

Figure 26. Reductions in cardiac function and morphology following exposure to ethanol commencing at stage 26. 98

Figure 27. *Xenopus* embryos exposed to ethanol initiating at stage 33/34 displayed reductions in ventricular morphology and function. ............................................................................. 101

Figure 28. *Xenopus laevis* embryos are capable of displaying expected cardiac responses to pharmacological agents by at least stage 37/38. ................................................................. 103

Figure 29. A simplified version of the Shroom3 pathway. ................................................. 109

# List of Appendices

Figure A1. Examination of end-diastolic dimension and end-systolic dimension for *Xenopus laevis* embryos at stage 47. ........................................................................................136

# List of Abbreviations

| | |
|---|---|
| **°C** | Degrees Celsius |
| **β** | Beta |
| **λ** | Lambda |
| **µL** | Microliter |
| **µM** | Micromolar |
| **µm** | Micrometer/Micron |
| **2D** | Two-dimensional |
| **3D** | Three-dimensional |
| **ADH** | Alcohol dehydrogenase |
| **ADP** | Adenosine diphosphate |
| **ALDH** | Aldehyde dehydrogenase |
| **AP** | Anterior-posterior |
| **aPKC** | Atypical protein kinase C |
| **ASD** | Atrial septal defect |
| **ASD2** | Apx/Shrm domain 2 |
| **ATP** | Adenosine triphosphate |
| ***bmp*** | Bone morphogenetic protein gene |
| **bmp** | Bone morphogenetic protein protein |
| **bmp2** | Bone morphogenetic protein 2 protein |
| **bpm** | Beats per minute |
| **C** | Control |
| **$Ca^{2+}$** | Calcium ion |
| **CHD** | Congenital heart defect |

| | |
|---|---|
| ***Chordin*** | Chordin gene |
| **CO** | Cardiac output |
| **CSA** | Cross-sectional area |
| **CSAV** | Cross-sectional area of the ventricular cavity |
| ***cTnI*** | Cardiac troponin I mRNA |
| **cyp26** | Cytochrome P450, family 26 protein |
| **cyp2E1** | Cytochrome P450, family 2, subfamily E, polypeptide 1 protein |
| **DMSO** | Dimethyl sulfoxide |
| **DOCT** | Doppler optical coherence tomography |
| ***Drosophila*** | *Drosophila melanogaster* |
| **ED** | End-diastole |
| **EDD** | End-diastolic dimension |
| **EGF** | Epidermal growth factor |
| **ES** | End-systole |
| **ESD** | End-systolic dimension |
| **F-actin** | Filamentous actin |
| **FAS** | Fetal alcohol syndrome |
| **FFOCT** | Full-field optical coherence tomography |
| **Fgf** | Fibroblast growth factor protein |
| **Fgf8** | Fibroblast growth factor 8 protein |
| ***FoxC1*** | Forkhead box C1 gene |
| **fps** | Frames per second |
| **FS** | Fractional shortening |
| **FV** | Flow velocity |

| | |
|---|---|
| **Galnt11** | Polypeptide N-Acetylgalactosaminyltransferase 11 protein |
| ***Gata4*** | Gata binding protein 4 gene |
| **GFP** | Green fluorescent protein |
| **GLUT1** | Glucose transporter family member 1 |
| ***Gsc*** | Goosecoid homeobox gene |
| **Gt** | Gene trap |
| **GTP** | Guanosine triphosphate |
| **$H_2O$** | Dihydrogen monoxide |
| ***Has*** | Heart and soul gene |
| **hCG** | Human chorionic gonadotropin |
| ***Heart and Soul*** | Heart and soul gene |
| **HH** | Hamburger-Hamilton |
| ***HoxA1*** | Homeobox A1 gene |
| ***HoxA2*** | Homeobox A2 gene |
| ***HoxB4*** | Homeobox B4 gene |
| ***HoxB9*** | Homeobox B9 gene |
| **HR** | Heart rate |
| **IGF** | Insulin-like growth factor |
| ***Isl-1*** | Islet-1 gene |
| **Isl-1** | Islet-1 protein |
| **IU** | International units |
| **LL** | Longitudinal length |
| **LMP** | Low-melting point |

| | |
|---|---|
| **LUT** | Lookup table |
| ***Mef2c*** | Myocyte enhancer factor 2c gene |
| **Mef2c** | Myocyte enhancer factor 2c protein |
| **mg** | Milligram |
| **min** | Minute |
| **mL** | Milliliter |
| **MLC** | Myosin light chain |
| **MLCK** | Myosin light chain kinase |
| **mm** | Millimeter |
| **MMR** | Marc’s Modified Ringers |
| **MRI** | Magnetic resonance imaging |
| **mRNA** | Messenger RNA |
| **n** | Sample size |
| **N-cadherin** | Neural cadherin |
| ***Nkx2.5*** | NK2 homeobox 5 gene |
| **Nkx2.5** | NK2 homeobox 5 protein |
| **NM** | Non-muscle myosin |
| **Notch** | Notch protein |
| **OCT** | Optical coherence tomography |
| ***Otx2*** | Orthodenticle homeobox 2 gene |
| **P** | Perimeter |
| **$P_i$** | Inorganic phosphate |
| **Par** | Partitioning defective protein |
| **PBS** | Phosphate buffered saline |

| | |
|---|---|
| **PFA** | Paraformaldehyde |
| **Pitx1** | Paired-like homeodomain 1 protein |
| ***Pitx2*** | Paired-like homeodomain 2 gene |
| **Pitx2** | Paired-like homeodomain 2 protein |
| **RA** | Retinoic acid |
| **RAA** | Retinoic acid receptor antagonist |
| ***Raldh2*** | Retinaldehyde dehydrogenase family member 2 gene |
| **Raldh2** | Retinaldehyde dehydrogenase family member 2 protein |
| **RAR** | Retinoic acid receptor |
| **RARE** | Retinoic acid responsive element |
| **RNA** | Ribonucleic acid |
| **ROCK** | Rho-associated, coiled-coil-containing protein kinase protein |
| **RXR** | Retinoid X receptor |
| **s** | Second |
| **SAN** | Sino-atrial node |
| **SEM** | Standard error of the mean |
| **shh** | Sonic hedgehog protein |
| ***Shroom3*** | Shroom family member 3 gene |
| **Shroom3** | Shroom family member 3 protein |
| **Smad1** | Mothers against decapentaplegic homolog family member 1 protein |
| **SOD** | Superoxide dismutase |
| **SSC** | Saline-sodium citrate |

| | |
|---|---|
| **SV** | Stroke volume |
| **TBS** | Tris-buffered saline |
| ***Tbx1*** | T-box 1 gene |
| ***Tbx5*** | T-box 5 gene |
| ***Tbx20*** | T-box 20 gene |
| **tgfβ** | Transforming growth factor beta |
| **THG** | Third harmonic generation |
| ***Tinman*** | Tinman gene |
| **TL** | Transverse length |
| **VSD** | Ventricular septal defect |
| **VV** | Volume of blood in the ventricular cavity |
| **VWT** | Ventricular wall thickness |
| ***Wnt*** | Wingless-type MMTV integration site family member 1 gene |
| **Wnt** | Wingless-type MMTV integration site family member 1 protein |
| **Wnt11** | Wingless-type MMTV integration site family member 11 protein |
| ***Zic3*** | Zinc finger protein of the cerebellum 3 gene |

# Chapter 1

# 1 Introduction

The morphogenetic movements involved in cardiogenesis are well defined in many animal species, including *Xenopus laevis*. There is an important need for understanding cardiogenesis because cardiac development is a delicately orchestrated process that, if disturbed, can result in the development of congenital heart defects (CHDs). Alterations in cardiac morphology have been studied following manipulation of normal organogenesis in many animal models, including *Xenopus*. However, how these morphological changes can influence cardiac function is not as well understood. Therefore, understanding the linkage between changes in cardiac morphology and cardiac function could lead to important insight into clinical cases of congenital heart defects.

For the purpose of understanding the model organism we are using to study CHDs, I will discuss the history and use of *Xenopus* in research.

## 1.1 *Xenopus* as a Model Organism

*Xenopus laevis* has proven to be an invaluable animal model and has previously been used to provide a rich history for many aspects of early development. For example, a recent publication in Nature Genetics examined the development of the kidney tubules through novel tissue elongation mechanisms (Lienkamp et al., 2012). This article addresses the requirement for planar cell polarity and non-canonical wnt signaling in the proper formation of rosettes, which are multicellular structures used in elongation. Through *in vivo* fluorescent imaging, this research team was able to visualize and identify the role of rosette intercalation in kidney development. *Xenopus* have also been used as an animal model to study organogenesis of the gut (Kenny et al., 2012). A key process in understanding development involves examination of the morphological movements of cells during embryonic development. To examine these movements, a research group used a non-invasive *in vivo* imaging modality referred to as X-ray microtomography. This work provided further insight into cellular movements during gastrulation (Moosmann et al., 2013). Lastly, embryogenesis requires appropriate cell division orientation. Through experiments with *Xenopus,* mechanisms underlying symmetric cell division were examined and discovered to be essential for tissue growth and spreading (Woolner and Papalopulu, 2012).

Several *Xenopus* studies have shed light on mechanisms involved in congenital heart disease. The examination of human patients suffering heterotaxy has identified a high prevalence of rare genic copy number variations (Fakhro et al., 2011). Heterotaxy can result in congenital heart defects (CHDs) involving the disruption of proper left-right patterning. Five genes that result in disruption of left-right cardiac patterning were identified in *Xenopus* using the candidate genes discovered from the patients. Additional experiments demonstrated a novel signaling cascade associated with heterotaxy involving Galnt11, which is a glycosylation enzyme (Boskovski et al., 2013). Galnt11 mediates the activity of notch and was identified as a candidate gene involved in heterotaxy in human patients. The notch signaling pathway was found to be essential for the appropriate balance between motile and immotile cilia at the midline where those cilia are important in the determination of laterality. Therefore, *Xenopus* studies are able to elucidate potential mechanisms involved in the etiology of heterotaxy in humans.

The initial characterization of specific signaling molecules required for cardiogenesis was first identified in *Xenopus*. These cardiogenic pathways include fgf (Amaya et al., 1993), bmp (Shi et al., 2000), inhibition of the canonical wnt pathway (Schneider and Mercola, 2001), and activation of non-canonical wnt signaling (Pandur et al., 2002). The roles of these signaling pathways will be discussed in greater detail in a later section.

Amphibians do not require a functional heart until later tadpole stages making it feasible to study severe cardiac defects in early hearts (Kaltenbrun et al., 2011; Mohun et al., 2000). Zebrafish are another animal species commonly used in developmental biology that also possess this important feature. Furthermore, the availability of multiple transgenic lines provides genetic tools that can facilitate the study of many diseases.

Another feature of *Xenopus* that is particularly useful for this project and for the study of congenital heart defects is a feature that is shared with zebrafish and shell-less chick cultures, which are also used to study cardiac development. That is the ability to view the heart without embryo manipulation due to the translucent nature of the tadpoles. By simply viewing the embryo from the ventral side, the heart can be clearly resolved using a microscope with the ventricle and truncus being easily distinguishable. Therefore, gross morphological complications in cardiac development can be clearly viewed through live-imaging or by *in situ* hybridization using a myocardium specific antisense RNA probe to detect cardiac mRNAs such as *cardiac troponin I* (*cTnI*) (Drysdale et al., 1994).

In summary, *Xenopus laevis* embryos can be used to investigate the possible effects that CHDs may have on cardiac morphology and function as it relates to humans (Lohr and Yost, 2000). A discussion of myocardial specification, morphogenesis, origin, and structure is appropriate in understanding the advantage of using *Xenopus* for studying cardiac development and will be discussed next.

## 1.2 Cardiogenesis in *Xenopus laevis*

### 1.2.1 Myocardial Specification

Initiation of cardiac development involves the specification of precardiac mesodermal progenitors during gastrulation through signals from both the deep endoderm and Spemann’s organizer in the dorsal mesoderm (Collop et al., 2006; Nascone & Mercola, 1995; Sater & Jacobson, 1989; Schneider & Mercola, 1999). Subsequently, the expression of early transcription factors, such as *nkx2*.5 and *gata4*, are activated, helping to specify the cardiomyocyte lineage (Haworth et al., 2008; Lohr and Yost, 2000). This culminates in the formation of two bilaterally symmetrical heart patches located beside Spemann’s organizer (Afouda and Hoppler, 2009; Collop et al., 2006; Lohr and Yost, 2000; Mohun et al., 2000).

*Tinman*, the homolog of *Nkx2.5*, was first characterized in *Drosophila melanogaster* to be required for cardiac specification (Bodmer, 1993). The loss-of-function phenotype, in *Drosophila*, includes a complete loss of the heart, hence the appropriate origin of the name assigned to this gene. Subsequently, mouse models demonstrated that loss of *Nkx2.5* expression caused the inability of cardiac morphogenesis to develop past the linear heart tube phase (Komuro and Izumo, 1993; Lyons et al., 1995). When *Xenopus* embryos were microinjected with mRNAs encoding mutated *nkx2.5* transcripts that were initially identified in human patients presenting with CHDs, the embryos had disrupted cardiogenesis with conduction defects and abnormalities of the atrioventricular valve and atrial septum similar to defects seen in human patients (Bartlett et al., 2007). Interestingly, although *tinman* appears critical for early cardiogenesis, it was not one of the genes recently identified as being efficient in directed differentiation of fibroblasts into myocardial cells. Instead, other key early transcription factors were capable of driving myocardial differentiation, including a combination of Tbx5, Gata4 and Mef2c (Fu et al., 2013).

The expression and interplay of numerous signaling pathways is essential for proper cardiogenesis and include, but are not limited to, inhibition of canonical wnt (Foley and Mercola, 2005; Pandur et al., 2002; Schneider and Mercola, 2001), bone morphogenetic protein (bmp) (Breckenride et al., 2001; Marvin et al., 2001), fibroblast growth factor (fgf) (Alsan and Schultheiss, 2002; Deimling and Drysdale, 2011) and notch (Rones et al., 2000).

The canonical and non-canonical wnt signaling pathways both serve a role in cardiac specification (Dyer and Kirby, 2009b). Inhibition of the canonical wnt pathway is required for cardiac induction, which was demonstrated through both over expression of pathway components and small molecule antagonist studies (Schneider and Mercola, 2001). In contrast, non-canonical wnt signaling stimulates cardiac differentiation through wnt11 in *Xenopus* and the non-canonical wnt pathway plays a role in repressing canonical wnt signaling (Afouda et al., 2008; Pandur et al., 2002). The repression of canonical wnt signaling is especially crucial in embryonic regions that display high levels of bmp activity (Marvin et al., 2001). Furthermore, bmp signaling is necessary for maintaining cardiac gene expression and differentiation of the myocardium following repression of canonical wnt signaling (Monzen et al., 1999; Schultheiss et al., 1997; Shi et al., 2000).

Research has demonstrated that fgf8 expression in chick is necessary for the expression of genes essential in myocardial differentiation (Alsan and Schultheiss, 2002). Expression of fgf8 resulted in increased expression of *nkx2.*5 and *mef2c* in regions with high expression of bmp2. Fgf signaling is also critical for cardiac differentiation throughout early development in *Xenopus* (Deimling and Drysdale, 2011). Therefore, fgf plays an evolutionarily conserved role in maintaining cardiac gene expression.

Notch signaling is responsible for mediating the balance between myocardial and non-myocardial cell fates. Activation of notch results in a down regulation of genes that culminate in myocardial differentiation, whereas inhibition of notch leads to myocardial differentiation (Rones et al., 2000). These initial studies were done prior to the discovery of the second heart field (see below) and thus this result could be related to regulating differentiation timing in those lineages.

### 1.2.2 Cardiac Morphogenesis

Cardiac morphogenesis requires both the formation of the cardiac layers and the myocardial movements required to form the mature heart. I will discuss both of these topics in the following sections.

#### 1.2.2.1 Functions of the Three Cardiac Layers

The heart has three layers that form its walls (Figure 1). The endocardium is the inner layer surrounding the cardiac lumen (Kolker et al., 2000; Lohr and Yost, 2000; Mohun et al., 2000). Surrounding the endocardium is the muscular layer, referred to as the myocardium. The myocardial layer will originate as a layer that is one cell thick, but progressively thickens during cardiac and embryonic development (Kolker et al., 2000; Lohr and Yost, 2000). The outer layer of the heart facing the pericardial cavity is the epicardium, which is formed last during cardiac looping (Kaltenbrun et al., 2011).

Regardless of morphological differences among vertebrates, there does appear to be evolutionary conservation of the molecular mechanisms underlying organogenesis, especially with respect to the heart (Bartlett et al., 2010; Lohr and Yost, 2000). Conservation of cardiac development is even observed between vertebrates and *Drosophila melanogaster* in which the heart is composed of merely a linear tube responsible for circulating haemolymph (Bodmer and Venkatesh, 1998).

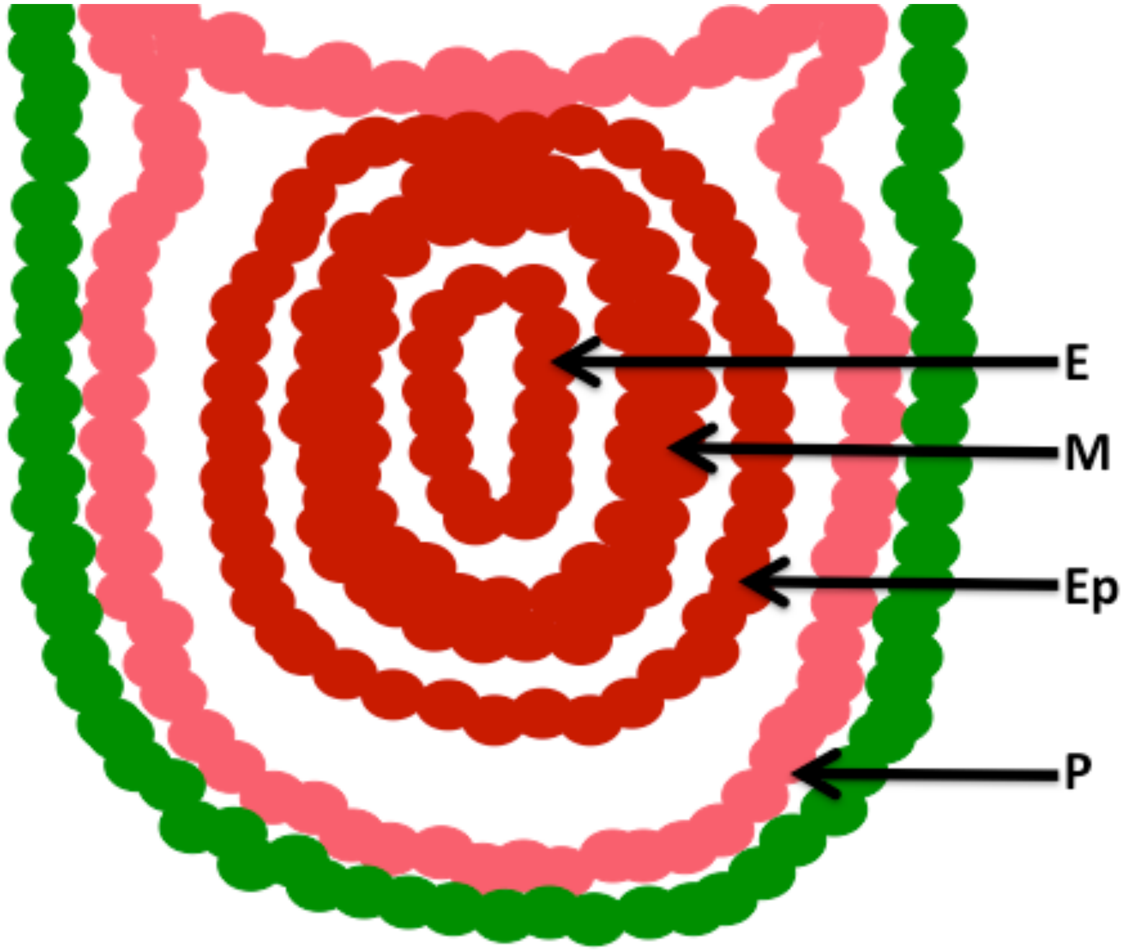

**Figure 1. The three layers of the heart.** An illustrated depiction of a transverse section of a *Xenopus laevis* embryo heart. The heart is comprised of the three red layers suspended within the pericardium. The epicardium comprises the outer sheet while the endocardium comprises the inner sheet. The myocardium can be found between the epicardium and endocardium. Legend: E = endocardium; P = pericardium; M = myocardium; Ep = epicardium

#### 1.2.2.2 Myocardial Movements

Cardiac development is well documented in *Xenopus* and can be characterized using a standardized embryonic staging system developed by Nieuwkoop and Faber (Nieuwkoop and Faber, 1994).

Following cardiac specification, two bilaterally symmetrical heart primordia are formed and proceed to migrate towards the ventral midline. Originally, the patches migrate dorso-anteriorly following gastrulation movements, but will subsequently migrate ventrally to the ventral midline during neurulation (Afouda and Hoppler, 2009; Lohr and Yost, 2000).

Afterwards, the two specified heart patches commence fusing to form a single linear heart primordium at stage 16 of development (Kolker et al., 2000; Lohr and Yost, 2000; Mohun et al., 2000). For this to occur, the two bilaterally symmetrical heart patches of myocardium located on either side of Spemann's organizer are physically united and suspended within the pericardial cavity forming a trough (Mohun et al., 2000). The term trough represents the morphology of the myocardium, which is initially a flat sheet, but upon separation from the endoderm commences to pinch and invaginate to form a V-shaped anlagen. Next, the trough of myocardial tissue commences surrounding and enclosing a single-cell thick endocardial tube. Eventually, the resultant linear cardiac tube consists of a myocardial layer surrounding the thin endocardial tube (Figure 1). Cardiac differentiation initiates during cardiac tube closure at stage 27 and this differentiation can be defined by the expression of genes necessary for end function (Figure 2A) (Kolker et al., 2000; Lohr and Yost, 2000; Mohun et al., 2000). Subsequently, by stage 33, the myocardial tube has completely closed, signaling the complete formation of the heart tube (Figure 2B).

After formation of the linear heart tube, the heart undergoes dorsal and rightward looping beginning at stage 33/34 (Figure 2C), resulting in the formation of an anticlockwise spiral or S-shaped tube by stage 35 (Figure 2D) (Afouda and Hoppler, 2009; Kolker et al., 2000; Lohr and Yost, 2000; Mohun et al., 2000). This non-linear tube consists of the outflow tract (also referred to as the truncus arteriosus) in the anterior end while the atria form the posterior end (Mohun et al., 2000). Cardiac looping is an essential process for subsequent valve formation and the development of the three cardiac chambers. The three chambers are comprised of the left atrium, right atrium, and a single ventricle. An additional sheet of cells, collectively known as the epicardium originating from the proepicardial anlagen, will develop and surround the muscular myocardium during cardiac looping (Jahr et al., 2008; Kaltenbrun et al., 2011). Subsequently, coordinated myocardial contractions cause the primitive heart to commence beating at approximately stage 35 (Lohr and Yost, 2000; Warkman and Krieg, 2007).

By stage 41, the truncus arteriosus and ventricle have thickened through the addition of layers and the ventricle becomes highly trabeculated, but not septated as is the case in mammals (Figure 2E) (Kolker et al., 2000; Lohr and Yost, 2000). Trabeculation refers to luminal projections of muscle located within the ventricle that aid in increasing the force of cardiac contraction. By stage 45/46, the distinct cardiac structures are easily discriminated. The spiral valve, located within the outflow tract, and the atrioventricular valve have fully formed at this developmental period (Figure 2F) (Bartlett et al., 2010; Kolker et al., 2000; Lohr and Yost, 2000; Mohun et al., 2000). The spiral valve is required for separation of oxygenated and deoxygenated blood in the single outflow tract and resembles the aorticopulmonary septum observed in humans (Kolker et al., 2000; Sadler, 1990). Lastly, an atrial septum separating the left and right atria extends from the dorsal wall resulting in partial atrial septation (Lohr and Yost, 2000; Mohun et al., 2000).

Therefore, the major elements comprising the mature heart can be considered complete by stage 46, which, at room temperature, is approximately four and a half days after fertilization (Kolker et al., 2000).

Recent developments have demonstrated added complexity to cardiac development as the cells that contribute to the heart do not all originate from one single population, as discussed next.

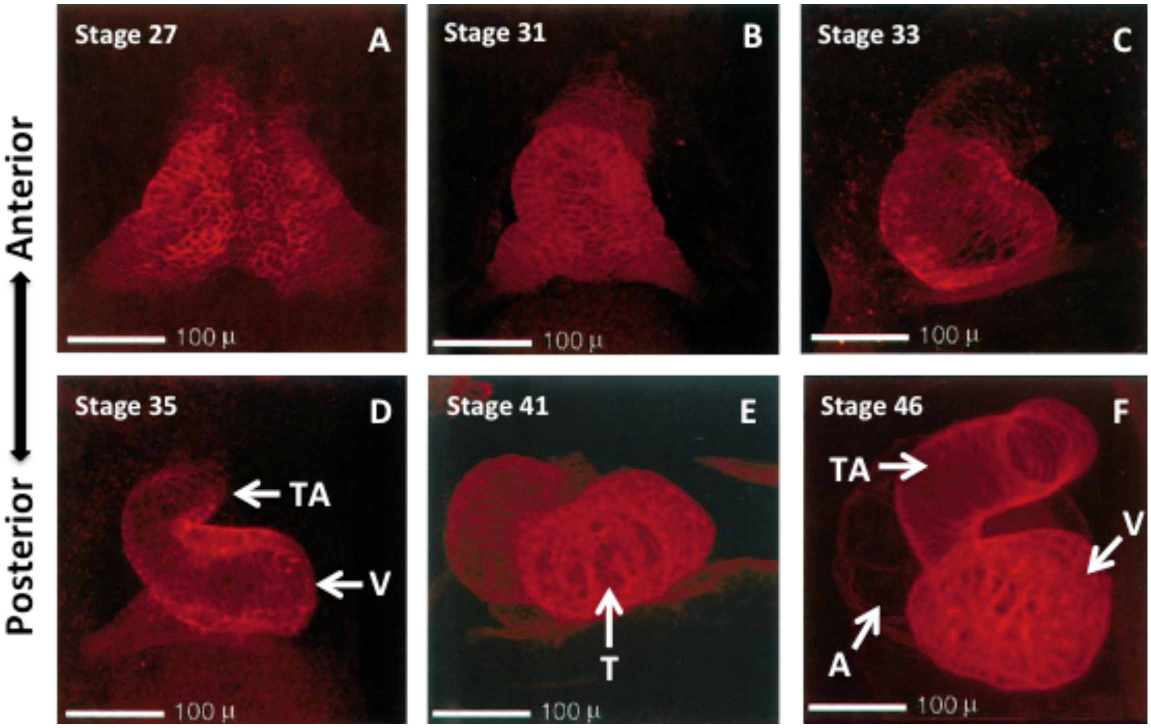

**Figure 2. Cardiac development in *Xenopus* embryos.** Confocal images of fixed *Xenopus* embryos using anti-tropomyosin staining for stages 27-33 and anti-cardiac troponin T staining for stages 35-46. Images are displayed from the ventral side of the embryo. Panel 2A depicts the closing of the cardiac anlagen to form a single cardiac primordium. This developmental interval also represents the initiation of cardiac differentiation. Next, panel 2B depicts the complete closure of the primordium to form a single linear heart tube consisting of an endocardial and myocardial layer. By panel C, the heart has begun to undergo dorsal and rightward looping and subsequently this process is complete by panel D. During this period, the ventricle and truncus arteriosus become distinguishable from the ventral side. Afterwards, the ventricle becomes highly trabeculated, which is depicted in panel 2E. The *Xenopus* embryo is primarily finished cardiac development by panel 2F, with completion of partial septation of the atria. Scale bar represents 100µm. Image was adapted from Kolker et al. (2000) with omission of the whole mount embryo depictions from the original figure and addition of arrows denoting the anterior-posterior axis. Legend: TA = truncus arteriosus; V = Ventricle; A = Atria; T = Trabeculation

### 1.2.3 Secondary Heart Field

The heart was initially believed to originate from a single population of cardiac progenitors. However, research over the last decade has identified the presence of two separate populations of cardiac progenitors that are both required for proper cardiac development (Dyer and Kirby, 2009b; Meilhac et al., 2003; Zaffran and Kelly, 2012).

The primary heart field is the region that gives rise to the initial cardiac tube, whereas the cells of the secondary heart field contribute to the developing myocardium by migrating into the arterial and venous poles of the original cardiac tube (Dyer and Kirby, 2009b). The partitioning of progenitors into the two pools is believed to originate either at gastrulation or earlier in development (Zaffran and Kelly, 2012). The cell population of the left ventricle is derived from the primary cardiac cell group, whereas the outflow tract and right ventricle originate from cells arising from the second population (Meilhac et al., 2003). The atria are thought to arise from a mixture of the two lineages (Dyer and Kirby, 2009b).

The presence of a secondary heart field has now been confirmed in *Xenopus* (Brade et al., 2007). The secondary heart field (or second heart field) serves a similar purpose to the mouse model although the relative contributions of each lineage to the different chambers has not been worked out. The second heart field provides cells required for expansion and extension of the linear heart tube at the arterial and venous poles.

Expression of *Islet-1* (*isl-1*) can be used to identify early cardiac progenitors within the mesoderm and this expression is conserved in *Xenopus* (Dyer and Kirby, 2009b; Sun et al., 2007). Extensive research in *Drosophila,* amphibians, amniotes, and mammals has contributed to understanding the importance of this gene in the establishment of a mature heart (Brade et al., 2007; Dyer and Kirby, 2009b). *Isl-1* is expressed in all cardiac progenitors, but its expression is lost in the primary heart field while being maintained in the secondary heart field (Dyer and Kirby, 2009b). Therefore, the secondary heart field can be identified based on the expression of *Isl-1*, which is maintained in the second heart field and down regulated in the primary heart field once differentiation is complete.

The expression of *Nkx2.5* contributes to the differences in temporal expression of *Isl-1* and primarily acts through inhibition of Smad1, which leads to further inhibition of Bmp signaling (Prall et al., 2007). This network allows for the differentiation of the primary population while the secondary lineage is held in a proliferative progenitor state until a later development period. The expression of *Isl-1* and *Nkx2.5* is not exclusive between the two populations, but rather the difference lies in the temporal regulation of differentiation (Dyer and Kirby, 2009b).

Addition of cells from the secondary heart field lengthens the outflow tract and probably serves a role in the proper rotation and alignment of the cardiac regions (Yelbuz et al., 2002b). The inability to maintain the progenitor pool results in a premature accumulation of myocardial cells to the initial cardiac tube (Dyer and Kirby, 2009b). Several loss of function studies have demonstrated the essential role that the second heart field serves in formation of a mature heart. For example, *Isl-1* knockout mice lack the development of an outflow tract, right ventricle, and much of the atria (Cai et al., 2003). Ablation of the secondary heart field in chick embryos resulted in several cardiac defects including overriding aorta, pulmonary atresia, and coronary artery anomalies indicating that the second heart field is necessary for proper orientation of the outflow tract (Ward et al., 2005). In the presence of antisense morpholinos targeting *isl-1* in *Xenopus*, there was abnormal cardiac looping and the resulting hearts were reduced in size (Brade et al., 2007).

Canonical Wnt signaling is maintained in the second heart field following the development of the initial cardiac tube. The loss of Wnt signaling has been associated with a reduced Isl1 positive cell population (or second heart field), resulting in outflow tract and right ventricular defects in mice (Cohen et al., 2007).

Sonic hedgehog (shh) is required for arterial pole development through its role in maintaining the secondary heart field (Dyer and Kirby, 2009a). Shh signaling is required for cell proliferation in the second heart field and loss of this signaling results in the inadequate ability to expand the arterial pole. Absence of Shh signaling has been linked to cardiac defects in mice and zebrafish, including patterning abnormalities in the outflow tract and disruption of neural crest cell development, which may be the cause of the outflow defects (Schilling et al., 1999; Washington Smoak et al., 2005).

Fgf serves a role in the addition of cells originating from the second heart field to the expanding outflow tract in mice to regulate morphogenesis (Park et al., 2008; Zhang et al., 2008). Fgf expression in the second heart field is required for the production of extracellular matrix, expression of Tgfβ, and expression of Bmp in the outflow tract of mice (Park et al., 2008). Disruption of downstream Fgf signaling in mice resulted in outflow tract defects, such as improper expansion, defective alignment, hypoplasia, and septal defects (Zhang et al., 2008).

Conditional Notch knockouts through *Mef2c* and *Isl-1* cre recombinase drivers resulted in an increased incidence of right ventricular and outflow tract defects in mice (High et al., 2009). The use of these cre recombinase lines allowed for the knockout of Notch signaling exclusively in cells of the second heart field. Therefore, the defects seen are intrinsic to the secondary heart field cell population.

My thesis is aimed at assessing cardiac function, therefore, I will now discuss the mature embryonic *Xenopus* heart.

### 1.2.4 Circulation and Cardiac Structure

Cardiac blood flow in *Xenopus* commences at the posterior end of the heart where the partially septated atria separate pulmonary and systemic venous returns (Figure 3) (Lohr and Yost, 2000; Mohun et al., 2000). The larger right atrium collects the systemic venous returns while the pulmonary venous returns accumulate in the smaller left atrium. Therefore, there is separation of oxygenated and deoxygenated blood. Afterwards, erythrocytes circulate through the atrioventricular valve into a single trabeculated ventricle (Lohr and Yost, 2000). In contrast to birds and mammals, *Xenopus* only have a single ventricle and atrioventricular valve for accommodating both the pulmocutaneous and systemic circulation. Subsequently, circulation proceeds from the ventricle to the truncus arteriosus, which contains two valves, including the spiral valve. These valves direct blood flow based on the relative resistance of the vasculature to either the pulmonary, carotid, or systemic arteries (Kolker et al., 2000). Conversely, the mammalian four-chambered heart consists of both an aorta and pulmonary artery to separate blood flow.

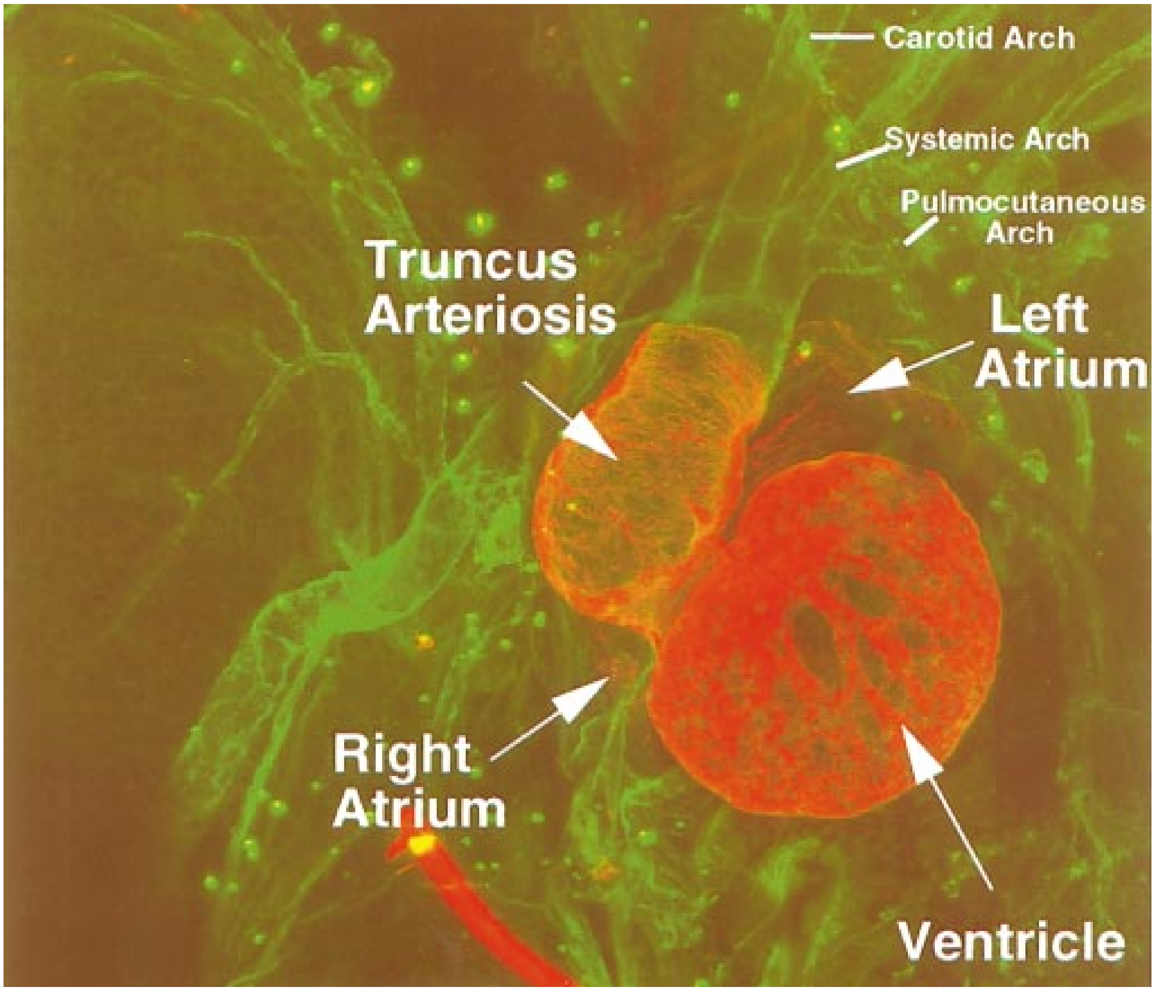
Carotid Arch
Systemic Arch
Pulmocutaneous Arch
Truncus Arteriosis
Left Atrium
Right Atrium
Ventricle

**Figure 3. A confocal microscopy image of a morphologically mature embryonic *Xenopus laevis* heart.** The embryo was fixed and immuno-labeled at stage 46. The red staining labels cardiac troponin T (myocardium) while green staining serves as a marker for type VI collagen (vasculature and endocardium). Images of longitudinal sections of the heart were combined to create an image from the ventral side. Image was adapted from Kolker et al. (2000) without modifications to the original image.

## 1.3 Congenital Heart Defects

As discussed above, cardiac development is a highly coordinated process. Therefore, it is not surprising that there is a strong association between disruptions during early cardiogenesis and the occurrence of congenital heart defects (CHDs) (Khoshnood et al., 2012). CHDs represent the most prevalent abnormality seen at birth and accounts for a substantial proportion of morbidity and mortality. Currently, estimations predict that CHDs affect approximately 1% of live births (Hoffman and Kaplan, 2002).

Congenital heart defects can manifest in numerous manners. Examples of CHDs in humans include heterotaxy, atrial septal defects (ASDs), functionally univentricular hearts, anomalies of the venous return, and ventricular septal defects (VSDs), which is the most prevalent CHD (Khoshnood et al., 2012). Furthermore, the outcome that the defect may have on cardiac function can vary depending on the defect.

The origin of CHDs can be explained by both genetic and environmental factors. CHDs with a genetic basis have been linked to disease states including Down's syndrome, Noonan syndrome, Holt-Oram syndrome, DiGeorge syndrome, Axenfeld-Reiger syndrome, and CHARGE syndrome (Bosman et al., 2015; Kaltenbrun et al., 2011). Our understanding of the single gene mutation basis of CHDs in humans originated with the gene *NKX2.5*, the human homologue of *Tinman* discussed previously (Schott et al., 1998). Human patients identified to be heterozygous for an autosomal dominant mutation that resulted in CHDs were evaluated and the mutation was mapped to the *NKX2.5* locus. The mutation could be associated with VSDs, ASDs, tetralogy of Fallot, pulmonary atresia, ventricular hypertrophy, or subvalvular aortic stenosis and all patients demonstrated atrioventricular conduction defects. Importantly, as shown eloquently in this study, a single mutation can result in different phenotypes among affected patients.

Since the discovery of *tinman,* an abundance of research has determined links between disruptions in numerous genes and the development of congenital heart disease. These include *Gata4*, *Tbx1, Tbx5*, *Tbx20, Zic3*, *Pitx2*, and *FoxC1* (Kaltenbrun et al., 2011). Most of these mutations share common characteristics, such as dominant inheritance and result in defects in cardiac structure and conduction.

## 1.4 Disruption of Cardiogenesis

Since disruption of cardiogenesis has been associated with the incidence of congenital heart defects, exposure to small molecules targeting specific morphogenetic pathways can be used to generate cardiac abnormalities (Khoshnood et al., 2012). I utilized several of these in my thesis and I will now provide an overview of the small molecules used and the pathways they impact.

### 1.4.1 Blebbistatin

Myosins comprise a group of motor proteins that, in combination with actin, use the energy released upon ATP hydrolysis to drive contraction (Allingham et al., 2005). The composition of myosins can be separated into four components: two heavy chains and two light chains (Tullio et al., 1997). Non-muscle myosin (NM) is present within muscle cells along with muscle myosin and is fundamental for actin cross-linking and contraction (Vicente-Manzanares et al., 2009). NM II, an isoform of NM, serves a role in the regulation of the actin cytoskeleton as well as in cell migration, adhesion, cytokinesis and cellular morphogenesis (Tullio et al., 1997; Vicente-Manzanares et al. 2009). Non-muscle myosin's role in cardiac development has been demonstrated through knockout experiments where NM-deficient mice displayed an increased incidence of VSDs and abnormalities of the outflow tract (Tullio et al., 1997). Numerous kinases have been discovered to be required for the phosphorylation and activation of the regulatory light chain of NM-II, including ROCK and myosin light chain kinase (MLCK) (Vicente-Manzares et al., 2009).

Blebbistatin is a small molecule that acts as a non-competitive inhibitor of non-muscle myosin II activity (Allingham et al., 2005; Dou et al., 2007; Swift et al., 2012). Specifically, blebbistatin binds to myosin causing it to stabilize in the myosin-ADP-$P_i$ complex state. Myosin maintains low affinity for actin due to the inability of myosin to release the phosphate. Hence, myosin does not bind to actin, which blocks the force-generating step required for a contraction (Dou et al., 2007; Swift et al., 2012). This effect is only observed with the (-)-blebbistatin enantiomer, while (+)-blebbistatin can serve as a control due to its lower binding affinity (Allingham et al., 2005). Blebbistatin has been demonstrated in mice to inhibit cardiac contractions independently of $Ca^{2+}$ influx (Dou et al., 2007).

### 1.4.2 Rockout

The Rho family of GTPases is essential in cell morphogenesis, cell migration, and organogenesis, including a necessary role in cardiac development (Morckel et al., 2012; Wei et al., 2002). The signaling activity of Rho is dependent on ROCK (Rho-associated kinases), which represents a group of serine/threonine kinases (Yarrow et al., 2005). Upon activation by Rho, ROCK is capable of phosphorylating downstream proteins including myosin light chain (MLC). However, ATP is required for these kinases to phosphorylate downstream effectors and initiate the appropriate response.

Rockout is a small molecule that inhibits Rho-associated kinases, specifically ROCK-II (Morckel et al., 2012; Yarrow et al., 2005). Rockout acts as a competitive inhibitor of ATP binding to ROCKII, thereby effectively decreasing phosphorylation of MLC.

### 1.4.3 Retinoic Acid and Retinoic Acid Receptor Antagonist

All-trans retionic acid is the biologically active form of vitamin A (Collop et al., 2006). The endogenous synthesis of retinoic acid (RA) primarily depends on the enzyme retinaldehyde dehydrogenase 2 (Raldh2) (Hochgreb et al., 2003; Xavier-Neto et al., 1999), while Cyp26 is the enzyme responsible for RA degradation (Haselbeck et al., 1999; Hollemann et al., 1998).

RA is essential for the regulation of numerous developmental processes, including cardiac development (Collop et al., 2006; Deimling and Drysdale, 2009; Glass and Rosenfeld, 2000; Ross et al., 2001; Zile, 2001). Retinoic acid traverses the cellular membrane, due to RA's lipophilic properties, then proceeds to form a complex in the nucleus with retinoic acid receptors (RARs) and retinoid X receptors (RXRs) that are bound to DNA. Subsequently, this complex can act as a transcription factor in the nucleus. In particular, this ligand-activated complex bound to retinoic acid responsive elements (RAREs) recruits co-activators that alter gene expression (Glass and Rosenfeld, 2000; Ross et al., 2001; Zile, 2001). In the absence of retinoic acid, or in the presence of retinoic acid receptor antagonists, the RAR/RXR heterodimer is still bound to the response elements on DNA, but represses the expression of RA-responsive genes (Deimling and Drysdale, 2009).

Previous experiments have demonstrated that RA is essential in the development of the heart of *Xenopus*, mammals, and birds (Collop et al., 2006; Drysdale and Crawford, 1994; Jiang et al., 1999; Keegan et al., 2005; Smith et al., 1997; Twal et al., 1995; Xavier-Neto et al., 2000). RA is required for the initial restriction of cardiac progenitor cells in zebrafish, therefore regulating the quantity of progenitor cells. Retinoic acid is also required for the subsequent closure of the heart tube from the symmetrical heart regions in *Xenopus* (Collop et al., 2006).

## 1.5 Assessing Cardiac Function

### 1.5.1 Rationale

The information provided demonstrates that cardiac development in *Xenopus* is useful for the study of CHDs. For my project, I chose to evaluate a novel approach to studying CHDs, which involves assessing cardiac function in *Xenopus* embryos.

However, my project relies on a relationship between cardiac morphology and function to characterize CHDs, therefore I will first discuss this link.

### 1.5.2 Relationship Between Cardiac Morphology and Function

Although the widely held belief is that morphology affects function, the reverse also appears to be true. Proper cardiac function is essential for normal morphogenetic developments. Disruption of haemodynamic forces in zebrafish resulted in cardiac morphological defects such as chamber, valve and cardiac looping abnormalities (Hove et al., 2003). Lack of myocardial function during late heart development resulting from absence of a heartbeat caused disruptions in the formation of the atrioventricular endocardial cushions (Bartman et al., 2004). Also, zebrafish with a reduced circulation had cell shape alterations, ultimately resulting in a decrease in cardiomyocyte elongation, which is required for proper ventricle formation (Auman et al., 2007).

Thus, cardiac function and morphology are inter-related and both are crucial for the proper maintenance of the other. Therefore, to start understanding this relationship, I studied cardiac function in *Xenopus* using video imaging in both normal hearts and in those with specific morphogenetic defects to begin examining the link between cardiac function and morphology.

### 1.5.3 Cardiac Function Terminology

My project primarily focused on cardiac function analysis. However, to understand the cardiac function experiments, I will first discuss common terminology that is used to characterize this process.

During a cardiac cycle, two major phases can be easily identified. End-diastole refers to the time point in the cardiac cycle when the maximum blood volume is contained within the ventricular cavity. At this point, the dimension of the ventricle is at its largest and this period is immediately before a cardiac contraction. In contrast, end-systole refers to the point in the cardiac cycle when the minimum amount of blood is present in the ventricular cavity. The dimension of the ventricle is also at its minimum and this occurs directly after a complete cardiac contraction.

An entire cardiac cycle can be used to compute the heart rate. Heart rate is measured in beats per minute (bpm) and can be calculated by determining the number of cardiac cycles spanning a minute.

Furthermore, cardiac function can be quantified through parameters such as thickness of the ventricular wall, ejection fraction, stroke volume, and cardiac output. Ventricular wall thickness is a measure of the distance from the endocardial border to the epicardial border. Ejection fraction refers to the percentage of blood that is ejected as a ratio of that contained at end-diastole, which is equivalent to the percentage of blood no longer present at end-systole. Similarly, stroke volume is a measure of the blood volume that is ejected after a complete cardiac contraction. Cardiac output is a measure of the volume of blood pumped by the heart per minute and can be calculated by multiplying the stroke volume by the heart rate. It is important to note that some of these are the same parameters that are used to assess cardiac function in human patients.

### 1.5.4 Previous Literature Examining Cardiac Function

The study of cardiac function not only requires knowledge of terminology, but also familiarity with the research that has emerged in this field. However, research focusing on CHDs is far more limited with respect to functional examination than compared to data based on static morphological findings. As for the studies that have analyzed cardiac function, these have primarily focused on other animal models, such as the chick (Li et al., 2012) and zebrafish (Gao et al., 2012).

Previous research on cardiac development using *Xenopus* can be divided into static morphological experiments and real-time *in vivo* imaging. The majority of research has simply used whole mount *in situ* hybridization and standard microscopy to document the images (for example, Collop et al., 2006; Deimling and Drysdale, 2009; Grover, 2009; Halabi, 2013). Additional imaging modalities used with respect to fixed *Xenopus* embryos include confocal microscopy (Jahr and Männer, 2011; Kolker et al., 2000), scanning electron microscopy (Jahr and Männer, 2011; Jahr et al., 2008), and histological sections used to generate 3D reconstructions (Jahr et al., 2008; Mohun et al., 2000; Yelin et al., 2007b).

In contrast, cardiac *in vivo* imaging of live *Xenopus laevis* has been limited, but does include imaging modalities such as echocardiography, involving the use of 2D imaging and pulse-wave Doppler ultrasound to generate high frequency sounds waves to produce an image (Bartlett et al., 2010). Studies examining adult *Xenopus* hearts used modified X-rays, which produced motion images by exploiting the differences in attenuation of tissues to X-radiation (Szigeti et al., 2014). Another technique used was Third Harmonic Generation (THG) utilized to visualize erythrocyte velocity and other hemodynamic properties within the tail vessels of *Xenopus* embryos; however this could potentially be modified to measure flow velocity in the aortic branches (Dietzel et al., 2014). THG uses similar principles to fluorescent microscopy and employs a label-free method in which a pulsing laser induces photons to be released from the biological tissue, such that an image can be obtained. Variations of optical coherence tomography (OCT) have also been used, taking advantage of various frequencies of light and the varying level of optical scattering within different tissues (Boppart et al., 1997; Mariampillai et al., 2007; Yang et al., 2003; Yazdanfar et al., 1997; Yelin et al., 2007b). Similarly, spectrally encoded confocal microscopy exploits the property of reflectance of near infrared light to penetrate through to deeper tissues (Yelin et al., 2007b). Hemoglobin contrast subtraction angiography utilizes the endogenous absorptive property of hemoglobin to generate a flow contrast that enhances visualization of cardiac chambers (Deniz et al., 2012). An additional technique used for *in vivo* live imaging of *Xenopus* is intrathoracic cardiac recording that employs the use of electrodes inserted in the thorax to examine electrical conduction (Bartlett et al., 2004).

However, these imaging modalities require specialized and expensive equipment. Therefore, my project utilized a novel imaging system that offers the advantages of being relatively inexpensive as it does not require specialized training and utilized relatively inexpensive equipment. In the following sections, I will introduce this video imaging system utilized for examining cardiac development.

### 1.5.5 History of the Novel Imaging System

Previously, the imaging system we have utilized was used to examine cardiac function in chick embryos. Experiments were undertaken to examine early cardiogenesis in the chick and to study crucial developmental intervals that determine proper development (Yelbuz et al., 2002a). A recent publication using a similar system was published examining chick hearts at numerous developmental time points in order to generate a comprehensive atlas of the heart (Al Naieb, 2013). The research team used the same equipment used in my study to observe real-time cardiac development in the chick (Orhan et al., 2007).

## 1.6 Rationale & Hypothesis

### 1.6.1 Rationale

A majority of previous experiments examining congenital heart defects in *Xenopus* based their findings on static morphological data. For example, our lab has exposed *Xenopus* embryos to various small molecules and documented their ability to alter cardiac development (Collop et al., 2006; Deimling and Drysdale, 2011; Grover, 2009; Halabi, 2013). Whole mount *in situ* hybridizations using probes against *cTnI* mRNA were used to identify myocardial tissue and, based on static observations, it was apparent that there were disruptions in cardiac morphology after treatment with specific small molecules. However, static morphological data is not necessarily indicative of altered cardiac function. Therefore, research into functional differences could prove extremely useful for the study of CHDs as it relates to humans where functional assessments are a key part of patient diagnosis.

I propose to test for potential changes in cardiac function and predict significant changes in cardiac performance resulting from CHDs. As well, I propose to document normal cardiac function in *Xenopus laevis* embryos using the novel video imaging system that provides higher resolution images compared to other commonly used imaging modalities. This video system is capable of obtaining high frame rates, which is useful when imaging a beating heart. I find that this novel imaging system and software can be a useful adjunct for the study of CHDs.

### 1.6.2 Hypothesis

I hypothesized that disruptions in cardiac morphology would result in significant changes in early cardiac function. Specifically, reductions in ventricular morphology would result in reductions in cardiac function, whereas increases in ventricular morphology would correspond to increases in cardiac function.

Furthermore, I hypothesized that this video imaging system would have the ability to accurately analyze ventricular function in *Xenopus laevis* embryos. This would allow for this imaging system to become a useful alternative to other imaging equipment for examining and characterizing functional alterations following disruption of cardiogenesis.

# Chapter 2

# 2 Materials and Methods

## 2.1 Embryo Collection

The embryos collected for experiments, not involving the transgenic animals, were gathered from matings of wild type *Xenopus laevis* males and females obtained from Xenopus 1 (Dexter, MI). The Nkx2.5-GFP transgenic females were obtained from the National Xenopus Resource (Woods Hole, MA). Wild type males were used as the sperm source regardless of whether the female was wild type or transgenic. The animal handling protocols for this thesis were approved by the Animal Care Committee at the University of Western Ontario, Canada (Protocol #: 2011-015).

Embryo collection firstly involved intramuscular injection of 700 international units (IU) of human chorionic gonadotropin (hCG) (Chorulon) into a sexually mature female *Xenopus laevis* to induce ovulation. After injection, the *Xenopus* were incubated overnight at a temperature ranging from 16° - 18°C.

To obtain fresh testes, I euthanized sexually mature wild-type *Xenopus laevis*. The euthanization protocol involved submerging the frog in water containing MS-222 (Tricaine; 3-aminobenzoic acid ethyl ester) (Sigma). Following anesthetization, the spinal cord was initially severed using scissors and pithing was undertaken to destroy the spinal cord. The testes were dissected out and maintained at 4°C in a petri dish containing 200% Steinberg's solution.

Squeezing of the females to gather ovum involved placing a small amount of 80% Steinberg's solution on a sterile petri dish. Eggs were squeezed into the dish and then fertilized *in vitro* by addition of a piece of minced testes. After fertilization was completed, embryos were de-jellied using 2.5% cysteine (pH 8.0 dissolved in distilled $H_2O$) (Bioshop). Subsequently, embryos were maintained in 20% Steinberg's solution (NaCl, KCl, $MgSO_4$, $Ca(NO_3)_2$, Tris-HCl, distilled $H_2O$) unless otherwise treated. All embryonic staging corresponded to Nieuwkoop and Faber's *Normal Table of Xenopus laevis* (Nieuwkoop and Faber, 1994).

## 2.2 Mounting and Live Imaging of Embryos

An embryo mounting technique, which was initially described by Kieserman et al. was developed using 0.8% low-melting point (LMP) agarose (Life Technologies) (Kieserman et al., 2010). This embedding procedure allowed me to maneuver the live embryo to visualize the ventral side without manipulation or anesthetization to obtain *in vivo* real-time cardiac images (Figure 4). The LMP agarose was dissolved in 1/3x MMR (4M NaCl, 1M KCl, 1M $MgSO_4$, 1M $CaCl_2$, 1M Hepes, 0.5M EDTA, distilled $H_2O$) to obtain the proper concentration.

The procedure involved placing an individual embryo into a small amount of LMP agarose. Next, the embryo was flipped onto its dorsal side so the ventral side and heart could be viewed easily. The agarose was then allowed to solidify and extra 1/3x MMR was added to prevent embryo desiccation. Embedding in the LMP agarose allowed for accurate cardiac imaging by largely eliminating motion artifacts, while requiring no embryo manipulation. Hence, this procedure permitted long-term imaging as well as re-use of the identical embryo for subsequent measurements in longitudinal or acute exposure studies.

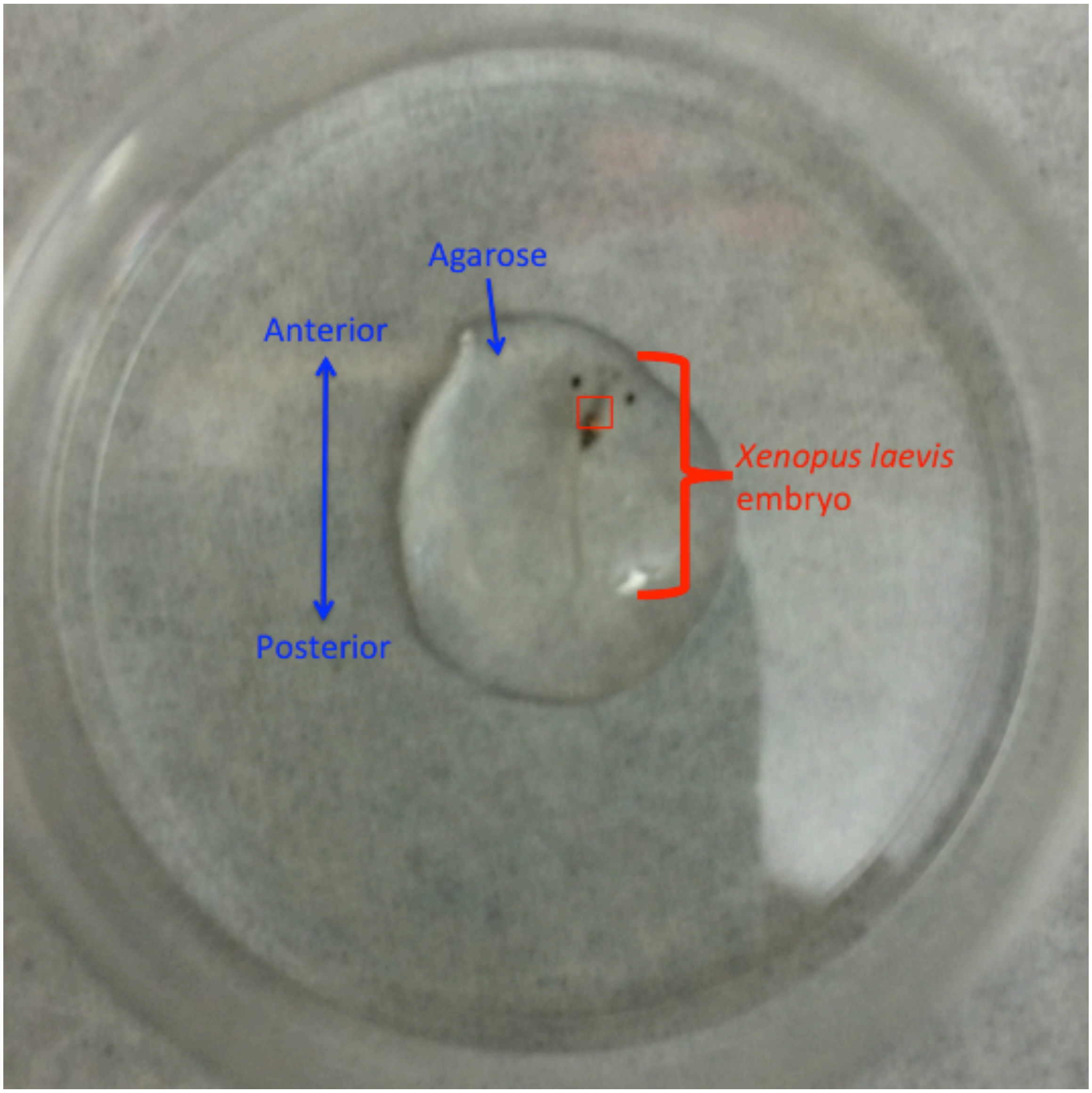

**Figure 4. Mounting of *Xenopus* embryos for live cardiac imaging.** *Xenopus laevis* embryos (red brace) of various stages were mounted using the protocol outlined by Kieserman et al., which embedded living embryos in 0.8% low-melting point agarose (blue arrow). This was performed in a petri dish and the embryo was later immersed in a salt solution to prevent desiccation. Embryos were maneuvered before the agarose solidified so the ventral side was easily viewable. Afterwards, *in vivo* cardiac images of live embryos were obtained. The heart is located above the gut and is outlined by the red box in the image. This technique was selected based on the fact that motion artifacts were largely eliminated while causing no negative cardiac repercussions.

## 2.3 IO Imaging System & HeartMetrics Program

### 2.3.1 Equipment

Both the imaging system and the cardiac function analysis program were obtained from IO Industries (London, Ontario). The equipment includes the DVR Express Core that captures the images from a Flare 2M360-CL colour video camera. The high-speed colour video camera is capable of obtaining a maximum of 359 frames per second (fps). The user can balance the frame rate and resolution to optimize images that are appropriate for the purpose of the experiment. For my experimental purposes, I selected a frame rate of 318.2 fps. The image capture software was designed to use hemoglobin as a contrast filter. The software can alter the image such that areas with blood appear black whereas areas depleted of blood are unaffected. However, additional alterations had to be performed to better image the *Xenopus* embryo so that the videos could be optimized prior to examining cardiac function.

The camera was mounted onto a stereomicroscope (Leica MZ12 or Leica M205 FA) and calibration files corresponding to the microscopes were created. These calibration files were applied to the videos for the purpose of obtaining accurately scaled measurements.

The camera feeds the video data to the DVR Express Core, which processes the images and sends the information to the computer software. The data analysis programs included HeartMetrics for guiding cardiac functional measurements and Microsoft Excel for computing functional measurements using algorithms and coordinates generated by HeartMetrics.

### 2.3.2 Program Procedure

Embryos were mounted and prepared for imaging according to the procedure described above (Kieserman et al., 2010). The heart could be observed without manipulation of the embryo since *Xenopus* embryos are relatively translucent at the time of cardiac imaging. Next, the embryo was then placed under a steremicrooscope and at this point, the heart was visible allowing the use of the HeartMetrics program and Flare camera.

After obtaining the videos, the files underwent a LUT (lookup table) transformation, which assisted in enhancing the contrast between the ventricular cavity and the ventricular wall based on the hemoglobin contrast image. Next, several labeling and selection functions of the HeartMetrics program were used. Labeling included the marking of seven to eight relatively equidistant points to trace the endocardial and epicardial borders during both end-systole and end-diastole. This was performed manually by the user for four end-diastole and three end-systole images and averaged for calculation of functional measurements. Subsequently, this data was exported to Microsoft Excel, which automatically used the algorithms in combination with the coordinates generated by HeartMetrics to calculate cardiac functional parameters.

### 2.3.3 Overview of the Imaging System

Colour images captured by the Flare camera are processed using a hemoglobin contrast filter to create monochromatic video files. This allows for regions containing hemoglobin, for example the ventricular cavity, to appear dark. In contrast, white regions signify little to no red colour due to the absence of hemoglobin, such as the ventricular wall. Furthermore, there are cardiac structures that appear grey signifying regions with low perfusion that primarily represent areas with trabeculation. Regions with a high density of trabeculation are considered contiguous with the ventricular wall and omitted from the dimensions of the ventricular cavity. It is important to note that due to the natural morphology of the *Xenopus* embryo, some areas that are not examined may appear to have variations in these shades as well, for example, the gut appears black.

A multitude of user functions are available for the HeartMetrics program (Figure 5). For the purposes of this project, the functions predominantly used included manually setting the time frame for four end-diastoles and three end-systoles. This allowed for heart rate to be computed. Manual labeling of the ventricle at end-diastole and end-systole were performed for both the epicardial and endocardial borders (Figures 6 and 7). The coordinates associated with the labels allowed for the calculation of other parameters, such as stroke volume, cardiac output, and ventricular wall thickness. A LUT transformation can be applied to increase the contrast of the image allowing for more accurate labeling of the ventricular borders.

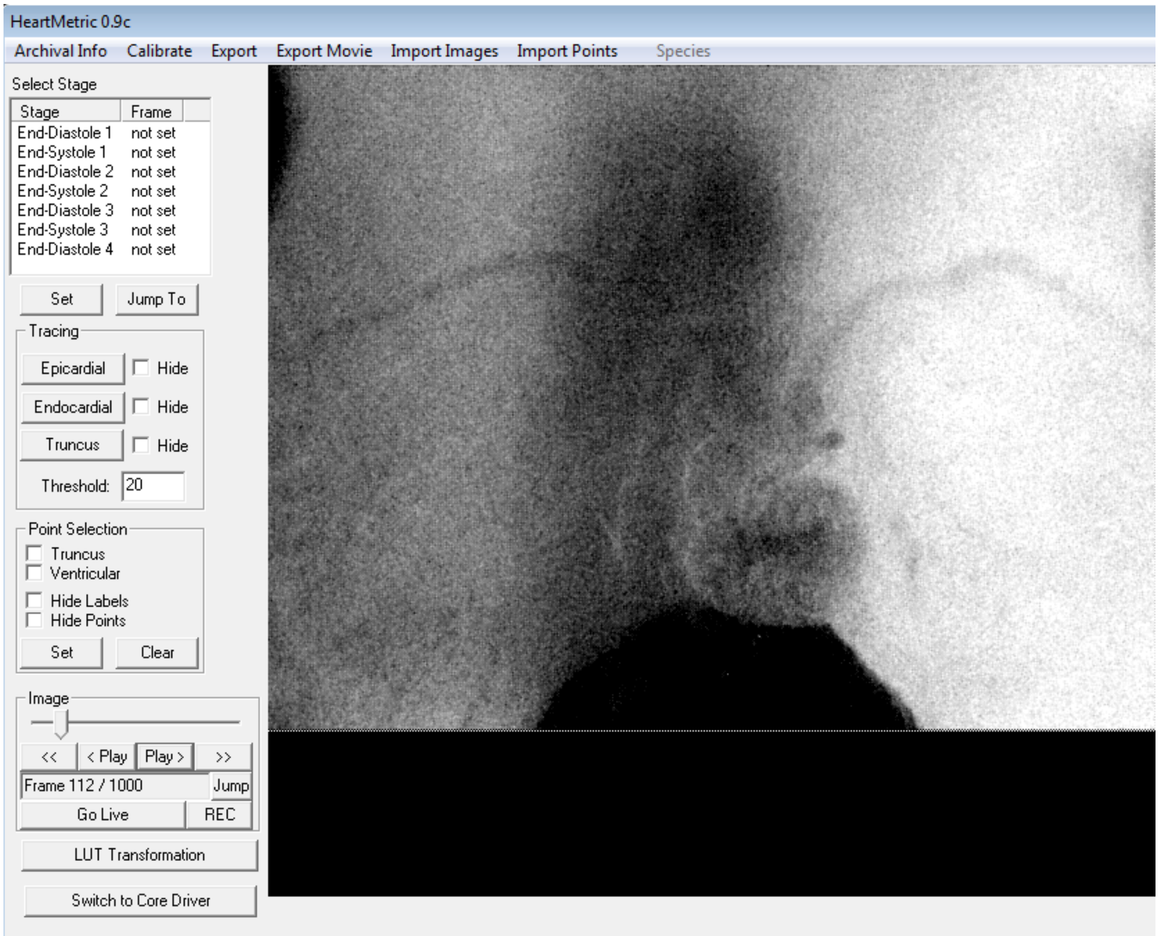
HeartMetric 0.9c
Archival Info
Calibrate
Export
Export Movie
Import Images
Import Points
Species
Select Stage
Set
Jump To
Tracing
Epicardial
Endocardial
Truncus
Hide
Point Selection
Truncus
Ventricular
Hide Labels
Hide Points
Set
Clear
Image
<<
< Play
Play >
>>
Jump
Go Live
REC
LUT Transformation
Switch to Core Driver

| Stage | Frame |
|---|---|
| End-Diastole 1 | not set |
| End-Systole 1 | not set |
| End-Diastole 2 | not set |
| End-Systole 2 | not set |
| End-Diastole 3 | not set |
| End-Systole 3 | not set |
| End-Diastole 4 | not set |

☐ Hide
☐ Hide
☐ Hide
Threshold: 20
☐ Truncus
☐ Ventricular
☐ Hide Labels
☐ Hide Points
Frame 112 / 1000

**Figure 5. Functions available for the HeartMetrics program.** Multiple functions are available for experimenters using HeartMetrics. The video file can be imported into the program and then the image is labeled using the functions located on the left hand side of the figure. For example, four end-diastole measurements and 3 end-systole measurements can be set for use in determining cardiac function. As well, the epicardium, endocardium, and truncus can be labeled. The point selection allows for marking of the endocardial and epicardial borders. The coordinates generated from outlining the epicardial and endocardial borders is then exported to Microsoft Excel to automatically compute cardiac function. The embryo depicted is at stage 48, which represents a developmental period when cardiogenesis is complete.

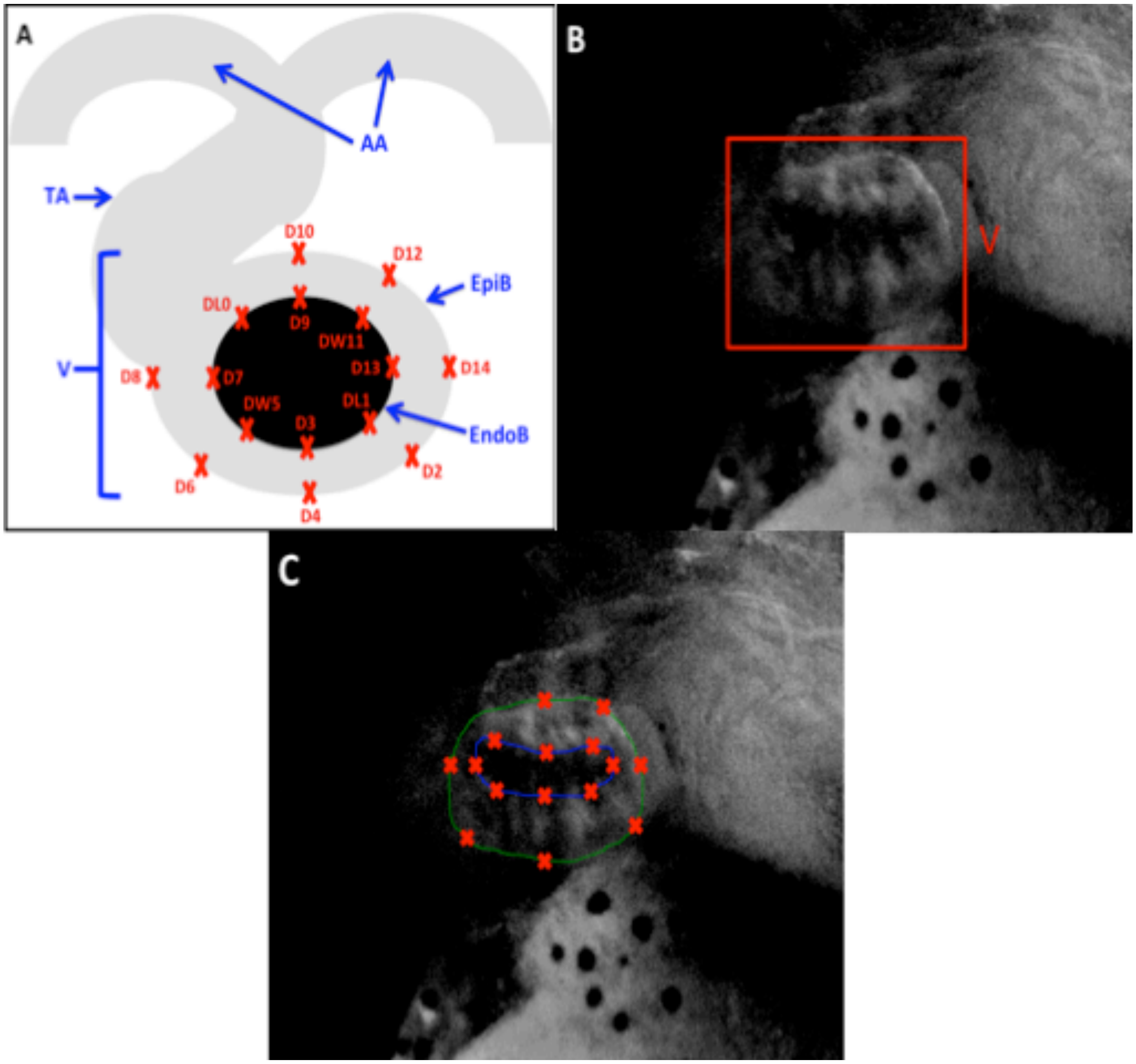
A
AA
TA
V
EpiB
EndoB
D10
D12
DL0
D9
DW11
D13
D14
D8
D7
DW5
D3
DL1
D6
D4
D2
B
V
C

**Figure 6. Depictions of end-diastole using HeartMetrics.** Panels A – C depict end-diastole as it would be observed on the HeartMetrics program after being processed by the hemoglobin contrast filter. Panel A depicts a schematic of end-diastole with the appropriate labels that would be marked using the HeartMetrics program (red crosses). This image is at stage 48 when the aortic arches become easily distinguishable and situated more ventrally. At this stage, gross changes in cardiac morphology have already been completed. The black region represents the ventricular cavity whereas the grey region represents the highly trabeculated areas and the ventricular wall. The coordinates assigned to the labels are averaged over four heartbeats and exported to Excel where algorithms are applied to generate measurements of cardiac function. Panel B depicts an imaged embryo during end-diastole using HeartMetrics. A LUT transformation has been applied to increase the contrast. The embryo represented is at stage 47 and gross morphological movements in cardiac development are complete. The red crosses are labeled to demonstrate the labeling function of HeartMetrics, which allows for the outlining of the epicardial and endocardial borders. This is in accordance with the procedure outlined for the previous panel. Panel C depicts the identical embryo as the previous panel, except the epicardium (green) and endocardium (blue) are labeled and the perimeters are drawn, which is another function of HeartMetrics. Legend: AA = aortic arch; TA = truncus arteriosus; EpiB = epicardial border; EndoB = endocardial border; V = ventricle

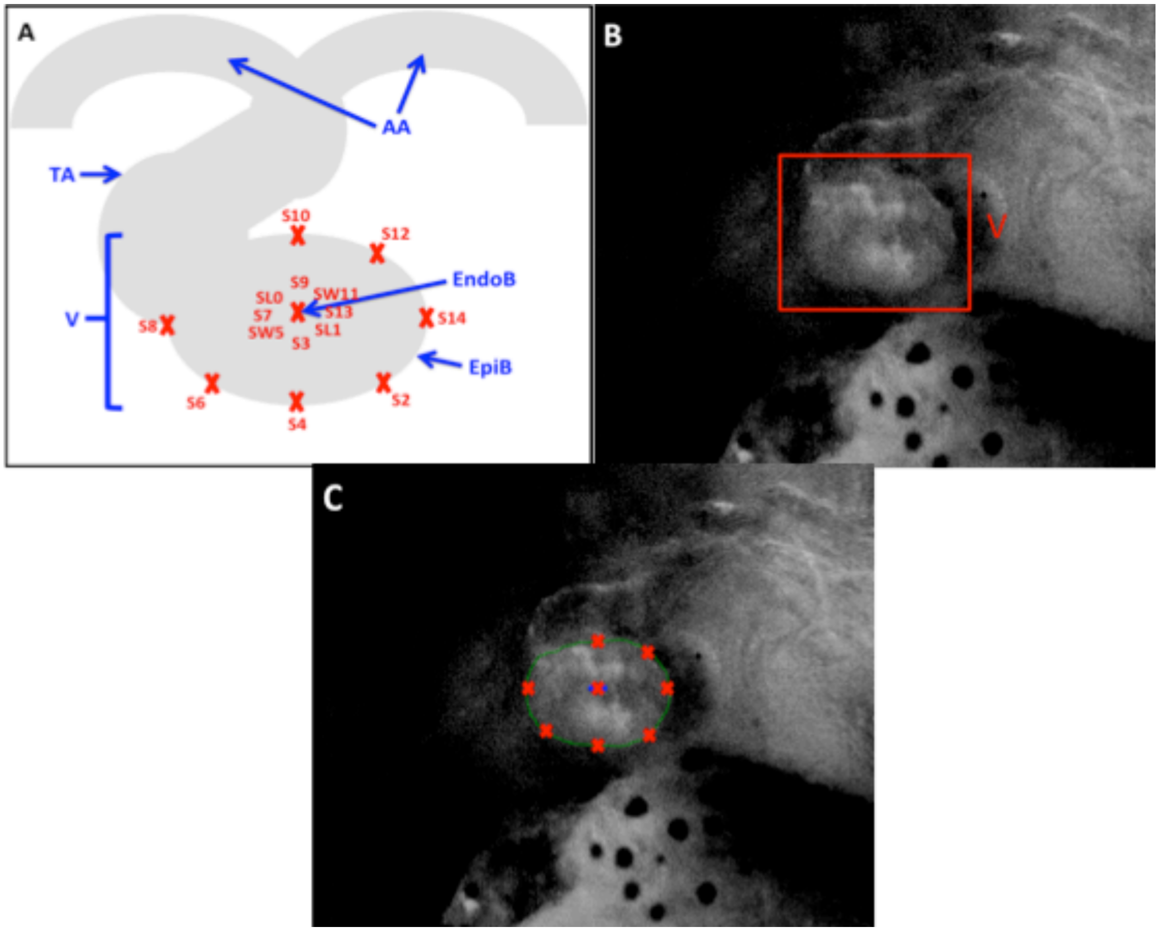
A
AA
TA
V
S10
S12
EndoB
S9
SL0
SW11
S7
S13
S14
S8
SW5
S3
SL1
EpiB
S6
S4
S2
B
V
C

**Figure 7. Depictions of end-systole using HeartMetrics.** End-systole is depicted in panels A – C to demonstrate the images generated using HeartMetrics. Images are processed using a hemoglobin contrast filter to optimize contrast. A schematic of end-systole is depicted in panel A with the corresponding labels that would be marked using the HeartMetrics program (red crosses). The embryo is representative of stage 48 of development, which corresponds to when the aortic arches become easily distinguishable and situated more ventrally. At this point, gross changes in cardiac morphology are complete. The grey region represents areas with high levels of trabeculation and the ventricular wall. The coordinates corresponding to the red crosses are averaged over four heartbeats. Subsequently, this data is exported to Microsoft Excel where algorithms are applied to compute cardiac function. A HeartMetrics image frame of a stage 47 embryo is depicted in panel B. A logarithmic LUT transformation was applied to increase the contrast of the image. The red crosses are marked to indicate the appropriate labeling functions that would be applied when operating the HeartMetrics program. The labeling function is used to outline the epicardial and endocardial borders. Panel C depicts the embryo shown previously in panel B, except the endocardium (blue) and epicardium (green) are labeled and the perimeters are drawn, which is an additional function of HeartMetrics. Legend: AA = aortic arch; TA = truncus arteriosus; EpiB = epicardial border; EndoB = endocardial border; V = ventricle

## 2.4 Computing Cardiac Function

As described previously, cardiac images were obtained and analyzed on HeartMetrics then exported to Microsoft Excel for computation. An ellipsoidal model for the ventricle shape was used to generate the measurements.

Measurements obtained for the normative sample included heart rate, stroke volume, cardiac output, ventricular wall thickness at end-diastole, and ventricular wall thickness at end-systole. Flow velocity was calculated for stage 48 embryos by tracing the distance traveled by a single erythrocyte over the course of one frame.

Cardiac parameters gathered for embryos treated with small molecules did not include functional examination at end-systole as discussed in a later section. Parameters were measured at end-diastole and included cross-sectional area of the ventricular cavity (CSAV), volume of blood in the ventricular cavity (VV), and ventricular wall thickness (VWT). Heart rate was also compared for each of the treatment groups.

### 2.4.1 Heart Rate

Heart rate (HR) was calculated by averaging the frames elapsed from end-diastole until the successive end-diastole (Refer to Figure 5). The computation also accounts for the pre-set frame rate of the system, which is 318.2 fps. Heart rate is represented as beats per minute (bpm).

$$\text{AF (frames)} = [(\text{ED2} - \text{ED1}) + (\text{ED3} - \text{ED2}) + (\text{ED4} - \text{ED3})] / 3$$

$$\text{HPS} = 318.2\text{fps} / \text{AF}$$

$$\text{HR (bpm)} = \text{HPS} \times 60$$

Legend: AF = average number of frames elapsed during one heart beat; ED = frame number at end-diastole; HPS = heart beats per second; HR = heart rate; fps = frames per second; bpm = beats per minute

### 2.4.2 Ventricular Wall Thickness

Ventricular wall thickness (VWT) was measured at either end-diastole or end-systole. The computation of these measurements utilizes the labels that were added to the HeartMetrics program that marked the endocardial and epicardial borders at three end-diastoles and three end-systoles (Refer to Figures 6 and 7). Labeling of points in HeartMetrics allowed for the generation of coordinates along the epicardial and endocardial borders that were subsequently used to calculate the diastolic and systolic ventricular wall thickness pairs. All calculations were averaged for seven measurements for each ventricular border. Measurements are computed in millimeters (mm).

$$\text{DVWTP1 (mm)} = |\,\text{DL1} - \text{D2}\,|$$

$$\text{DVWTP2 (mm)} = |\,\text{D3} - \text{D4}\,|$$

$$\text{DVWTP3 (mm)} = |\,\text{DW5} - \text{D6}\,|$$

$$\text{DVWTP4 (mm)} = |\,\text{D7} - \text{D8}\,|$$

$$\text{DVWTP5 (mm)} = |\,\text{D9} - \text{D10}|$$

$$\text{DVWTP6 (mm)} = |\,\text{DW11} - \text{D12}\,|$$

$$\text{DVWTP7 (mm)} = |\,\text{D13} - \text{D14}\,|$$

$$\text{VWT}_\text{D}\text{ (mm)} = (\,\text{DVWTP1} + \text{DVWTP2} + \text{DVWTP3} + \text{DVWTP4} + \text{DVWTP5} + \text{DVWTP6} + \text{DVWTP7}\,) / 7$$

Legend: DVWTP = Diastolic ventricular wall thickness pair; $\text{VWT}_\text{D}$ = average ventricular wall thickness (end-diastole); mm = millimeters

$$\text{SVWTP1 (mm)} = |\,\text{SL1} - \text{S2}\,|$$

$$\text{SVWTP2 (mm)} = |\,\text{S3} - \text{S4}\,|$$

$$\text{SVWTP3 (mm)} = |\,\text{SW5} - \text{S6}\,|$$

$$\text{SVWTP4 (mm)} = |\, S7 - S8 \,|$$

$$\text{SVWTP5 (mm)} = |\, S9 - S10 \,|$$

$$\text{SVWTP6 (mm)} = |\, SW11 - S12 \,|$$

$$\text{SVWTP7 (mm)} = |\, S13 - S14 \,|$$

$$VWT_S = (\ SVWTP1 + SVWTP2 + SVWTP3 + SVWTP4$$

$$+ SVWTP5 + SVWTP6 + SVWTP7\ ) / 7$$

Legend: SVWTP = Systolic ventricular wall thickness pair; $VWT_S$ = average ventricular wall thickness (end-systole); mm = millimeters

### 2.4.3 Stroke Volume & Volume of Blood in the Ventricular Cavity at End-Diastole

Stroke volume (SV) is considered equivalent to the volume of blood in the ventricular cavity (VV) at end-diastole for the normative sample in this project because approximately 100% ejection fraction was observed. Stroke volume is the volume of blood pumped by the heart for one cardiac contraction and if no blood is present in the ventricle at end-systole then the entire volume of blood at end-diastole was pumped during the single contraction. Stroke volume is considered synonymous to diastolic traced ventricular ellipsoidal volume (DTVEV) in the HeartMetrics program. Labeling of the endocardium at end-diastole in HeartMetrics is required for computing stroke volume (Refer to Figure 6). The points labeled in HeartMetrics along the endocardial border during end-diastole were used to generate the ventricular lengths. The value is averaged over four end-diastoles and represented in microliters (μL).

$$\text{DVL (mm)} = |\, DL0 - DL1 \,|$$

$$\text{DVED2 (mm)} = |\, DW5 - DW11 \,|$$

$$\text{DTVEV (mm}^3\text{)} = SV = 4/3 \times \pi \times DVL \times DVED2^2$$

$$DTVEV_{av}\ (\text{mm}^3) = SV_{av} = (\ DTVEV1 + DTVEV2 + DTVEV3 + DTVEV4\ ) / 4$$

$$DTVEV_{av}\ (\mu L) = SV_{av} = DTVEV_{av}\ (mm^3)\ /\ 1000 \times 1000$$

Legend: DVL = diastolic ventricular length; DVED = Diastolic ventricular end dimension; DTVEV = diastolic traced ventricular ellipsoidal volume; SV = stroke volume; $DTVEV_{av}$ = average diastolic traced ventricular ellipsoidal volume; $SV_{av}$ = average stroke volume; mm = millimeters; μL = microliters

### 2.4.4 Cross-sectional Area of the Ventricular Cavity

Cross-sectional area of the ventricular cavity (CSAV) represents the 2D region of the ventricular cavity that is occupied by erythrocytes at end-diastole. CSAV can be computed in a similar manner to stroke volume, except it is calculated in two dimensions instead of three dimensions. Therefore, the units are represented as an area in millimeters$^2$ (mm$^2$) as opposed to a volume. This calculation requires the labeling of the endocardial border at end-diastole in the HeartMetrics program (Refer to Figure 6). The coordinates generated by labeling points in HeartMetrics along the endocardial border at end-diastole were used to compute the ventricular lengths.

$$DVL\ (mm) = |\ DL0 - DL1\ |$$

$$DVED2\ (mm) = |\ DW5 - DW11\ |$$

$$CSAV\ (mm^2) = \pi \times DVL \times DVED2$$

$$CSAV_{av}\ (mm^2) = (\ CSAV1 + CSAV2 + CSAV3 + CSAV4\ )\ /\ 4$$

Legend: DVL = diastolic ventricular length; DVED = Diastolic ventricular end dimension; mm = millimeters; CSAV = cross-sectional area of the ventricular cavity; $CSAV_{av}$ = average cross-sectional area of the ventricular cavity

### 2.4.5 Cardiac Output

Cardiac output (CO) represents the volume of blood ejected from the heart per minute and is measured in microliters/minute (μL/min). Cardiac output can be calculated by simply multiplying the stroke volume by the heart rate.

$$\text{CO } (\mu\text{L/min}) = \text{SV } (\mu\text{L}) \times \text{HR (bpm)}$$

Legend: CO = cardiac output; µL = microliters; min = minutes; SV = stroke volume; HR = heart rate; bpm = beats per minute

### 2.4.6 Flow Velocity

Flow velocity (FV) was not computed using the pre-programmed HeartMetrics algorithms, but was calculated separately using cell labeling on HeartMetrics (Refer to Figure 5) (Movie 5). This parameter involved computing the distance in millimeters that was traveled by a single erythrocyte in one frame. The x- and y-coordinates of the erythrocyte were provided after the data was exported to Microsoft Excel. Subsequently, the distance traveled was calculated as the hypotenuse by using the Pythagorean Theorem and the x- and y- coordinates generated by HeartMetrics. Depending on the calibration used, the HeartMetrics program allowed me to identify the value of pixels in 1 millimeter. Furthermore, the user is aware of the frame rate of the captured video, which was 318.2 fps in these experiments. Flow velocity was then averaged over four separate measurements and assigned units of millimeters/second (mm/s). The data was gathered directly after end-diastole during ventricular contraction. During this interval, cardiac contraction and velocity of erythrocytes are at a relative maximum.

$$\text{DTP (pixels)} = (\,|\,X1 - X2\,|^{2} + |\,Y1 - Y2\,|^{2}\,)^{1/2}$$

$$\text{DTM (mm)} = \text{DTP} / \text{CU}$$

$$\text{DT}_{\text{av}} \text{ (mm)} = (\text{ DTM1} + \text{DTM2} + \text{DTM3} + \text{DTM4 }) / 4$$

$$\text{FV (mm/s)} = \text{DT}_{\text{av}} \times 318.2 \text{ fps}$$

Legend: DTP = distance traveled in pixels; X1 = x-coordinate of erythrocyte in first frame; X2 = x-coordinate of erythrocyte in second frame; Y1 = y-coordinate of erythrocyte in first frame; Y2 = y-coordinate of erythrocyte in second frame; DTM = distance traveled in millimeters; mm = millimeters; CU = calibration unit (number of pixels in one millimeter); $\text{DT}_{\text{av}}$ = average distance travelled; FV = flow velocity; s = seconds; fps = frames per second

## 2.5 *Xenopus* Treatments

### 2.5.1 Known Modulators of Heart Rate

*Xenopus laevis* embryos were exposed to classical modulators of heart rate at various stages depending on the nature of the experiment. The embryos were exposed to the modulators at stage 37/38 to stage 45 to determine the developmental interval in which cardiac response to pharmacological agents originates. For the heart rate studies, classical modulators were applied once embryos matured to stages 46-48.

Three of the modulators used are known to increase heart rate in *Xenopus*: atropine (Sigma), (-)-epinephrine (Sigma), and (-)-isoproterenol hydrochloride (Sigma) (Shutt and Bowes, 1979; Callaway, 2013; Cirić and Susić, 1980). An individual embryo was submerged in the solution for 3 minutes before being removed and embedded in 0.8% LMP agarose. Subsequently, cardiac images were acquired and used to measure heart rate in beats per minute. The embryos were subjected to increasing concentrations of atropine, including: 0mg/mL (distilled $H_2O$) [0mM], 0.05mg/mL [0.17mM], 0.1mg/mL [0.35mM], 0.5mg/mL [1.73mM], and 1mg/mL [3.46mM]. The concentrations of epinephrine included: 0mg/mL (distilled $H_20$) [0mM], 0.05mg/mL [0.27mM], 0.1mg/mL [0.55mM], 0.5mg/mL [2.73mM], and 1mg/mL [5.46mM]. The increasing concentrations of isoproterenol included: 0mg/mL (distilled $H_20$) [0mM], 0.05mg/mL [0.20mM], 0.1mg/mL [0.40mM], 0.5mg/mL [2.02mM], and 1mg/mL [4.04mM]. Concentrations were obtained by dissolving the pharmacological agent in distilled water.

The pharmacological agent (±)-metoprolol (+)-tartrate salt (Sigma) has been shown in the literature to decrease heart rate, therefore metoprolol was used in this study to contrast the other classical modulators (Fujito et al., 2014). The procedure for this pharmacological agent was similar to the procedure outlined above for the other drugs, except that the concentrations used included: 0mg/mL (distilled $H_20$) [0mM], 0.5mg/mL [0.73mM], 1mg/mL [1.46mM], 5mg/mL [7.30mM], and 10mg/mL [14.60mM].

An experiment involving the combination of atropine and metoprolol was performed. Initially, embryos were submerged in 0mg/mL (distilled $H_20$) to obtain baseline measurements of heart rate. Next, the embryo was submerged in successively increasing concentrations of atropine (0.05mg/mL, 0.1mg/mL, and 1mg/mL). Afterwards, embryos were immersed in solutions with successively increasing concentrations of metoprolol that were dissolved in a 1:1 ratio with 1mg/mL of atropine (0.5mg/mL, 1mg/mL, 10mg/mL).

Concentration 1: 0mg/mL of drug

Concentration 2: 0.05mg/mL atropine

Concentration 3: 0.1mg/mL atropine

Concentration 4: 1mg/mL atropine

Concentration 5: 1mg/mL atropine + 0.5mg/mL metoprolol

Concentration 6: 1mg/mL atropine + 1mg/mL metoprolol

Concentration 7: 1mg/mL atropine + 10mg/mL metoprolol

Heart rate was determined using the equation outlined previously and measured in beats per minute.

### 2.5.2 Small Molecule Treatments on Embryos

*Xenopus laevis* embryos were submerged in treatments at various stages including stages 8.5, 14, 26, and 33/34 depending on the experiment. The concentrations of the treatments included 100μM (-)-blebbistatin (Calbiochem), 100μM (+)-blebbistatin (Calbiochem), 20μM Rockout (EMD), 1μM retinoic acid (RA) (Sigma), and 1μM retinoic acid receptor antagonist (RAA; also known as AGN193109) (Allergan #193109) (Agarwal et al., 1996). Concentrations used were chosen based on experiments previously performed by members of the lab that demonstrated defects in cardiac morphology through *in situ* hybridizations (Collop et al., 2006; Halabi, 2013).

Every small molecule, except for ethanol, was dissolved in dimethylsulfoxide (DMSO) (Fisher Scientific) and then brought to working concentration using 20% Steinberg's solution. DMSO was used as the vehicle control for each experiment, except for the ethanol experiment. The concentration of DMSO was 1µL/mL for the Rockout and retinoic acid experiments, whereas the concentration of DMSO for the blebbistatin experiment was 10µL/mL. (+)-blebbistatin is an inactive enantiomer and served as another control for the specificity of (-)-blebbistatin activity.

Embryos were removed from their respective treatments after 24 hours at room temperature, except for the ethanol experiments. Afterwards, embryos were submerged in 20% Steinberg's solution following several washes. Cardiac images were captured once embryos matured to stage 46 and onwards. After video imaging as described above, embryos were fixed in MEMPFA (4% Paraformaldehyde dissolved in distilled $H_2O$, 1mM $MgSO_4$, 100mM Mops pH 7.5, 2mM EGTA pH 8.0) at room temperature for 2 hours or for 16 hours at 4°C in preparation for whole mount *in situ* hybridization. Embryos were then dehydrated in cold 100% methanol for storage at 4°C.

The procedure for the ethanol experiments was slightly modified from the protocol outlined above for the other small molecules. The embryos were either exposed to 20% Steinberg's solution or 1.5% ethanol (Fisher Scientific) dissolved in 20% Steinberg's solution. *Xenopus* embryos were maintained in the treatment until the time of imaging at stage 46 and onwards. The solution was replaced at least every 24 hours due to the volatility of ethanol.

## 2.6 Whole Mount *In Situ* Hybridization

The whole mount *in situ* hybridization protocol was based on Deimling et al. (Deimling et al., 2015). *Xenopus* embryos were submerged in potassium chloride prior to fixation to permit collection of morphology parameters following cardiac arrest at end-diastole.

BM Purple (Roche) was used for the colourometric reaction. Antisense probes against *cTnI* mRNA were used to specifically label the myocardium (Drysdale et al., 1994; Kolker et al., 2000; Lohr and Yost, 2000; Mohun et al., 2000). Embryos were fixed for an additional 20 minutes in MEMPFA to create a permanent stain. Subsequently, the embryos were bleached using bleaching solution (1% $H_2O_2$, 50% formamide, and 0.5% SSC) to increase the contrast of the probe-labeled regions by removing the endogenous pigmentation. Bleaching was performed for 16 hours at 4°C or 3 hours at approximately 25°C.

Individual images of each embryo were collected using Northern Eclipse (Empix Imaging; Mississauga, ON, Canada) with the Leica MZ12 and DFC450 camera.

## 2.7 Cardiac Morphology Measurements

Measuring cardiac morphology for treatment groups involved examining the *in situ* hybridization images. Images acquired were further analyzed using straight-line and curved functions of Northern Eclipse. Measurements of the ventricle included longitudinal length (LL), transverse length (TL), perimeter (P), and cross-sectional area (CSA).

## 2.8 Origin of Cardiac Response

Transgenic Nkx2.5-GFP embryos were generated using the same methods described above and embryos were allowed to mature until stages 37-39 before imaging. In contrast, wild-type embryos were used after maturing to stages 40-45. Embryos were then embedded in 0.8% LMP agarose and visualized under the Leica M205 FA stereoscope. The origin of cardiac response in my experiments is defined as the initial developmental interval in *Xenopus* where the heart is first able to display autonomic responses following exposure to pharmacological agents (Armour, 1999).

The fluorescent feature of the stereoscope allowed for the heart to be visualized for embryos ranging from stages 37 to 39, which is ordinarily challenging due to the natural pigmentation of the embryo. The time elapsed for 10 heartbeats was measured and used later for computation of heart rate. The heart rate was averaged for three separate measurements due to the variability of the method. Subsequently, embryos were exposed to 1mg/mL of isoproterenol for 3 minutes preceding imaging. The identical procedure was performed as stated above to determine heart rate. Heart rate was determined in beats per minute (bpm).

$$T_{10,av}\,(s) = (\,T_{10,1} + T_{10,2} + T_{10,3}\,)\,/\,3$$

$$T_1 \text{ (s)} = T_{10,av} / 10$$

$$HR \text{ (bpm)} = 60 / T_1$$

Legend: $T_{10}$ = time elapsed for 10 heartbeats; $T_{10,av}$ = average time elapsed for 10 heartbeats; $T_1$ = time elapsed for one heartbeat; s = seconds; HR = heart rate; bpm = beats per minute

Conversely, wild-type embryos that had matured to stages 40-45 were collected and baseline heart rates were measured after immersing the embryo in $H_2O$ for 3 minutes. Videos were collected using the Flare camera and later analyzed using HeartMetrics to measure the heart rate averaged over 4 heartbeats. Afterwards, embryos were submerged in 1mg/mL of isoproterenol for an additional 3 minutes preceding imaging. Heart rate was measured using the equation outlined previously and stated in beats per minute.

## 2.9 Statistical Analyses

All statistical analyses were performed on GraphPad Prism 6.0 software.

### 2.9.1 Normative Sample

*Xenopus laevis* embryos that ranged from stages 45 to 48 were used to represent the normative sample. The results obtained from these embryos were analyzed using a one-way ANOVA paired with a Tukey's post-hoc test. Significance was represented by p-values less than 0.05.

### 2.9.2 Classical Modulators of Heart Rate

Dose-response experiments included data using atropine, epinephrine, isoproterenol, and metoprolol. Data was analyzed using a non-linear fit regression where the x- and y-axes were represented as linear.

### 2.9.3 Comparison of Cardiac Function & Morphology Following Disruption of Cardiogenesis

Cardiac function and morphology were analyzed using a two-way ANOVA paired with a Sidak test. This included analysis of embryos treated with RA and RAA, (-)-blebbistatin, Rockout, and ethanol. Each data set was compared to individual control groups containing genetically identical offspring. Significance was represented by p-values less than 0.05.

Heart rate was also measured for each treatment and analyzed using a two-way ANOVA paired with a Sidak test. Significance was represented by p-values less than 0.05.

### 2.9.4 Origin of Cardiac Response

The cardiac response data was analyzed using a non-linear fit regression. Both the x- and y-axes were treated as linear.

# Chapter 3

# 3 Results

Note: All supplementary movies are shown at a frame rate of 30 fps instead of the original 318 fps to avoid playback errors experienced by some media players. The heart can be identified by the beating tissue located in the center of the image with the pixels cycling between dark and light, which corresponds to the cardiac cycle.

## 3.1 Establishing Normal Cardiac Function Parameters for *Xenopus* embryos

In order to evaluate our video imaging system's ability to measure cardiac function in *Xenopus*, functional data was collected for a normative sample of *Xenopus* embryos that could be used to compare to previous methods. In addition, some of the functional assessments we performed have not, to our knowledge, been previously documented for *Xenopus*, therefore, our results will expand our knowledge of early cardiogenesis in this model organism.

The video imaging system provided the ability to study embryos at four developmental stages during which cardiogenesis is considered relatively complete (Kolker et al., 2000). The stages assessed included stages 45, 46, 47, and 48 (Movies 1, 2, 3, and 4, respectively). A sample size of fifty embryos was used to characterize each stage when assessing functional data. The embryos were not studied longitudinally, so each stage is considered to be a separate non-identical subset. Although I attempted to assess embryos earlier than stage 45 and later than stage 48, there were optical considerations that created more difficulty and less accuracy in measuring function. Embryos earlier than stage 45 were difficult to assess due to decreased hemodynamics and increased pigmentation, as well as increased opacity on the ventral ectoderm. Embryos older than early stage 48 were considerably larger than younger embryos creating an increased working distance that decreased the sharpness of the epicardial and endocardial contours. This will be explained more thoroughly in a section addressing limitations of this system.

### 3.1.1 Ejection Fraction

A previous study (Deniz et al., 2012) concluded, after utilizing hemoglobin contrast subtraction angiography, that *Xenopus tropicalis,* a closely related species, ordinarily have 100% ejection fraction thereby completely emptying the ventricle of blood by end-systole. Images captured using our system corroborate this finding (for an example, refer to Movie 1). Therefore, in my experiments I assumed approximately 100% ejection fraction such that blood volume in the ventricle at end-systole is negligible in comparison to ventricular volume at end-diastole.

### 3.1.2 Heart Rate

The heart rate of 50 separate embryos at each stage was obtained and used to compare the four developmental intervals (Figure 8). The mean heart rate at stage 45 was observed to be 91.7bpm, whereas the average heart rate was calculated to be 124.6bpm by stage 46. The mean computed at stage 47 was 139.3bpm and the average heart rate at stage 48 was 144.2bpm. Overall, heart rate increased significantly as the embryo developed from stage 45 through to stage 47, although there was no significant increase in heart rate from stage 47 to 48. I noted that heart rate varies considerably in this species as compared to other animal models. In addition, the most dramatic increase appears to be following maturation of stage 45 embryos to stage 46.

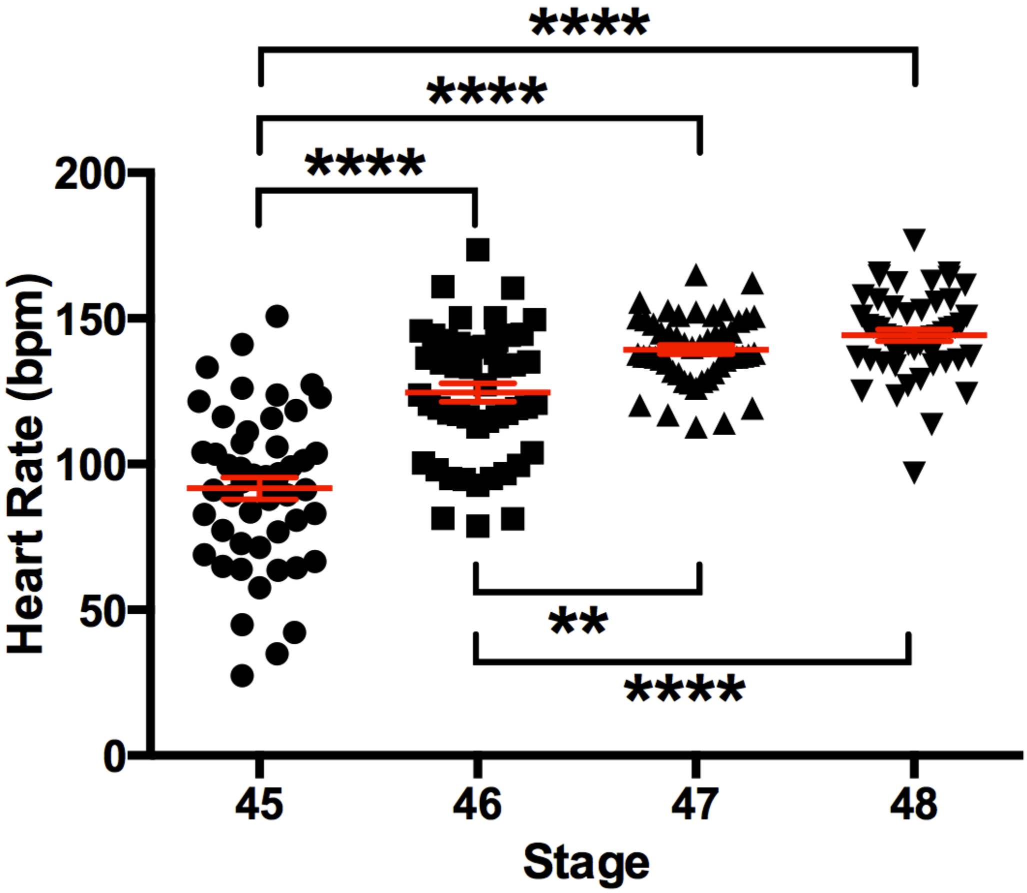

**Figure 8. Heart rate increases in *Xenopus laevis* embryos from stages 45 to 48.** The average heart rate of *Xenopus laevis* embryos was analyzed at four stages of cardiac development. There were significant increases in heart rate from stage 45 through to stage 47, although no significant difference was observed between stages 47 and 48. A one-way ANOVA paired with a Tukey's post-hoc test was used to compare the heart rate data. The means are indicated by the center of the red bars and the end bars represent ±SEM. n = 50 for each group; **$p \leq 0.01$; ****$p \leq 0.0001$

### 3.1.3 Ventricular Wall Thickness

Ventricular wall thickness (VWT) was measured at both end-diastole and end-systole at stages 45 to 48 (Figure 9).

Significant increases in ventricular wall thickness at end-diastole were observed (Figure 9A). The mean at stage 45 was determined to be $4.95 \times 10^{-2}$mm. An increase in thickness was observed by stage 46 with an average calculated to be $6.03 \times 10^{-2}$mm. The mean computed at stage 47 was $6.68 \times 10^{-2}$mm, whereas the average VWT by stage 48 was $7.40 \times 10^{-2}$mm. A significant increase in ventricular wall thickness at end-diastole was shown when comparing every stage examined.

Additionally, VWT at end-systole was also examined (Figure 9B). The mean ventricular wall thickness at end-systole for stage 45 was $9.29 \times 10^{-2}$mm. At stage 46, the mean VWT was $9.71 \times 10^{-2}$mm, whereas the average was $1.19 \times 10^{-1}$mm for stage 47. Embryos at stage 48 had an average ventricular wall thickness of $1.25 \times 10^{-1}$mm at end-systole. A significant increase in VWT was observed when comparing stage 45 to either stage 47 or 48. A significant increase was also detected between stage 46 and the two later stages. There was no significant difference between stages 45 and 46 and no significant increase was observed between stages 47 and 48.

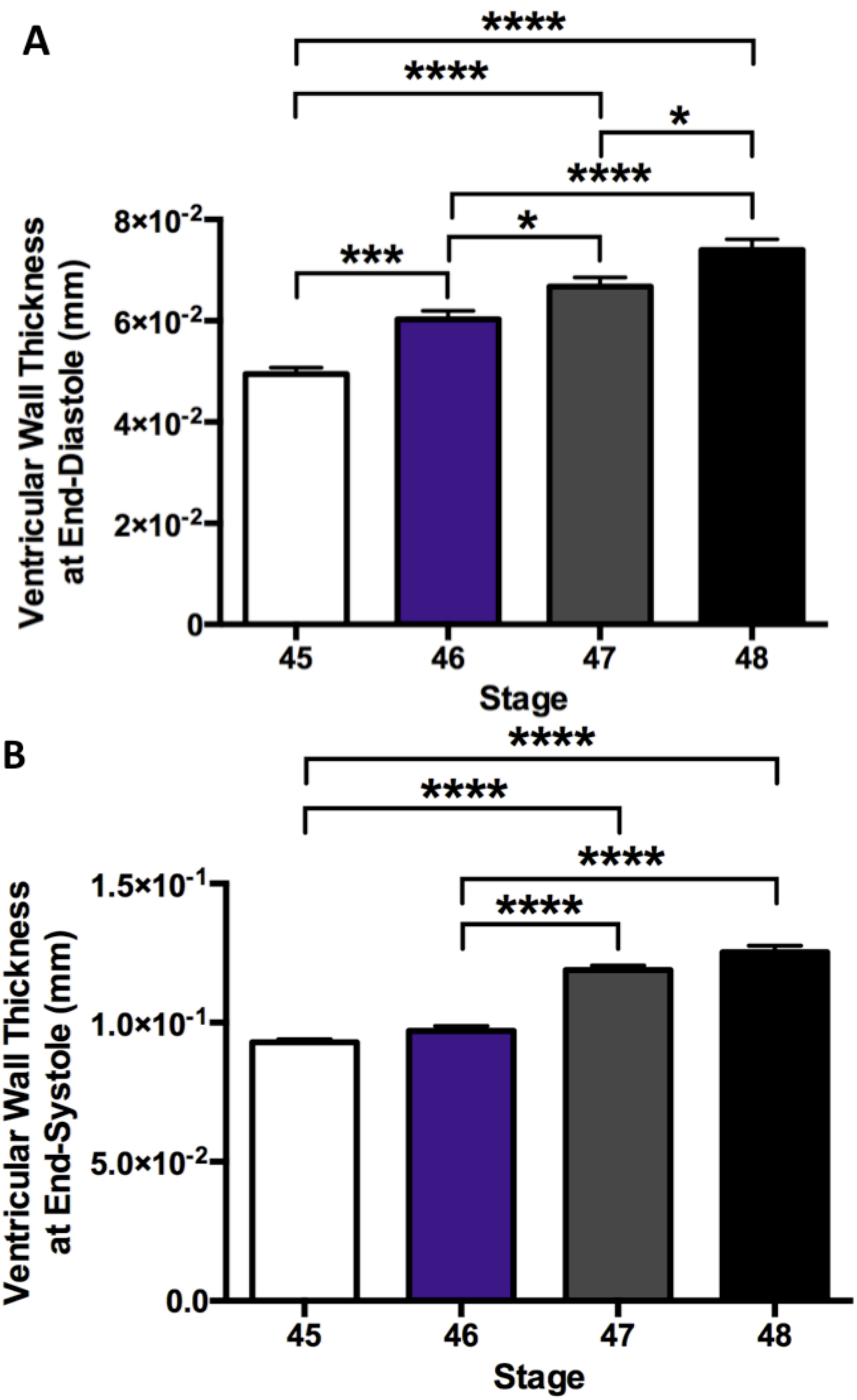
A
****
****
*
****
*
***
Ventricular Wall Thickness at End-Diastole (mm)
8×10-2
6×10-2
4×10-2
2×10-2
0
45
46
47
48
Stage
B
****
****
****
****
Ventricular Wall Thickness at End-Systole (mm)
1.5×10-1
1.0×10-1
5.0×10-2
0.0
45
46
47
48
Stage

**Figure 9. Average ventricular wall thickness of *Xenopus laevis* embryos increases from stages 45 to 48.** The average ventricular wall thickness (VWT) at end-diastole was analyzed at stages 45, 46, 47, and 48 (Panel A). An increase in VWT was observed as embryos matured through the four stages. A significant difference was determined between all groups that were analyzed. As well, the average ventricular wall thickness was also examined at end-systole (Panel B). No significant differences were observed following comparison of stage 45 and stage 46 as well as no significant increase between stages 47 and 48. However, increases in VWT were observed when comparing stage 45 to stages 47 and 48 or through comparison of stage 46 and the two later developmental stages. Analysis of the data involved a one-way ANOVA paired with a Tukey's post-hoc test. The end bars represent ±SEM. n = 50 for each group; $*p \leq 0.05$; $***p \leq 0.001$; $****p \leq 0.0001$

### 3.1.4 Stroke Volume and Cardiac Output

Another parameter that was analyzed to determine cardiac function in early *Xenopus* embryos was stroke volume (SV) (Figure 10A). Stroke volume represents the volume of blood that is pumped by the heart for a single cardiac contraction. A collective 200 embryos were measured spanning four developmental stages. Importantly, ejection fraction was assumed to be approximately 100% implying that the blood volume in the ventricular cavity at end-systole was approximately zero. This is based on both previous observations and our own video images (Deniz et al., 2012) (Movie 1). Significant increases in stroke volume were observed when stages 45 or 46 were compared to stages 47 and 48. Embryos at stages 45 and 46 were not statistically different and no significant difference was observed when comparing stages 47 and 48. The mean stroke volume at stage 45 and 46 was $1.2 \times 10^{-3}$μL and $1.8 \times 10^{-3}$μL, respectively. The mean computed at stage 47 was $3.8 \times 10^{-3}$μL and the mean SV for stage 48 embryos was calculated to be $3.9 \times 10^{-3}$μL.

Cardiac output (CO) was measured for *Xenopus* embryos during stages 45, 46, 47, and 48 (Figure 10B). Cardiac output represents the volume of blood pumped by the heart in a minute and is dependent on stroke volume and heart rate. There was an overall increase in CO observed as the embryos progressed through the stages. The average CO for stage 45 was $1.2 \times 10^{-1}$μL/min. For stage 46 embryos, the average cardiac output was calculated to be $2.3 \times 10^{-1}$μL/min, whereas the mean for stage 47 embryos was $5.3 \times 10^{-1}$μL/min. The mean cardiac output computed for stage 48 was determined to be $5.7 \times 10^{-1}$μL/min. A significant increase in CO was observed following comparison of stage 45 embryos and every other stage. A functionally significant increase was observed following comparison of stage 46 with the two most mature stages. The only stages that were not statistically different following comparison were stages 47 and 48.

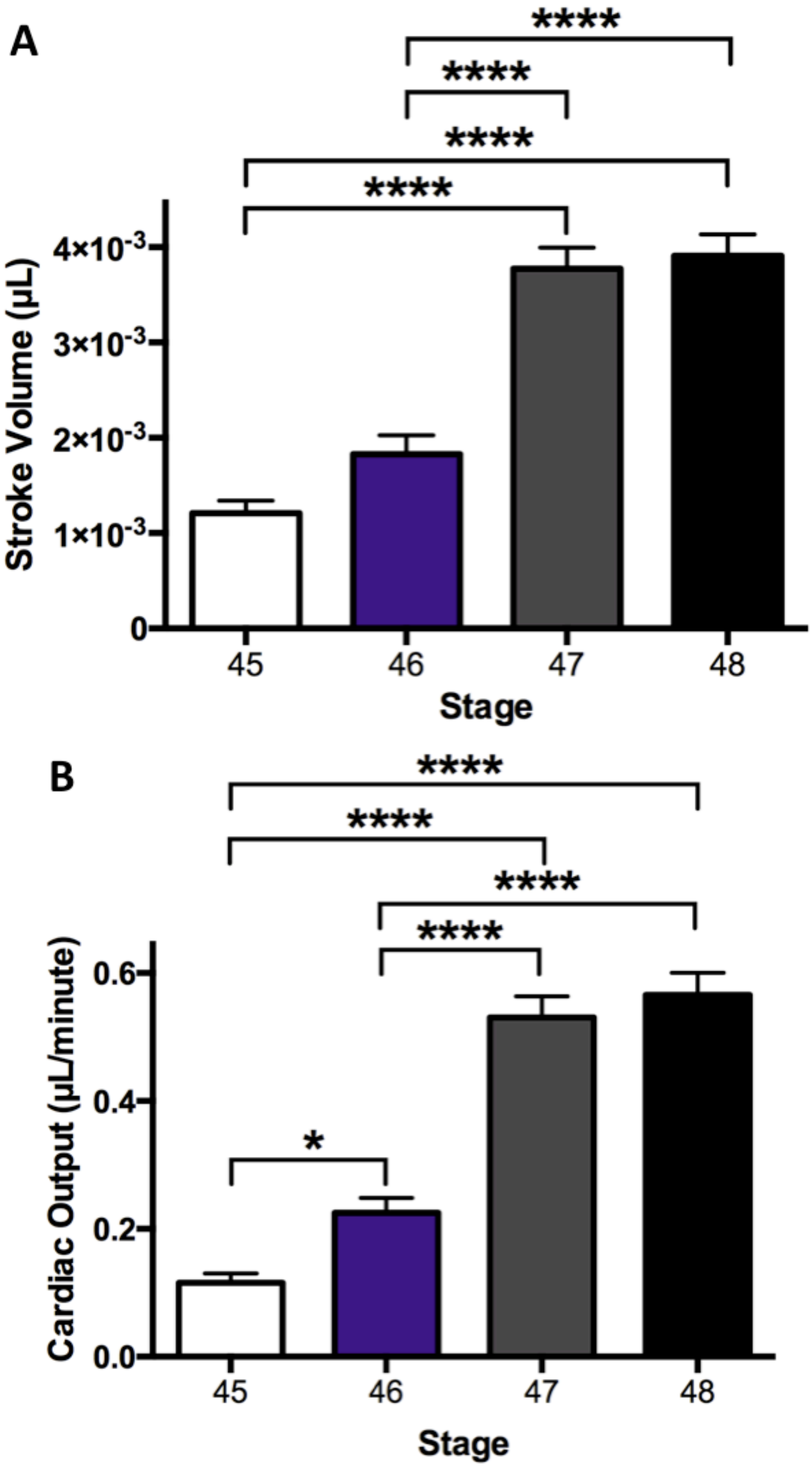
A
****
****
****
****
Stroke Volume (µL)
4×10$^{-3}$
3×10$^{-3}$
2×10$^{-3}$
1×10$^{-3}$
0
45
46
47
48
Stage
B
****
****
****
****
*
Cardiac Output (µL/minute)
0.6
0.4
0.2
0.0
45
46
47
48
Stage

**Figure 10. Average stroke volume and cardiac output increases between stages 45 and 48 in *Xenopus laevis* embryos.** The average stroke volume was determined from embryos spanning stages 45 to 48 (Panel A). No statistical differences were observed between the two earlier stages as well as between the two later stages. However, a statistically significant increase was detected between stage 45 embryos and the two most mature stages. A statistical increase was demonstrated between stage 46 and the two later stages. Furthermore, cardiac output was assessed for the four developmental stages (Panel B). A statistically significant difference was observed following comparison of stage 45 embryos with every other stage. Stage 46 embryos were also identified as being significantly different from every other stage for cardiac output. There was no significant difference when comparing stage 47 against stage 48. A one way-ANOVA paired with a Tukey's post-hoc test was used to compare the stages. The end bars represent ±SEM. n = 50 for each group; $^*p \leq 0.05$; $^{****}p \leq 0.0001$

### 3.1.5 Flow Velocity

Flow velocity (FV) was computed through the use of the HeartMetrics software. This parameter involved tracking the velocity of individual erythrocytes in the anterior portion of the left aortic arch directly after end-diastole when cardiac contraction was at a maximum. The embryos used in the normative sample to measure cardiac function were not the identical embryos used for this experiment. This experiment involved the measurement of laminar flow within the center of the vessel, as turbulent flow along the vessel walls could not be measured using the method selected.

The flow velocity was measured for fourteen embryos that were morphologically normal (Figure 11; Movie 5). *Xenopus* embryos were at stage 48 at the time of imaging. The average flow velocity was determined to be 4.0mm/s, however, considerable variability in the measurements was observed.

### 3.1.6 Conclusions

The video imaging system was able to assess cardiac function between stages 45 and 48 in *Xenopus laevis* development. We found small, but significant increases in heart rate and cardiac function as embryos matured.

However, in order to further verify the ability of this system to detect changes in cardiac function in *Xenopus*, we proposed to use pharmacological agents that have well-documented effects on heart rate.

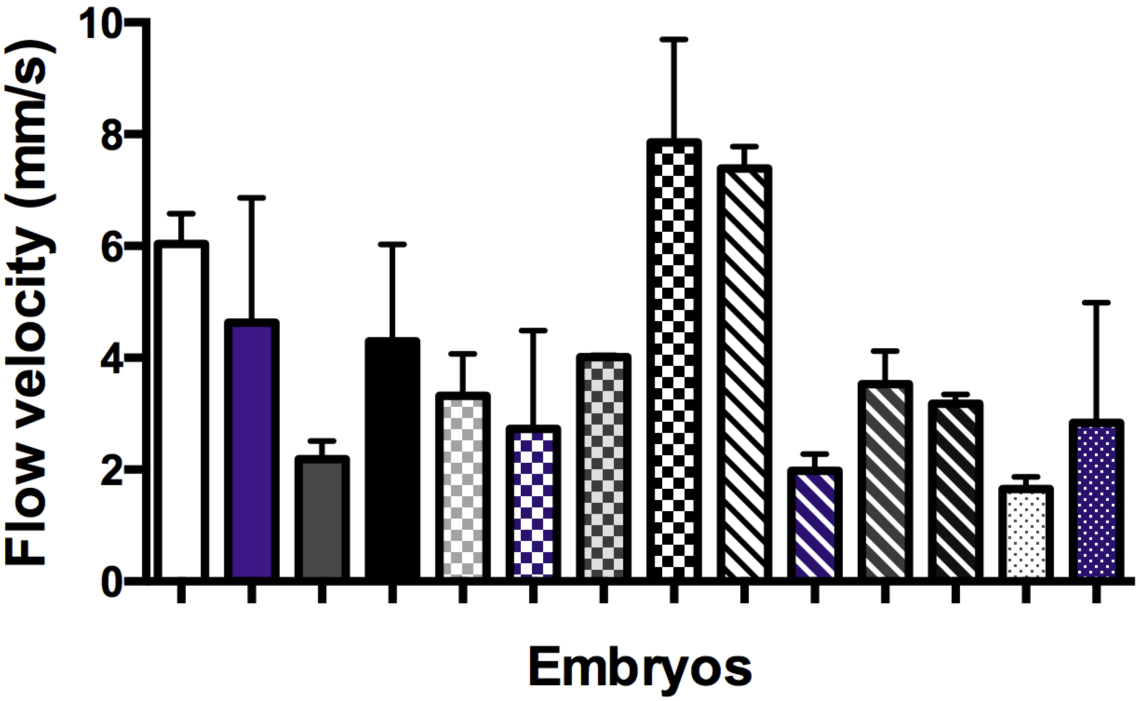

**Figure 11. Flow velocity in the left aortic arch of stage 48 *Xenopus* embryos.** The figure depicts the individual flow velocities of fourteen separate stage 48 *Xenopus laevis* embryos. Each measurement was performed four times and averaged to provide representative data. To perform the experiment, individual erythrocytes were tracked in the anterior portion of the left aortic arch directly after end-diastole. The average flow velocity was determined to be 4.0mm/s with a standard error of mean of 2.0mm/s. n = 14

## 3.2 Classical Modulators of Heart Rate

### 3.2.1 Rationale

The sino-atrial node (SAN) is the cardiac region that acts as the pacemaker of the heart (Tripathi et al., 2001). The spontaneous electrical activity generated by the SAN normally serves as the origin of the organism's heart rate and rhythmicity. The rate and rhythmicity of the heart can be manipulated using various pharmacological agents.

The effect that these pharmacological agents have on heart rate is well documented, so the outcomes following administration of these drugs to *Xenopus laevis* embryos are predictable. Therefore, exposure of *Xenopus* embryos to these pharmacological agents can be used to determine if we can assess changes in cardiac function using our system.

To modify heart rate, we chose to use atropine, epinephrine, isoproterenol, and metoprolol. The *Xenopus laevis* embryos used in these experiments ranged from stages 46 to 48 because we could test function at these stages. We were able to demonstrate predictable changes in heart rate using our imaging system.

### 3.2.2 Atropine, Epinephrine, and Isoproterenol

Atropine is recognized to act as an antagonist for the acetylcholine receptors located in the parasympathetic nervous system (Shutt and Bowes, 1979). Exposure to atropine causes tachycardia or an increase in heart rate. Based on the experiment performed, atropine increased heart rate in an expected manner (Figure 12A). The highest concentration resulted in a 21.5% increase in heart rate compared to the basal heart rate. Maximal sensitivity to atropine appears to start at approximately 0.05mM-0.1mM (concentrations 2 and 3) and the response shows saturation following administration of higher doses.

Epinephrine, otherwise referred to as adrenaline, is a hormone endogenous to the human body. Exogenous administration of epinephrine has been cited in the literature to increase heart rate (Callaway, 2013). We observed a concentration-dependent increase in heart rate in *Xenopus* embryos following epinephrine exposure (Figure 12B). Heart rate was increased by 20.5% compared to baseline at the highest concentration of epinephrine.

Isoproterenol exerts its pharmacological effects by serving as a beta-adrenergic agonist and has commonly been referred to as isoprenaline. Isoproterenol administration has been shown to induce increases in heart rate (Cirić and Susić, 1980). Following exposure to increasing concentrations of isoproterenol, an increase in heart rate was observed for *Xenopus* embryos (Figure 12C). The highest concentration of isoproterenol produced a 20.1% increase in heart rate compared to baseline measurements. Maximal sensitivity to isoproterenol appears to be attained at concentration 3 (0.1mM), therefore, concentrations 4 and 5 show a plateau signifying saturation.

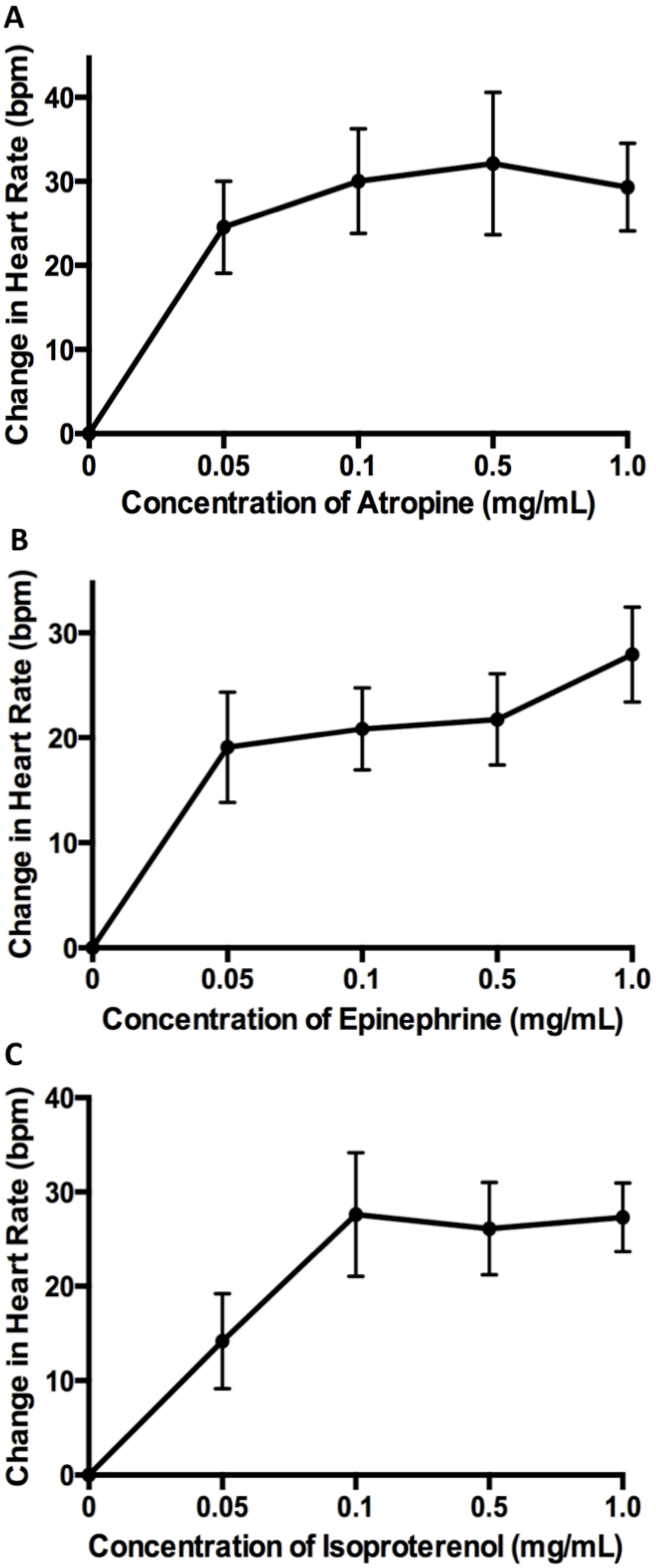
A
Change in Heart Rate (bpm)
0
10
20
30
40
0
0.05
0.1
0.5
1.0
Concentration of Atropine (mg/mL)
B
Change in Heart Rate (bpm)
0
10
20
30
0
0.05
0.1
0.5
1.0
Concentration of Epinephrine (mg/mL)
C
Change in Heart Rate (bpm)
0
10
20
30
40
0
0.05
0.1
0.5
1.0
Concentration of Isoproterenol (mg/mL)

**Figure 12. Atropine, epinephrine, and isoproterenol exposure result in increases in heart rate for *Xenopus* embryos.** *Xenopus laevis* embryos were subjected to various concentrations of atropine (Panel A), epinephrine (Panel B), and isoproterenol (Panel C) to examine whether the expected increase in heart rate could be detected using our imaging system. *Xenopus* embryos had matured to stages 46-48 prior to assessment. The data demonstrates a positive correlation between concentration of drug and heart rate for each pharmacological agent studied. A non-linear regression was used to analyze the data and both axes are shown as linear. The end bars represent ±SEM. n = 7, 7, and 6 for the atropine, epinephrine, and isoproterenol experiments, respectively; bpm = beats per minute

### 3.2.3 Metoprolol and Drug Combinations

In contrast, metoprolol is a β-blocking agent that is clinically used to treat tachycardia (Fujito et al., 2014). Therefore, the pharmacological properties of metoprolol culminate in a decrease in heart rate after administration. As predicted, metoprolol exposure resulted in a reduction in heart rate in a concentration-dependent manner (Figure 13A). Acute metoprolol exposure resulted in a 57.3% reduction in heart rate at the highest concentration in comparison to baseline heart rate.

Next, a combination of atropine and metoprolol was used to observe the antagonistic effects that these pharmacological agents have on heart rate (Figure 13B). To accomplish this, a baseline measurement of heart rate was measured and is represented as concentration 1 in the figure. Subsequently, *Xenopus* embryos were exposed to increasing concentrations of atropine, therefore, an initial increase in heart rate was expected. This was confirmed by an increase in heart rate during exposure to concentrations 2, 3 and 4. Afterwards, increasing concentrations of metoprolol were mixed with 1mg/mL of atropine. This resulted in a dose-dependent reduction in heart rate from concentrations 5 to 7. The heart rate is shown below baseline measurements at the highest concentration of metoprolol.

### 3.2.4 Conclusions

Our imaging system appears to be capable of detecting heart rate changes accurately. In addition, we can conclude that *Xenopus* embryos respond to classical heart rate modulators as expected when treated between stages 46-48.

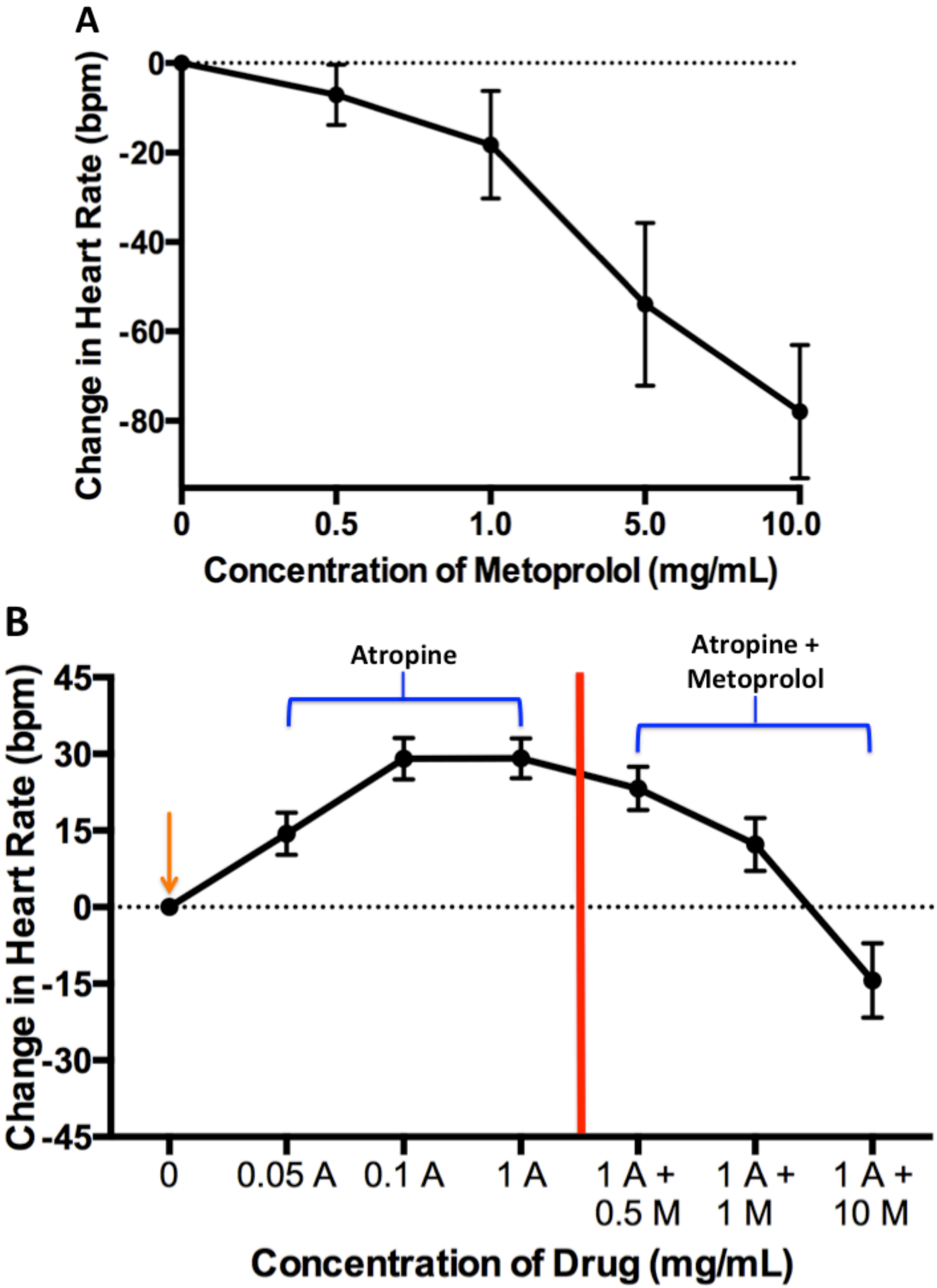
A
Change in Heart Rate (bpm)
0
-20
-40
-60
-80
0
0.5
1.0
5.0
10.0
Concentration of Metoprolol (mg/mL)
B
Atropine
Atropine +
Metoprolol
Change in Heart Rate (bpm)
45
30
15
0
-15
-30
-45
0
0.05 A
0.1 A
1 A
1 A +
0.5 M
1 A +
1 M
1 A +
10 M
Concentration of Drug (mg/mL)

**Figure 13. *Xenopus* embryos exposed to metoprolol and atropine demonstrated the expected changes in heart rate.** Exposure of *Xenopus laevis* embryos to metoprolol was documented to observe whether decreases in heart rate could be detected (Panel A). The data indicates that increasing concentrations of metoprolol caused a subsequent reduction in heart rate. Analysis of heart rate utilized a non-linear regression with both axes depicted as linear. Conversely, *Xenopus laevis* embryos were exposed to a combination of atropine and metoprolol to observe the antagonistic effects that these pharmacological agents have on heart rate (Panel B). Initially, heart rate was measured before any pharmacological agents were used (orange arrow). Subsequently, embryos were exposed to increasing concentrations of atropine and an increase in heart rate was observed. Next, increasing concentrations of metoprolol were added to 1mg/mL of atropine and a concentration-dependent decrease in heart rate was observed. A non-linear regression was used to assess the data and both axes were represented as linear. The end bars represent ±SEM. n = 7 and 8 for the metoprolol and combination experiments, respectively; bpm = beats per minute; A = atropine; M = metoprolol

## 3.3 Functional Changes Due to Morphological Alterations

The previous experiments focused on embryos that were allowed to develop normally. However, my overall objective was to test if we could see changes in cardiac function in embryos with morphological defects. We would predict that embryos with such defects would have significant alterations in cardiac function. To our knowledge, using this novel imaging system would be the first time that changes in cardiac function are analyzed in *Xenopus* embryos with known morphological changes.

### 3.3.1 Blebbistatin and Rockout

As mentioned previously, blebbistatin acts as an inhibitor of non-muscle myosin II, which acts downstream of ROCK signaling (Allingham et al., 2005; Amano et al., 1996; Dou et al., 2007; Swift et al., 2012). Experiments performed by Halabi demonstrated that exposure of *Xenopus laevis* embryo to (-)-blebbistatin initiating at stage 26 resulted in the disappearance of flexion points in the closing heart tube at stage 31/32. The absence of flexion points signifies disruption of proper cardiac tube closure. This was demonstrated through *in situ* hybridization using antisense mRNA probes against *cardiac troponin I* to selectively stain the myocardium (Halabi, 2013).

To further demonstrate that the changes were due to inhibition of ROCK signaling, we exposed embryos to Rockout, a second ROCK inhibitor. Rockout inhibits the ability of ROCK-II to phosphorylate MLC, thereby inhibiting ROCK activity, as is the case with blebbistatin. *In situ* hybridizations performed by Halabi demonstrated that Rockout disrupts cardiogenesis if *Xenopus* embryos are exposed starting at stage 26. As with the blebbistatin treatment, the flexion points did not develop properly as expected (Halabi, 2013).

Embryonic treatments were performed at stages 26 and 33/34 to observe cardiac disruptions resulting from ROCK inhibition. For the blebbistatin treatment, *Xenopus* embryos were either immersed in DMSO, (+)-blebbistatin, or (-)-blebbistatin, in which both DMSO and (+)-blebbistatin acted as control groups. For the Rockout treatment, embryos were either exposed to DMSO or Rockout. Embryos were exposed to the respective treatment for 24 hours at room temperature before being transferred to 20%

Steinberg's solution. Embryos were maintained until maturing to stage 46 and onwards prior to cardiac imaging and subsequent fixation for *in situ* hybridization.

Based on HeartMetrics images, there does appear to be a defect in cardiac looping for embryos exposed to (-)-blebbistatin when treated at both developmental periods. For my experiments, *in situ* hybridization for *cardiac troponin I* expression was used to selectively stain the myocardium for blebbistatin-exposed embryos (Figure 14A) and Rockout-exposed embryos (Figure 14B). In contrast to the data provided following blebbistatin exposure, there did not appear to be gross cardiac looping defects for Rockout-exposed embryos.

Heart rate was measured to identify potential variations in heart rate following exposure to blebbistatin (Figure 15A). A statistical increase in heart rate was only confirmed for embryos exposed to (-)-blebbistatin at stage 26, but not at stage 33/34. For the Rockout treatment, heart rate was also measured to examine the effect of Rockout on heart rate (Figure 15B). Rockout was determined to have no statistically significant effect on heart rate at either of the treatment stages.

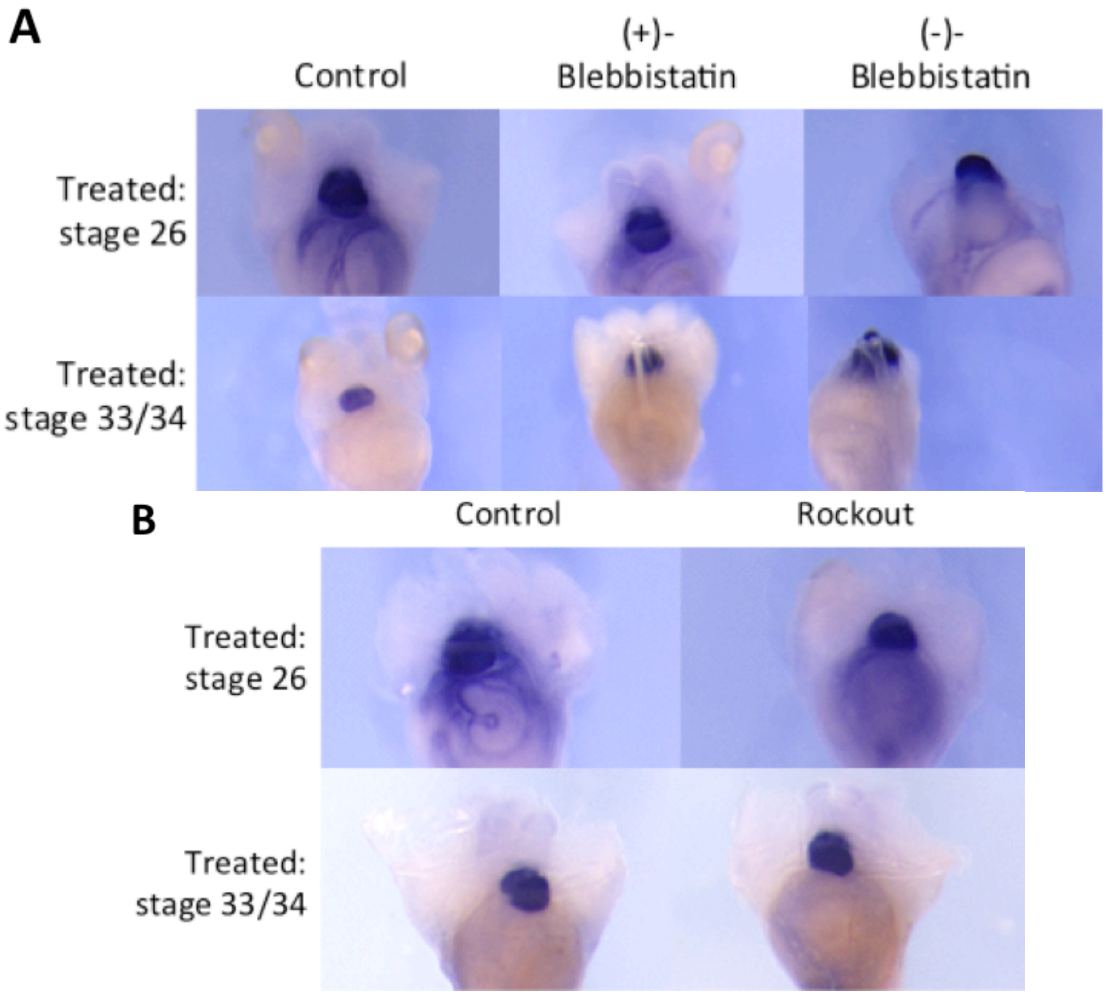
A
Control
(+)-
Blebbistatin
(-)-
Blebbistatin
Treated:
stage 26
Treated:
stage 33/34
B
Control
Rockout
Treated:
stage 26
Treated:
stage 33/34

**Figure 14. Abnormal cardiac morphogenesis in *Xenopus laevis* embryos following exposure to blebbistatin and Rockout.** Following embryo fixation, the myocardium was selectively stained through *in situ* hybridization using an antisense mRNA probe against *cardiac troponin I* mRNA. *Xenopus laevis* embryos were exposed to DMSO, (+)-blebbistatin, or (-)-blebbistatin commencing at stage 26 or 33/34 (Panel A). Both the DMSO- and (+)-blebbistatin-exposed embryos served as control groups. Significant reductions in ventricular morphology were observed in the (-)-blebbistatin-exposed embryos following treatment at stage 26. No significant alterations in ventricular morphology were noted following exposure at stage 33/34. As well, *Xenopus laevis* embryos were exposed to either DMSO or Rockout initiating at stages 26 and 33/34 (Panel B). The ventricular dimensions of embryos treated at stage 26 with Rockout demonstrated significant reductions. A significant increase in area of the ventricle was noted following Rockout exposure at stage 33/34.

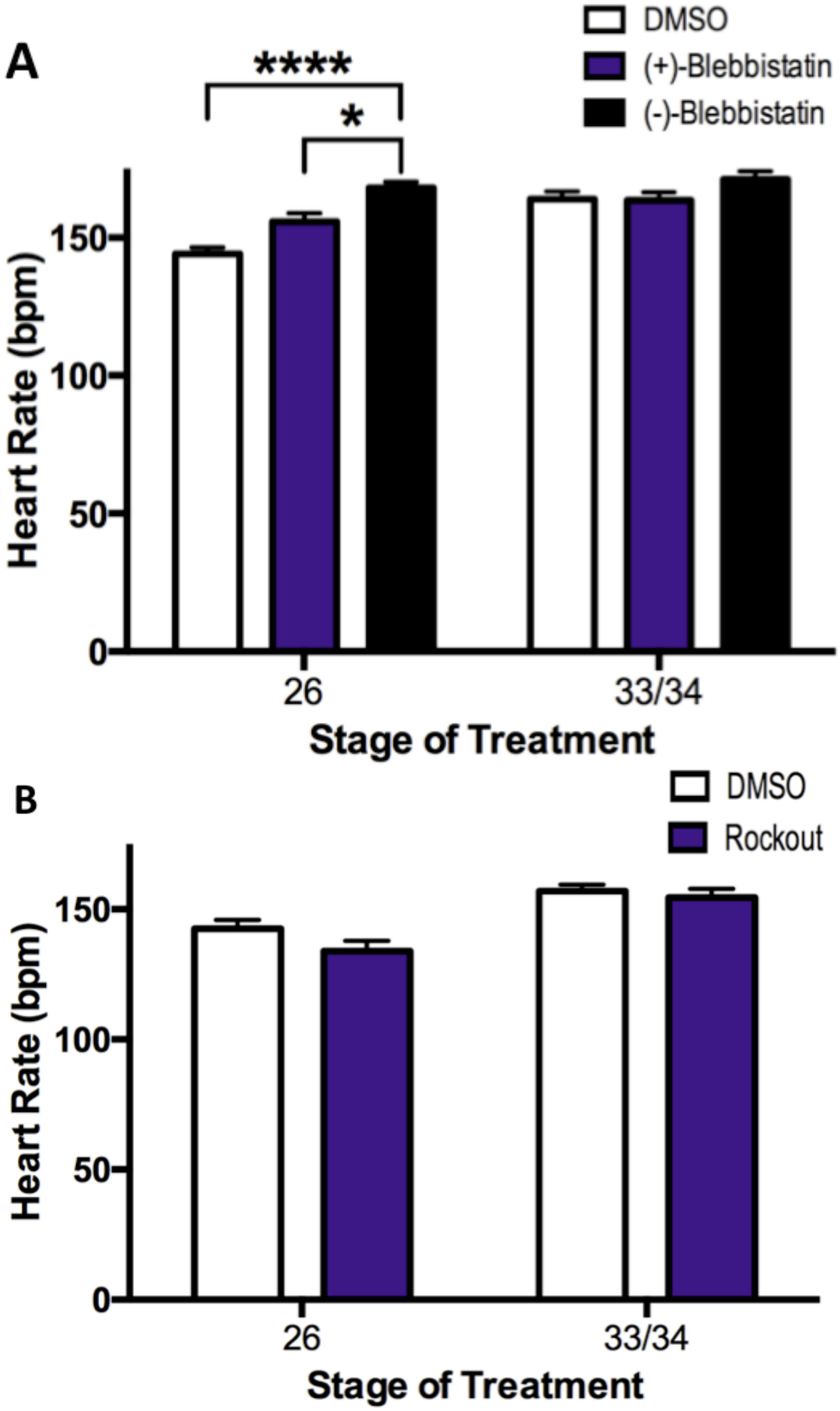
A
DMSO
(+)-Blebbistatin
(-)-Blebbistatin
****
*
Heart Rate (bpm)
0
50
100
150
26
33/34
Stage of Treatment
B
DMSO
Rockout
Heart Rate (bpm)
0
50
100
150
26
33/34
Stage of Treatment

**Figure 15. Increase in heart rate of *Xenopus* embryos following exposure to blebbistatin, but not following exposure to Rockout.** Heart rate was measured and analyzed following exposure to either DMSO, (+)-blebbistatin, or (-)-blebbistatin (Panel A). No significant differences were observed for heart rate following exposure at stage 33/34. A significant increase in heart rate was detected following exposure to (-)-blebbistatin at stage 26 compared to both of the control groups. Comparison of heart rate for DMSO- and Rockout-exposed embryos is shown in panel B. No significant differences in heart rate were observed following exposure to Rockout at either stage examined. Heart rate was measured in beats per minute (bpm) and data analysis involved a two-way ANOVA paired with a Sidak test. The end bars represent ±SEM. n = 6 for each group; $^{*}p \leq 0.05$; $^{****}p \leq 0.0001$

#### 3.3.1.1 Treatment of *Xenopus laevis* embryos at stage 26 with blebbistatin and Rockout

*Xenopus laevis* embryos were exposed to either DMSO, (+)-blebbistatin, or (-)-blebbistatin (Movie 6) initiating at stage 26. This coincides with the developmental time point directly before cardiac differentiation and during closure of the linear heart tube (Kolker et al., 2000; Lohr and Yost, 2000; Mohun et al., 2000).

As predicted, the embryos treated with DMSO and (+)-blebbistatin did not differ with respect to cardiac function (Figure 16A). In contrast, statistically significant reductions in cross-sectional area of the ventricular cavity and ventricular wall thickness were observed for the (-)-blebbistatin-treated embryos compared to both control groups. No significant difference was observed between any of the groups when examining volume of blood in the ventricular cavity.

For the Rockout treatment, *Xenopus laevis* embryos were exposed at stage 26 to either DMSO or Rockout (Movie 7). Based on the cardiac function analysis at end-diastole, a significant decrease in ventricular wall thickness was detected in the Rockout-exposed embryos (Figure 16B). Cross-sectional area of the ventricular cavity and volume of blood in the ventricular cavity were not significantly different.

Subsequently, the embryos underwent *in situ* hybridization using an antisense mRNA probe against *cardiac troponin I* to examine whether morphological changes could be detected following disruption of cardiogenesis. Statistically significant decreases were observed for transverse length, perimeter, and cross-sectional area of the ventricle for embryos exposed to (-)-blebbistatin (Figure 17A). Significant differences were not detected with respect to longitudinal length of the ventricle when comparing all three groups. As predicted, no significant differences existed between the DMSO and (+)-blebbistatin groups. Rockout exposure resulted in significant reductions in perimeter and cross-sectional area of the ventricle (Figure 17B). Rockout did not significantly alter the longitudinal or transverse length of the ventricle.

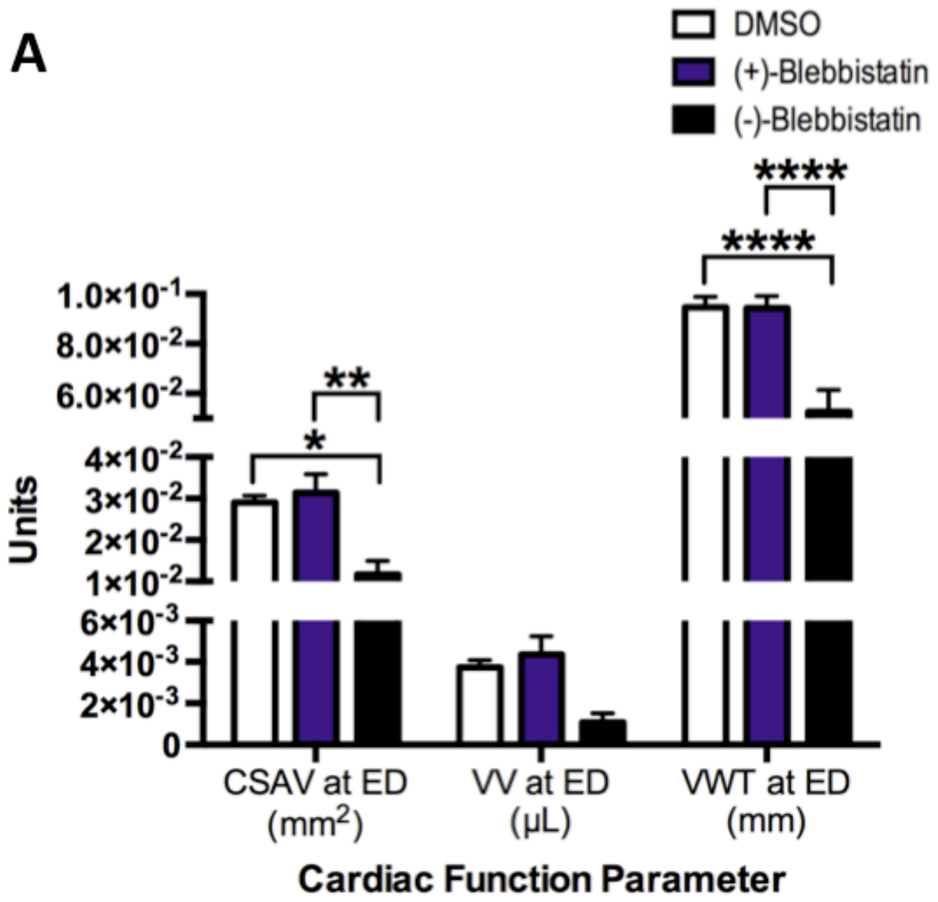
A
DMSO
(+)-Blebbistatin
(-)-Blebbistatin
****
****
**
*
1.0×10-1
8.0×10-2
6.0×10-2
4×10-2
3×10-2
2×10-2
1×10-2
6×10-3
4×10-3
2×10-3
0
Units
CSAV at ED (mm2)
VV at ED (μL)
VWT at ED (mm)
Cardiac Function Parameter

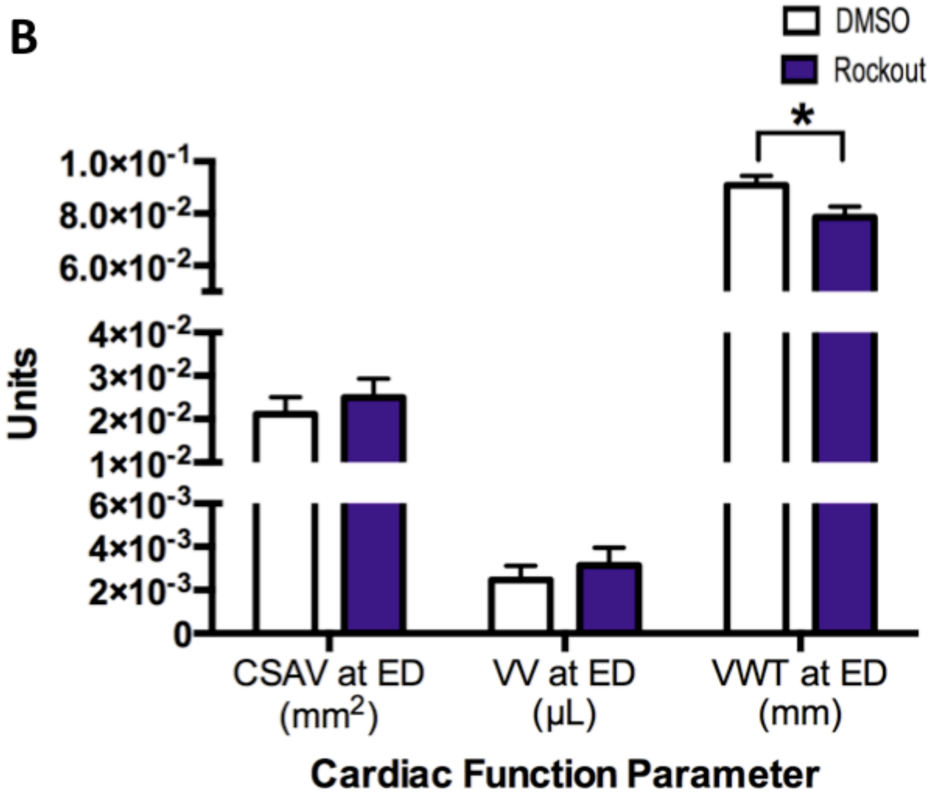
B
DMSO
Rockout
*
1.0×10-1
8.0×10-2
6.0×10-2
4×10-2
3×10-2
2×10-2
1×10-2
6×10-3
4×10-3
2×10-3
0
Units
CSAV at ED (mm2)
VV at ED (μL)
VWT at ED (mm)
Cardiac Function Parameter

**Figure 16. Reductions in cardiac function following exposure of *Xenopus laevis* embryos to blebbistatin and Rockout at stage 26.** Cardiac function was analyzed for treated embryos using parameters at end-diastole (ED). *Xenopus laevis* embryos were exposed to either DMSO, (+)-blebbistatin, or (-)-blebbistatin commencing at stage 26 (Panel A). Both DMSO and (+)-blebbistatin, the inactive enantiomer, served as control groups. No significant differences were observed between the DMSO group and the (+)-blebbistatin-treated embryos. There were significant reductions in cross-sectional area of the ventricular cavity (CSAV) and ventricular wall thickness (VWT) for the embryos exposed to (-)-blebbistatin compared to both of the control groups. No significant differences were observed for volume of blood in the ventricular cavity (VV) between any of the groups. As well, *Xenopus laevis* embryos were exposed to either DMSO (control) or Rockout initiating at stage 26 (Panel B). Cardiac function at end-diastole was examined and a significant reduction in VWT was observed in the Rockout-treated group. CSAV and VV were not significantly different between the two groups. Analysis of functional data was performed using a two-way ANOVA paired with a Sidak test. The end bars represent ±SEM. $n = 6$ for each group; $^{*}p \leq 0.05$; $^{**}p \leq 0.01$; $^{****}p \leq 0.0001$

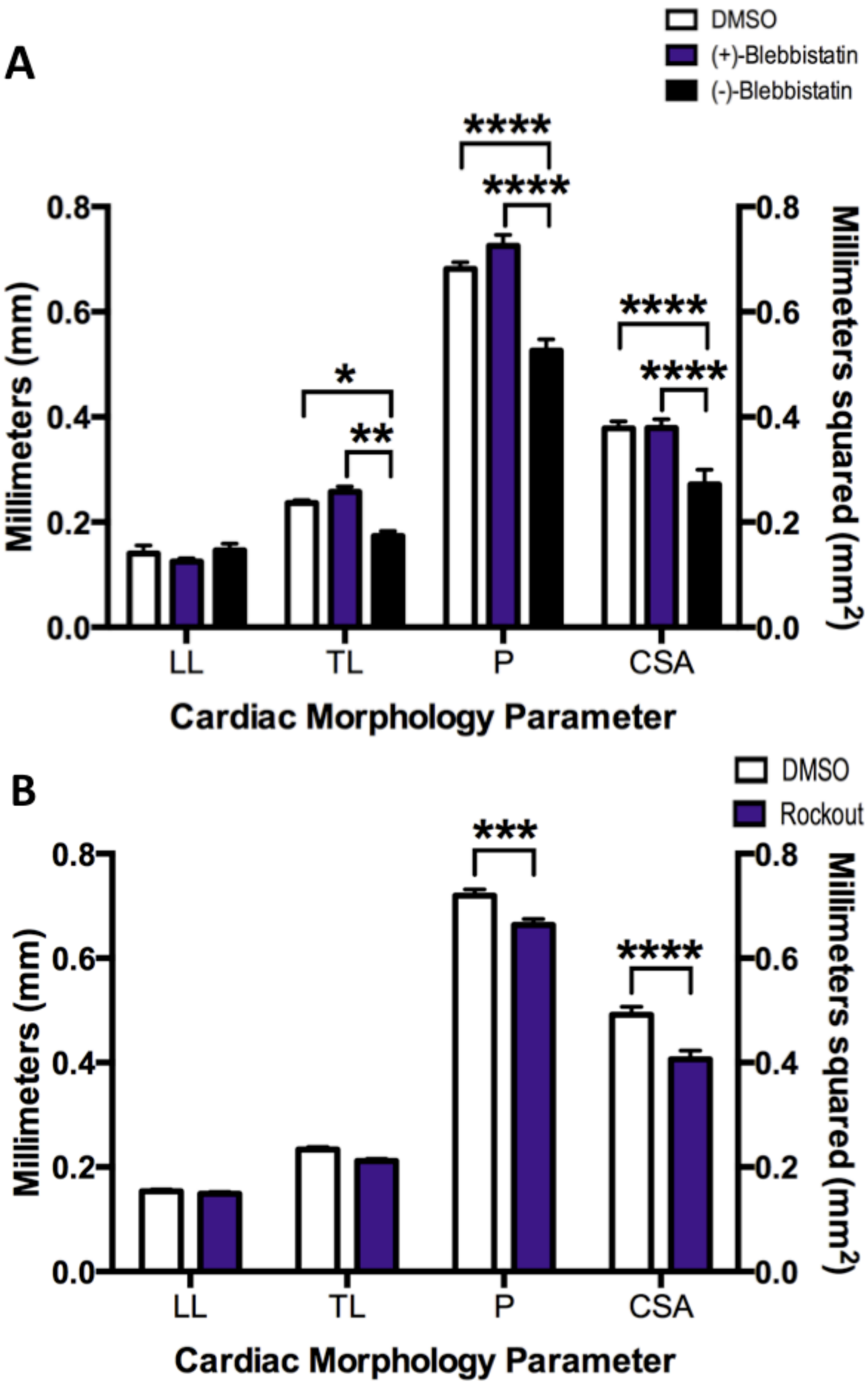
A
DMSO
(+)-Blebbistatin
(-)-Blebbistatin
Millimeters (mm)
Millimeters squared ($mm^2$)
0.0
0.2
0.4
0.6
0.8
*
**
****
****
****
****
LL
TL
P
CSA
Cardiac Morphology Parameter
B
DMSO
Rockout
Millimeters (mm)
Millimeters squared ($mm^2$)
0.0
0.2
0.4
0.6
0.8
***
****
LL
TL
P
CSA
Cardiac Morphology Parameter

**Figure 17. Reductions in ventricular size in *Xenopus* embryos exposed to blebbistatin and Rockout at stage 26.** *Xenopus laevis* embryos were exposed to small molecules that disrupt cardiogenesis to examine morphological alterations. *Xenopus laevis* embryos were exposed to DMSO, (+)-blebbistatin, or (-)-blebbistatin starting at stage 26 (Panel A). DMSO- and (+)-blebbistatin-treated embryos were considered to be control groups. Significant differences in ventricular parameters were not observed between the two control groups. In contrast, significant reductions were observed in transverse length (TL), perimeter (P), and cross-sectional area (CSA) of the ventricle in the (-)-blebbistatin group compared to both control groups. No significant differences were identified between any of the groups with respect to longitudinal length (LL) of the ventricle. Stage 26 *Xenopus* embryos were also exposed to DMSO (control) or Rockout (Panel B). No significant differences were observed between the DMSO- and Rockout-treated groups when comparing LL and TL of the ventricle. Significant ventricular reductions in P and CSA were detected for the Rockout-exposed embryos. Ventricular morphology was assessed following fixation and *in situ* hybridization of embryos using an antisense mRNA probe against *cardiac troponin I.* Analysis of morphology data used a two-way ANOVA paired with a Sidak test and the end bars represent ±SEM. n = 58, 36, 56 for the DMSO, (+)-blebbistatin, and (-)-blebbistatin groups, respectively; n = 66 and 69 for the DMSO- and Rockout-treated groups, respectively; *$p \leq 0.05$; **$p \leq 0.01$; ***$p \leq 0.001$; ****$p \leq 0.0001$

#### 3.3.1.2 Treatment of *Xenopus laevis* embryos at stage 33/34 with blebbistatin and Rockout

*Xenopus laevis* embryos were exposed to the respective treatments initiating at stage 33/34. During this developmental period, the linear heart tube has completely closed and is beginning to undergo rightward looping to determine chamber and valve formation (Afouda and Hoppler, 2009; Bartlett et al., 2010; Kolker et al., 2000; Lohr and Yost, 2000; Mohun et al., 2000).

For the blebbistatin treatment, embryos were either exposed to DMSO, (+)-blebbistatin, or (-)-blebbistatin (Movie 8). No significant functional alterations were observed following exposure to (-)-blebbistatin when compared to both control groups (Figure 18A).

*Xenopus* embryos were exposed to either DMSO or Rockout (Movie 9). Rockout did not significantly alter cardiac function with respect to any of the parameters examined (Figure 18B). This included end-diastolic measurements of cross-sectional area of the ventricular cavity, volume of blood in the ventricular cavity, and ventricular wall thickness.

Subsequently, *Xenopus* embryos were fixed such that the myocardium could be labeled through a whole-mount *in situ* hybridization using an antisense mRNA probe against *cardiac troponin I*. This permitted morphological analysis following cardiac disruption through inhibition of ROCK activity.

No significant morphological differences were detected in the ventricle size following exposure to (-)-blebbistatin commencing at stage 33/34 (Figure 19A).

As well, no significant differences were observed between the control and Rockout-treated groups for longitudinal length, transverse length, and perimeter of the ventricle (Figure 19B). However, a statistically significant increase was observed in cross-sectional area for the Rockout-exposed embryos.

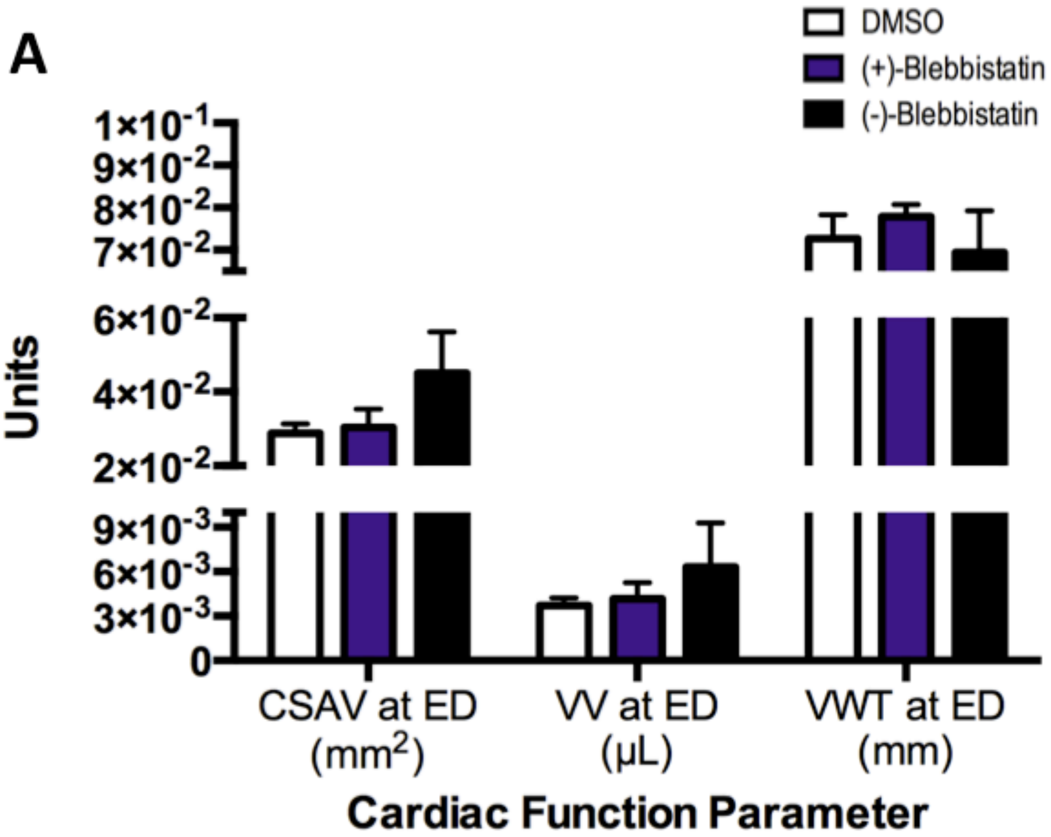
A
DMSO
(+)-Blebbistatin
(-)-Blebbistatin
Units
1×10-1
9×10-2
8×10-2
7×10-2
6×10-2
4×10-2
2×10-2
9×10-3
6×10-3
3×10-3
0
CSAV at ED (mm2)
VV at ED (µL)
VWT at ED (mm)
Cardiac Function Parameter

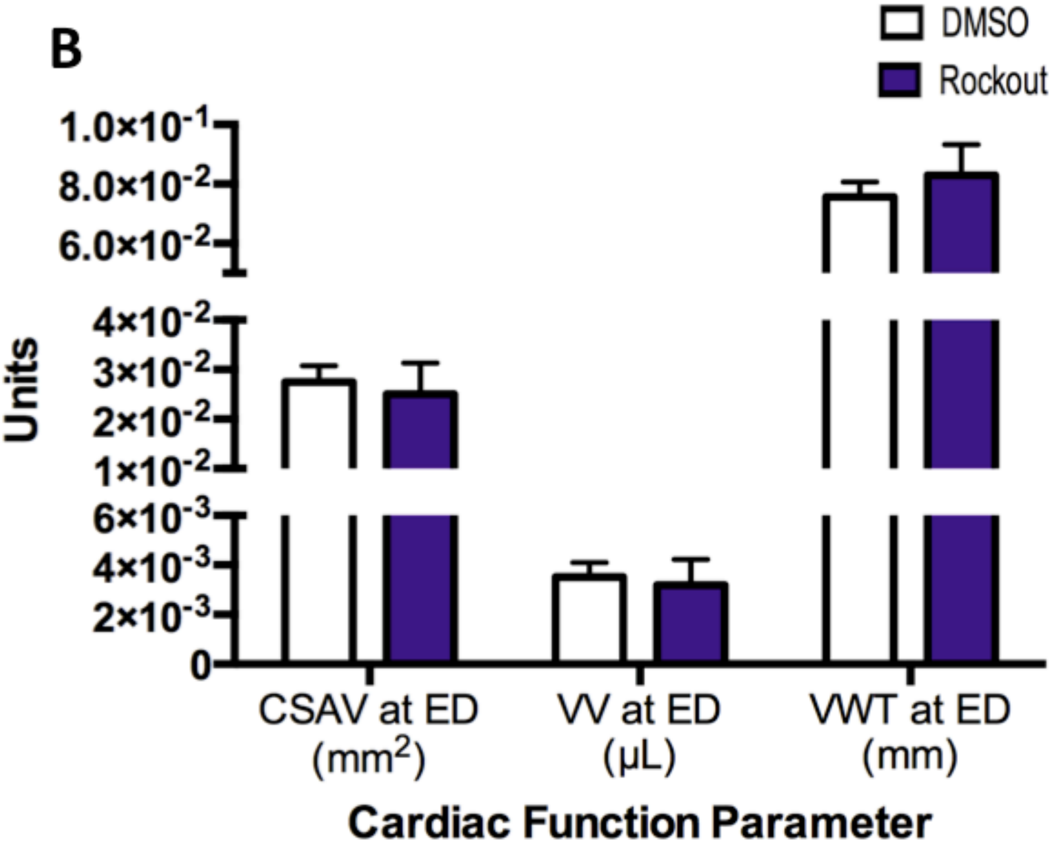
B
DMSO
Rockout
Units
1.0×10-1
8.0×10-2
6.0×10-2
4×10-2
3×10-2
2×10-2
1×10-2
6×10-3
4×10-3
2×10-3
0
CSAV at ED (mm2)
VV at ED (µL)
VWT at ED (mm)
Cardiac Function Parameter

**Figure 18. Cardiac function was not significantly altered in *Xenopus* embryos exposed to blebbistatin and Rockout at stage 33/34.** Cardiac function was compared for *Xenopus* embryos following disruption of cardiac development at stage 33/34. *Xenopus laevis* embryos were immersed in DMSO, (+)-blebbistatin, or (-)-blebbistatin (Panel A). Both the DMSO-treated and (+)-blebbistatin-treated embryos served as control groups since (+)-blebbistatin is an inactive enantiomer. Cardiac function at end-diastole (ED) was analyzed and significant differences were absent between any of the treatment groups examined. Parameters examined included cross-sectional area of the ventricular cavity (CSAV), volume of blood in the ventricular cavity (VV), and ventricular wall thickness (VWT). Panel B displays the Rockout experiment in which *Xenopus laevis* embryos were exposed to the control vehicle (DMSO) or Rockout. No significant functional differences were observed between the treatment groups. The data analysis required a two-way ANOVA paired with a Sidak test and the end bars represent ±SEM. n = 6 for each group

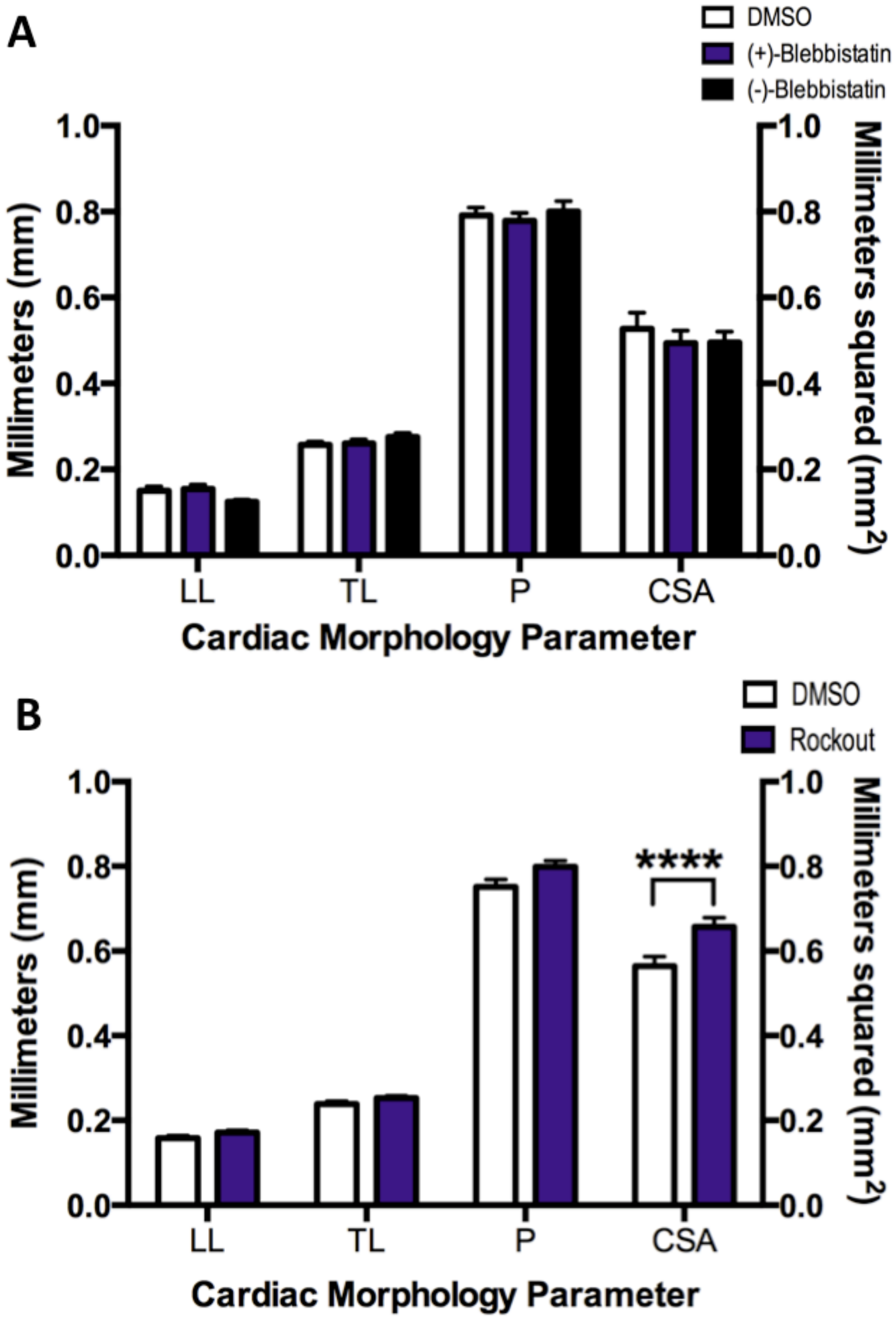
A
DMSO
(+)-Blebbistatin
(-)-Blebbistatin
Millimeters (mm)
Millimeters squared (mm$^2$)
1.0
0.8
0.6
0.4
0.2
0.0
LL
TL
P
CSA
Cardiac Morphology Parameter
B
DMSO
Rockout
Millimeters (mm)
Millimeters squared (mm$^2$)
1.0
0.8
0.6
0.4
0.2
0.0
****
LL
TL
P
CSA
Cardiac Morphology Parameter

**Figure 19. Exposure of *Xenopus* embryos to blebbistatin at stage 33/34 did not significantly alter ventricular morphology, although Rockout exposure resulted in an increase in ventricular dimension.** Cardiogenesis was disrupted using blebbistatin or Rockout commencing at stage 33/34 to examine morphological changes. Panel A depicts *Xenopus laevis* embryos that were exposed to DMSO, (+)-blebbistatin, or (-)-blebbistatin. There were no significant differences between the three treatment groups examined. The ventricular parameters used for the examination of cardiac morphology included longitudinal length (LL), transverse length (TL), perimeter (P), and cross-sectional area (CSA). Panel B displays *Xenopus* embryos exposed to either DMSO (control) or Rockout. No significant ventricular differences were detected between the DMSO- and Rockout-treated groups when comparing LL, TL, and P. A significant increase in ventricular CSA was observed for the embryos exposed to Rockout. Ventricular morphology was assessed following embryo fixation and whole mount *in situ* hybridization using an antisense mRNA probe against *cardiac troponin I.* Morphological data was compared using a two-way ANOVA paired with a Sidak test. The end bars represent ±SEM. n = 20, 24, 49 for the DMSO, (+)-blebbistatin, and (-)-blebbistatin groups, respectively; n = 33 and 37 for the DMSO and Rockout groups, respectively; $^{****}p \leq 0.0001$

#### 3.3.1.3 Conclusions

The data demonstrates that (-)-blebbistatin does disrupt cardiac function and morphology when embryos are exposed at stage 26. There was an overall decrease in ventricular morphology and function in the group treated with the active enantiomer. Conversely, no significant cardiac alterations were recorded following exposure to (-)-blebbistatin at stage 33/34.

Rockout also appears to induce changes in cardiac morphology and function that are reminiscent of the embryos exposed to (-)-blebbistatin. However, Rockout-treated embryos did not display as severe of a phenotype and cardiac looping defects were absent.

### 3.3.2 Retinoic Acid and Retinoic Acid Receptor Antagonist

The rationale for using these small molecules primarily arose from observations that cardiogenesis is disrupted in *Xenopus* embryos after exposure to RA and RAA during neurulation (Collop et al., 2006). Embryos that received exogenous retinoic acid demonstrated smaller hearts although a heart tube was fully formed. However, embryos with blocked RA signaling through exogenous treatment with retinoic acid receptor antagonists demonstrated lack of proper tube formation, although myocardial differentiation was still observed.

My project involved exposing embryos to RA and RAA commencing at stages 14, 26 and 33/34. Embryos were divided and submerged in DMSO, RA, or RAA, with DMSO serving as the control group. *Xenopus* embryos were exposed to the respective treatment for 24 hours at room temperature before being transferred to 20% Steinberg’s solution. Embryos were maintained until maturing to stage 46 and onwards prior to cardiac imaging and fixation.

I performed whole mount *in situ* hybridization to label the myocardium using an antisense mRNA probe that selectively labels *cardiac troponin I*. The cardiac morphology of embryos in both the control and treated groups are displayed following treatment (Figure 20A). The HeartMetrics videos enabled the ability to visualize cardiac looping defects following disruption of retinoic acid signaling with RA and RAA, except no looping defects were apparent following exposure to RAA at the latest stage examined.

Heart rate was measured to examine the effect of disturbing RA signaling on cardiac rhythmicity (Figure 20B). RA and RAA exposure did not result in statistically significant effects following exposure at the two later stages. Exposure at stage 14 resulted in a significantly reduced heart rate for the RA- and RAA-treated groups compared to the control.

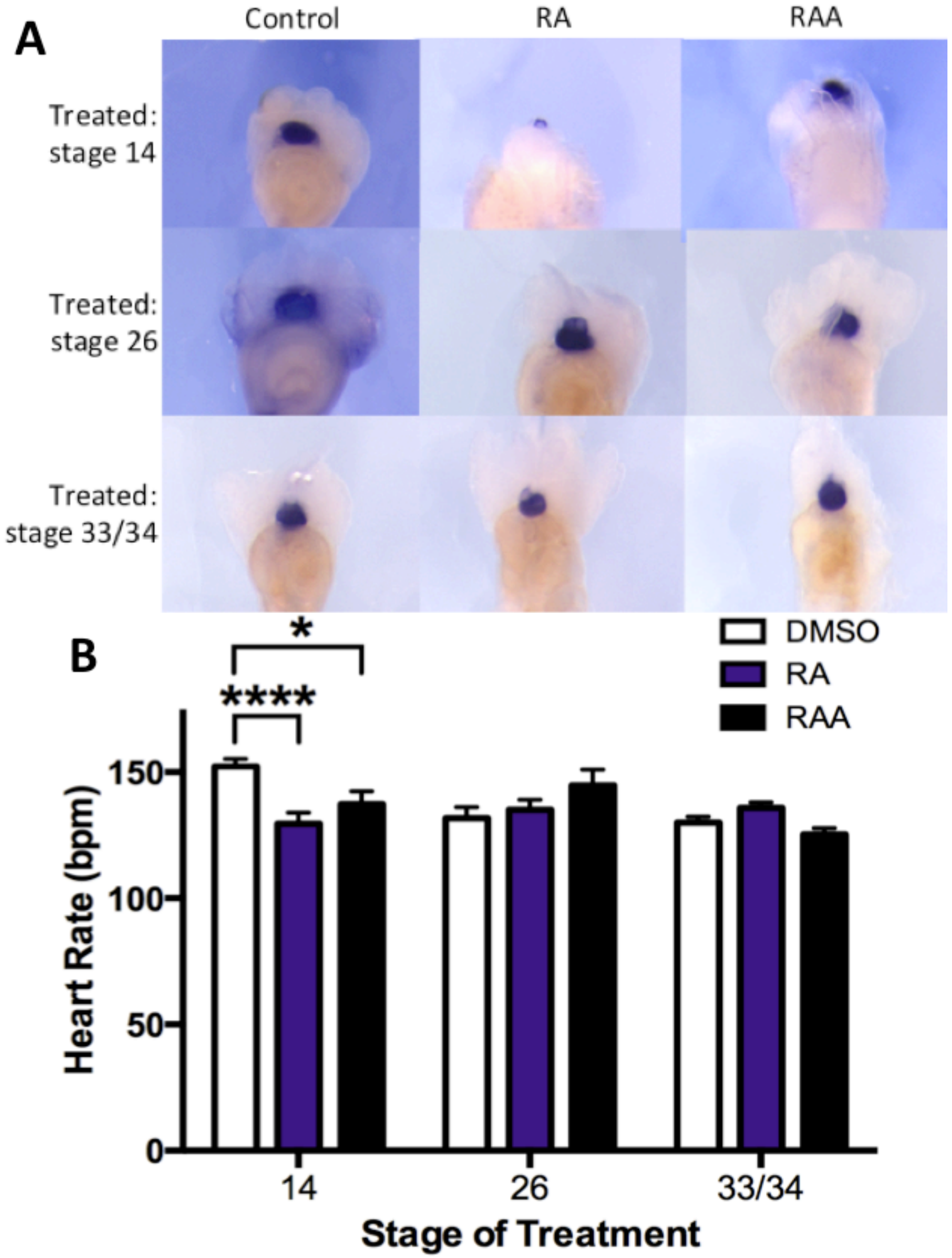
A
Control
RA
RAA
Treated: stage 14
Treated: stage 26
Treated: stage 33/34
B
*
****
DMSO
RA
RAA
Heart Rate (bpm)
150
100
50
0
14
26
33/34
Stage of Treatment

**Figure 20. *Xenopus laevis* embryos had reductions in heart rate and ventricular dimensions following exposure to retinoic acid and retinoic acid receptor antagonist.** *Xenopus* embryos were either exposed to DMSO (control), retinoic acid (RA), or retinoic acid receptor antagonist (RAA) commencing at stages 14, 26, and 33/34. Whole mount *in situ* hybridization was performed on *Xenopus* embryos using an antisense mRNA probe against *cardiac troponin I* to selectively outline the myocardium (Panel A). RA and RAA exposure resulted in decreased ventricular dimensions compared to the control. As well, heart rate was compared to examine the effect of disrupting retinoic acid signaling on cardiac rhythmicity (Panel B). No significant differences were observed for heart rate following exposure at stages 26 and 33/34. A significant reduction in heart rate was observed following exposure to both RA and RAA at stage 14. Heart rate was measured in beats per minute (bpm) and compared using a two-way ANOVA paired with a Sidak test. The end bars represent ±SEM. $n = 6$ for treatment at stages 14 and 33/34; $n = 8$ for treatment at stage 26; $*p \leq 0.05$; $****p \leq 0.0001$

#### 3.3.2.1 Treatment of *Xenopus laevis* embryos at stage 14 with RA and RAA

Treatment at stage 14 required exposure of the embryos either to DMSO, RA (Movie 10), or RAA (Movie 11). This stage represents an interval in neurulation that is prior to the migration of the two cardiac anlages that later form a single linear heart primordium, although specification has occurred by this time (Kolker et al., 2000; Lohr and Yost, 2000; Mohun et al., 2000).

A significant decrease was observed for cross-sectional area of the ventricular cavity and ventricular wall thickness when comparing the RA- and RAA-exposed embryos to the control group at end-diastole (Figure 21A). No significant differences in volume of blood in the ventricular cavity were observed. There were no significant differences observed between the RA- and RAA-treated groups.

Following analysis of cardiac function, *Xenopus* embryos were fixed and analyzed by *in situ* hybridization. An antisense mRNA probe recognizing *cardiac troponin I* mRNA was used to selectively label the myocardium such that cardiac morphology could be examined (Figure 21B). Ventricular reductions were observed in the RA-treated group for transverse length, perimeter, and cross-sectional area compared to the DMSO-exposed embryos. The RAA-treated group had a significantly decreased perimeter and cross-sectional area compared to the control group. The transverse length did not differ between the RAA- and DMSO-treated embryos. Longitudinal length of the ventricle was not significantly different between any of the groups. The RA- and RAA-treated embryos were not statistically different, except for the cross-sectional area of the ventricle, which was significantly reduced in the RA-treated group.

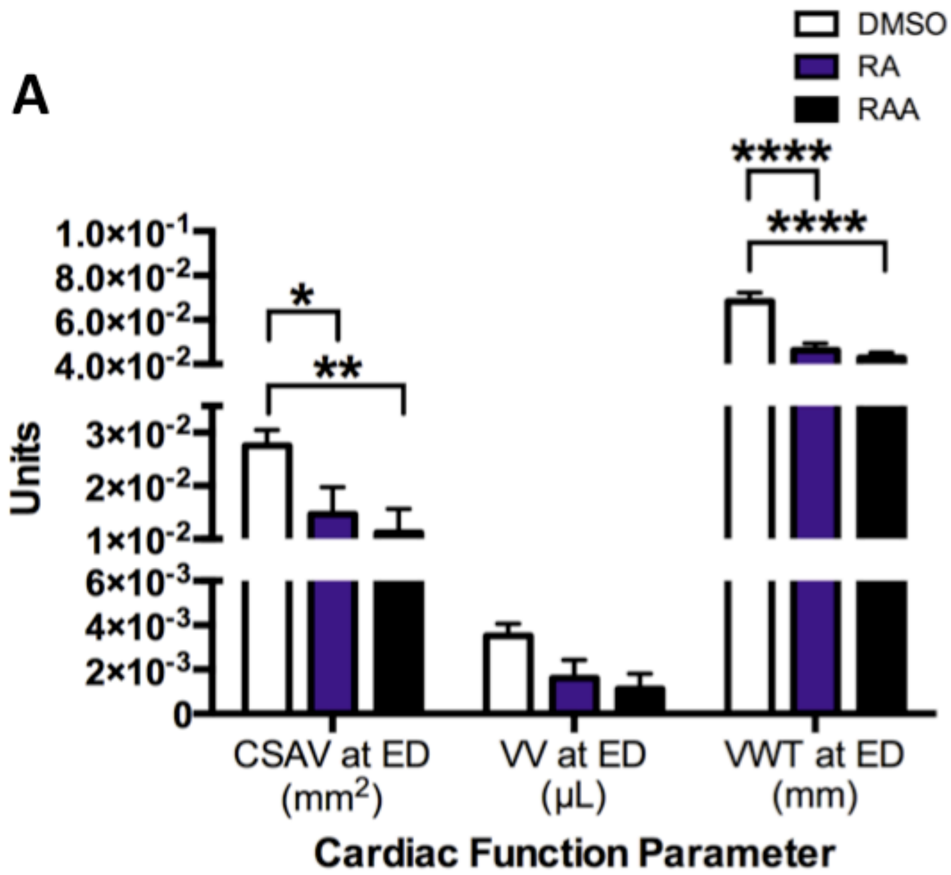
A
DMSO
RA
RAA
Units
1.0×10-1
8.0×10-2
6.0×10-2
4.0×10-2
3×10-2
2×10-2
1×10-2
6×10-3
4×10-3
2×10-3
0
*
**
****
****
CSAV at ED (mm2)
VV at ED (μL)
VWT at ED (mm)
Cardiac Function Parameter

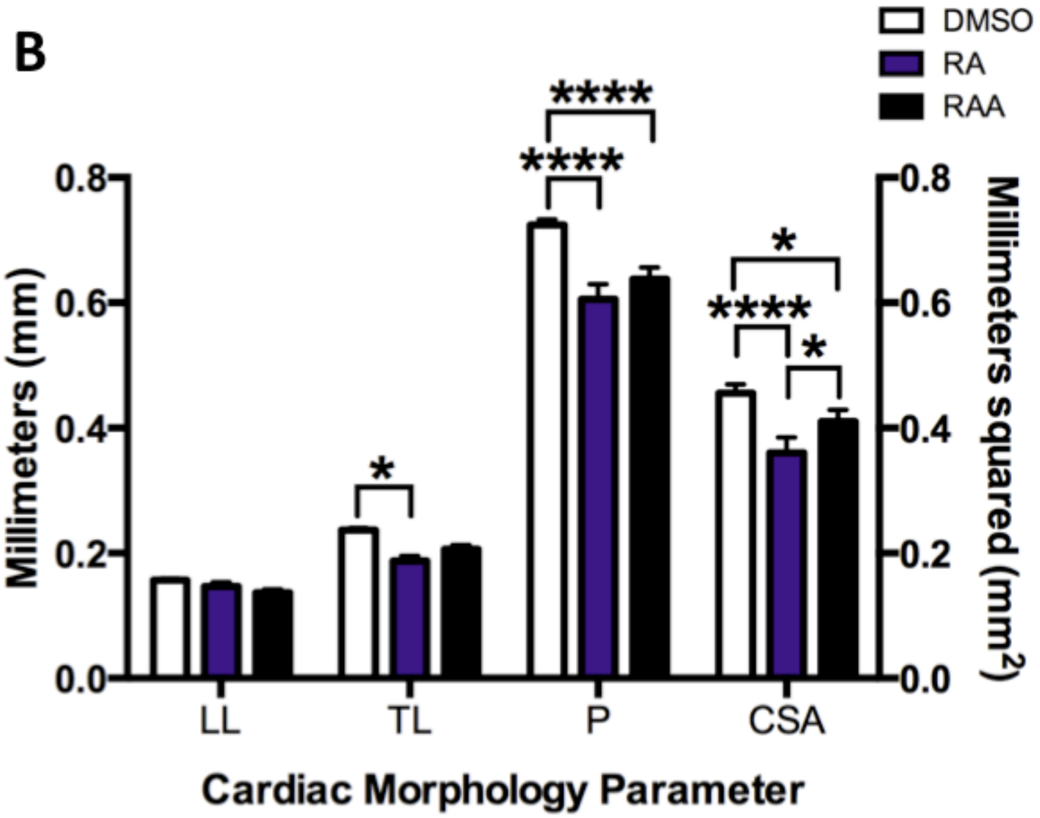
B
DMSO
RA
RAA
Millimeters (mm)
Millimeters squared (mm2)
0.8
0.6
0.4
0.2
0.0
*
****
****
*
****
*
LL
TL
P
CSA
Cardiac Morphology Parameter

**Figure 21. Exposure of *Xenopus laevis* embryos to retinoic acid and retinoic acid receptor antagonist at stage 14 resulted in decreased cardiac function and altered morphology.** In order to examine the effect of disrupted retinoic acid signaling, *Xenopus* embryos were exposed either to DMSO, retinoic acid (RA), or retinoic acid receptor antagonist (RAA) commencing at stage 14. Cardiac function was analyzed using parameters at end-diastole (ED) (Panel A). A significant reduction was observed for both the RA- and RAA-treated groups when compared to the control group for cross-sectional area of the ventricular cavity (CSAV) and ventricular wall thickness (VWT). No significant functional differences were identified between the RA- and RAA-treated groups. Volume of blood in the ventricular cavity (VV) was not altered following treatment with either RA or RAA. Panel B displays the comparison of ventricular morphology following *in situ* hybridization using an antisense mRNA probe against *cardiac troponin I*. No significant differences were observed for longitudinal length (LL) when comparing all three groups. Significant reductions were observed for perimeter (P) and cross-sectional area (CSA) for both the RA- and RAA-treated groups when compared to the control embryos. A significant reduction was detected for transverse length (TL) of the ventricle after treatment with RA compared to the control, while no significant difference was observed for this parameter when comparing RAA- and DMSO-treated embryos. There were no significant differences observed between the RA- and RAA-treated embryos, except with respect to CSA. A two-way ANOVA paired with a Sidak test was used to analyze the cardiac data. As well, the end bars represent ±SEM. $n = 6$ for each group for the functional analysis; $n = 85$, 61, and 67 for the DMSO-, RA-, and RAA-exposed embryos, respectively, for the morphological comparison; $^{*}p \leq 0.05$; $^{**}p \leq 0.01$; $^{****}p \leq 0.0001$

### 3.3.2.2 Treatment of *Xenopus laevis* embryos at stage 26 with RA and RAA

Treatment at stage 26 was used to disrupt cardiogenesis immediately prior to cardiac differentiation and during closure of the linear heart tube (Kolker et al., 2000; Lohr and Yost, 2000; Mohun et al., 2000). For this experiment, *Xenopus laevis* embryos were exposed to DMSO (control), RA (Movie 12), or RAA (Movie 13) to analyze the effect that disruption of retinoic acid signaling would have on cardiogenesis.

There were no significant functional differences between the RAA- and DMSO-exposed groups for any of the diastolic parameters examined (Figure 22A). No significant functional differences were observed between any of the groups when comparing volume of blood in the ventricular cavity. Conversely, a significant reduction was detected in the RA-treated group when compared to the control embryos for cross-sectional area of the ventricular cavity. There was no statistically significant difference detected between the RA- and RAA-treated groups for cross-sectional area of the ventricular cavity. A significant reduction was observed for diastolic ventricular wall thickness for embryos exposed to RA compared to both of the other groups.

Following analysis of cardiac function, *Xenopus* embryos were fixed such that *in situ* hybridization could be performed to selectively stain the myocardium for morphological comparison (Figure 22B). No significant differences were observed when comparing all three groups in terms of longitudinal and transverse length of the ventricle. Significant differences were observed when analyzing cross-sectional area of the ventricle with reductions observed in the RA- and RAA-treated groups compared to the control. A significant reduction in perimeter of the ventricle was observed in the RAA-treated group compared to the control embryos. There was no significant difference observed for perimeter following comparison of the DMSO- and RA-exposed embryos. No significant differences were observed between the RA- and RAA-treated groups.

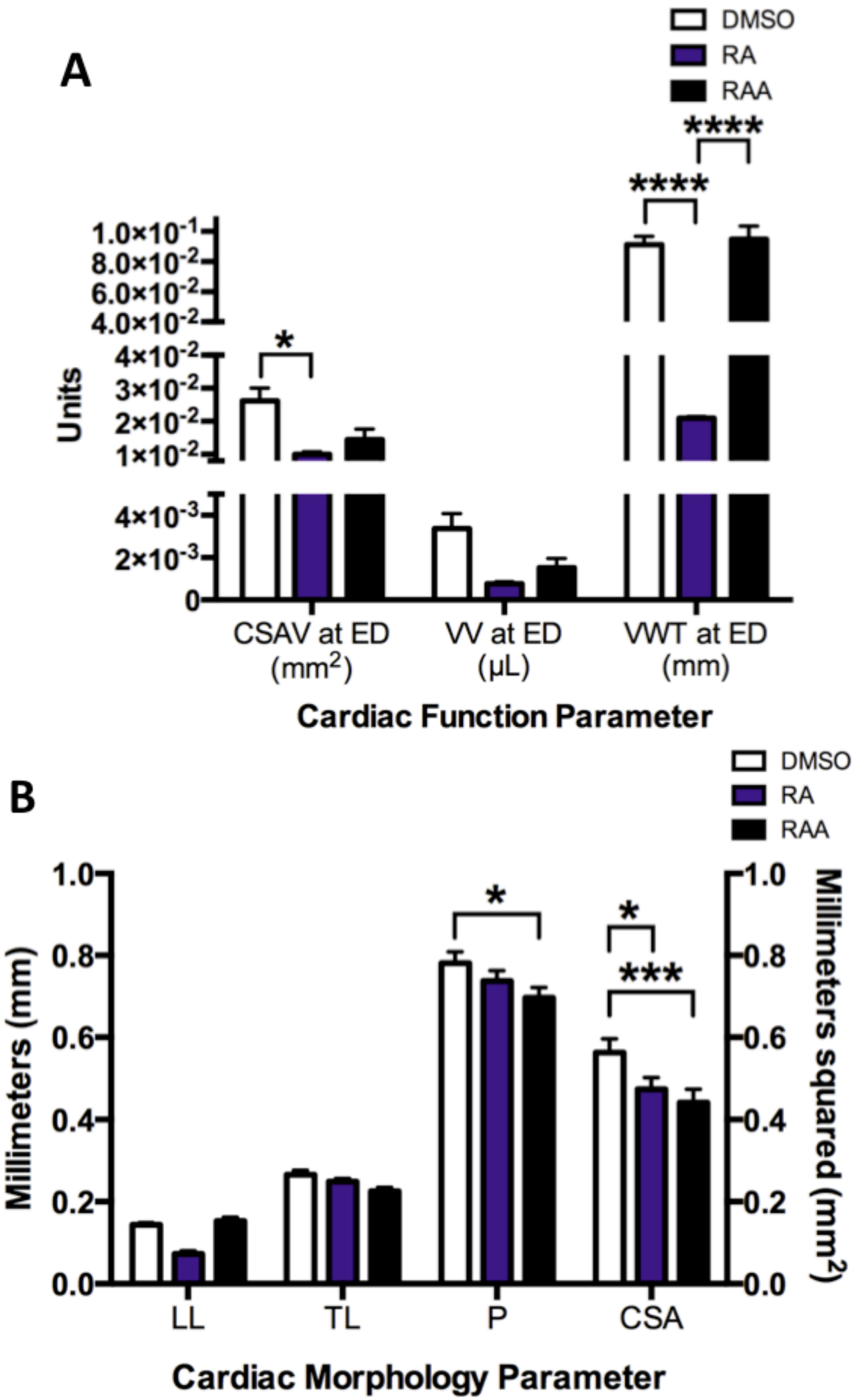
A
DMSO
RA
RAA
Units
1.0×10⁻¹
8.0×10⁻²
6.0×10⁻²
4.0×10⁻²
4×10⁻²
3×10⁻²
2×10⁻²
1×10⁻²
4×10⁻³
2×10⁻³
0
*
****
****
CSAV at ED (mm²)
VV at ED (µL)
VWT at ED (mm)
Cardiac Function Parameter
B
DMSO
RA
RAA
Millimeters (mm)
Millimeters squared (mm²)
1.0
0.8
0.6
0.4
0.2
0.0
*
*
***
LL
TL
P
CSA
Cardiac Morphology Parameter

**Figure 22. Retinoic acid and retinoic acid receptor antagonist exposure initiating at stage 26 resulted in reductions in ventricular morphology and function.** To observe the effects of disturbing retinoic acid signaling, *Xenopus* embryos were exposed to either DMSO, retinoic acid (RA) or retinoic acid receptor antagonist (RAA) initiating at stage 26. Functional examination at end-diastole (ED) detected no significant differences between the RAA and control group for all three diastolic parameters examined (Panel A). Significant reductions in cross-sectional area of the ventricular cavity (CSAV) and ventricular wall thickness (VWT) were observed for the RA-treated group when compared to the DMSO-exposed embryos. The volume of blood in the ventricular cavity (VV) was not significantly altered between any of the groups. A significant difference between the RA and RAA groups was only observed for VWT. Panel B shows the comparison of ventricular morphology following embryo fixation and whole mount *in situ* hybridization. No significant differences were observed for longitudinal length (LL) or transverse length (TL) when comparing every group. Significant reductions in perimeter (P) and cross-sectional area (CSA) of the ventricle were detected in the RAA-treated group compared to the DMSO-treated embryos. Although no significant difference was observed for P, there was a significant reduction in CSA for RA-treated embryos compared to the control group. There were no statistically significant differences detected between the RA- and RAA-exposed embryos. Functional and morphological data was compared using a two-way ANOVA paired with a Sidak test. The end bars represent ±SEM. n = 8 for each group for the functional comparison; n = 28, 19, and 17 for the DMSO, RA, and RAA groups, respectively, for the morphological comparison; $^{*}p \leq 0.05$; $^{***}p \leq 0.001$; $^{****}p \leq 0.0001$

### 3.3.2.3 Treatment of *Xenopus laevis* embryos at stage 33/34 with RA and RAA

Stage 33/34 corresponds to a period when the linear heart tube has completely closed and is beginning to undergo rightward looping (Afouda and Hoppler, 2009; Bartlett et al., 2010; Kolker et al., 2000; Lohr and Yost, 2000; Mohun et al., 2000). This looping process is essential for proper chamber and valve formation. Initiating at stage 33/34, *Xenopus* embryos were exposed either to DMSO (control), exogenous RA (Movie 14), or RAA (Movie 15).

Based on the functional comparison, significant decreases in cross-sectional area of the ventricular cavity and ventricular wall thickness were identified in the RA-treated embryos compared to the other two groups (Figure 23A). There were no significant functional differences observed between the RAA- and DMSO-exposed groups. Volume of blood in the ventricular cavity was not altered for any of the groups.

After examining cardiac function, *Xenopus* embryos were fixed to undergo *in situ* hybridization using a myocardium-specific antisense mRNA probe in order to compare ventricular morphology (Figure 23B). There were no significant differences observed.

### 3.3.2.4 Conclusions

This novel imaging system was able to detect significant alterations in cardiac function and morphology following disruption of retinoic acid signaling at various developmental time points. Overall, reductions in ventricular dimension were observed following disruption of retinoic acid signaling. Furthermore, cardiac looping defects were generally observed after exposure to RA or RAA.

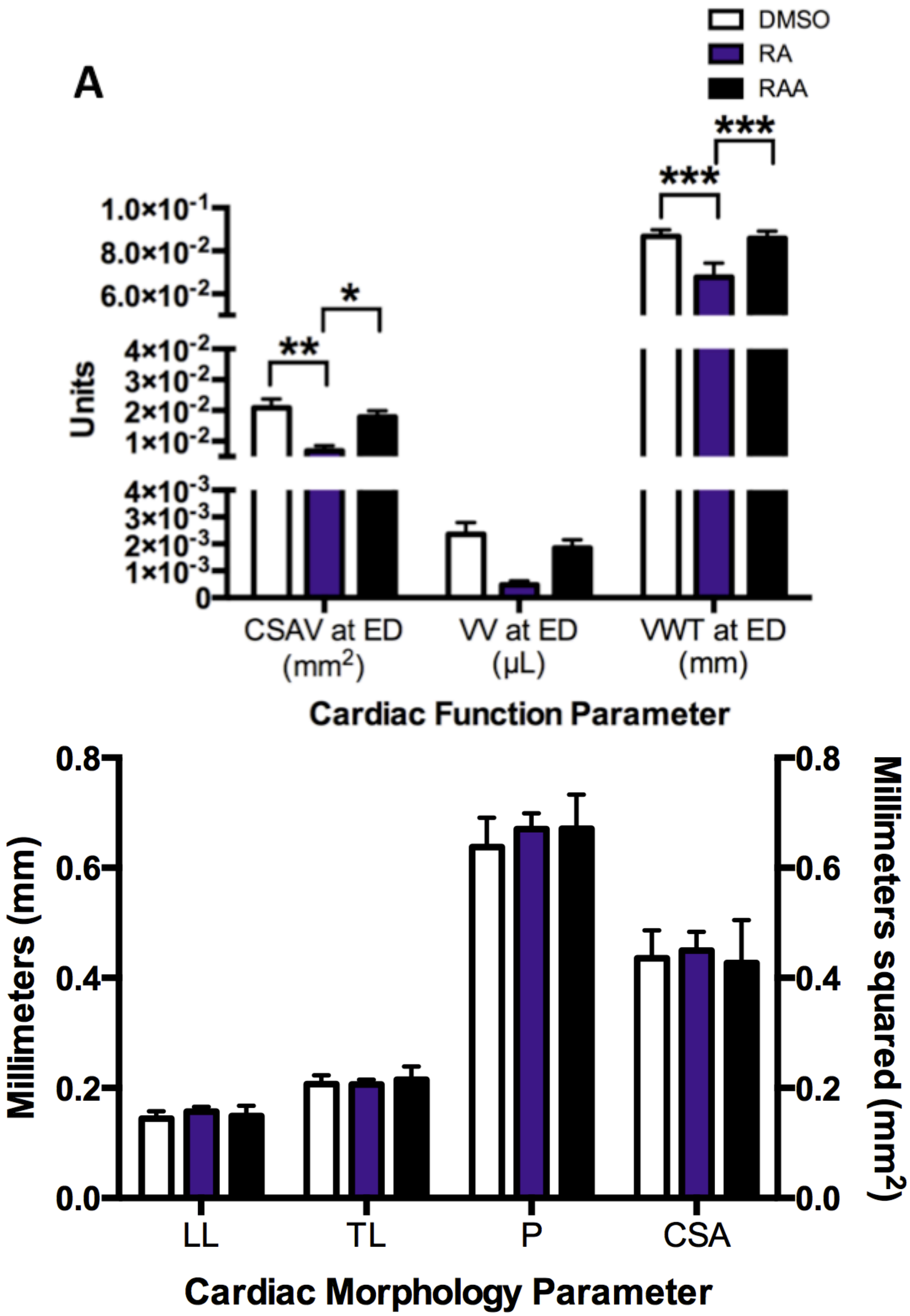
A
DMSO
RA
RAA
Units
1.0×10⁻¹
8.0×10⁻²
6.0×10⁻²
4×10⁻²
3×10⁻²
2×10⁻²
1×10⁻²
4×10⁻³
3×10⁻³
2×10⁻³
1×10⁻³
0
**
*
***
***
CSAV at ED (mm²)
VV at ED (μL)
VWT at ED (mm)
Cardiac Function Parameter
Millimeters (mm)
Millimeters squared (mm²)
0.8
0.6
0.4
0.2
0.0
LL
TL
P
CSA
Cardiac Morphology Parameter

**Figure 23. Disruption of retinoic acid signaling resulted in significant reductions in cardiac function, but did not result in statistically significant changes in ventricular morphology.** The functional and morphological effects resulting from disturbances in retinoic acid signaling were examined in *Xenopus* embryos using exogenous retinoic acid (RA) and retinoic acid receptor antagonist (RAA). Embryos were exposed to DMSO, RA, or RAA commencing at stage 33/34 and analyzed at end-diastole (ED) for functional alterations (Panel A). Significant reductions were observed for cross-sectional area of the ventricular cavity (CSAV) and ventricular wall thickness (VWT) in the RA-treated group compared to the two other groups. RAA- and DMSO-exposed embryos were not significantly different in cardiac function. No significant differences were observed following examination of volume of blood in the ventricular cavity (VV). Panel B shows the comparison of ventricular morphology. There were no statistically significant alterations observed. Ventricular parameters examined included longitudinal length (LL), transverse length (TL), perimeter (P), and cross-sectional area (CSA). This was examined following *in situ* hybridization using an antisense mRNA probe against *cardiac troponin I*. A two-way ANOVA paired with a Sidak test was used to compare the parameters, as well as the end bars represent ±SEM. n = 6 for each group for the functional comparison; n = 19, 31, and 20 for the DMSO, RA, and RAA groups, respectively, for the morphological comparison; $^{*}p \leq 0.05$; $^{**}p \leq 0.01$; $^{***}p \leq 0.001$

### 3.3.3 Ethanol

My next experiments involved deviating from small molecules previously used in our lab. A plethora of research has been dedicated to confirming ethanol's role as a teratogen leading to the development of fetal alcohol syndrome (FAS) (Jones and Smith, 1973). It is estimated that approximately 54% of children that have been associated with symptoms of FAS have been shown to display corresponding cardiac defects (Abel, 1990).

A study conducted by Yelin et al. demonstrated that exposure to various concentrations of ethanol caused cardiac defects in *Xenopus* embryos (Yelin et al., 2007b). A majority of embryos exposed to 1.5% ethanol during the mid-blastula transition showed changes in cardiac morphology including less mature trabeculae. Therefore, I sought to verify those findings using our high-speed video camera and HeartMetrics software. Since trabeculae are contiguous with the ventricular wall in my experiments, then I expect a reduction in ventricular wall thickness following ethanol exposure to correspond with the less mature trabeculae observed by the other research group.

I exposed *Xenopus laevis* embryos to either a control solution (20% Steinberg's solution) or 1.5% ethanol dissolved in 20% Steinberg's solution. *Xenopus* embryos were maintained in the respective treatments until stage 46 and onwards, at which point cardiac imaging and fixation were performed.

Representative embryos from both the control and ethanol-treated groups are shown below after treatment at stages 8.5, 26, and 33/34 (Figure 24A). The figure depicts the *in situ* hybridization images that outline the myocardium. The HeartMetrics program allowed for the visualization and identification of relatively normal cardiac looping following ethanol exposure, except for looping abnormalities when exposed at stage 8.5.

Heart rate was measured and analyzed following embryo exposure to ethanol (Figure 24B). Ethanol exposure did not cause statistically significant changes in heart rate, regardless of the stage of treatment.

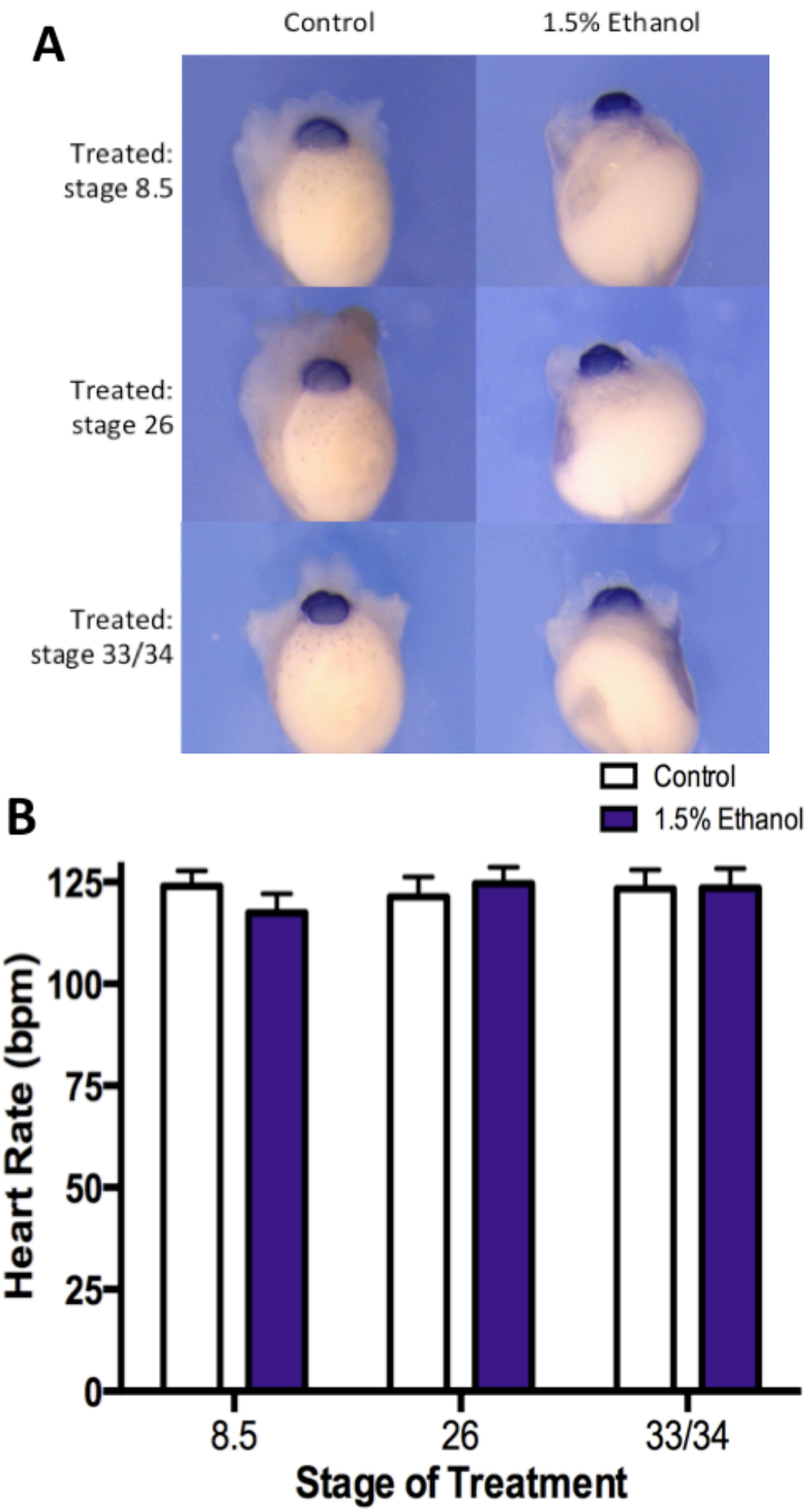
A
Control
1.5% Ethanol
Treated: stage 8.5
Treated: stage 26
Treated: stage 33/34
B
☐ Control
■ 1.5% Ethanol
Heart Rate (bpm)
0
25
50
75
100
125
8.5
26
33/34
Stage of Treatment

**Figure 24.** ***Xenopus laevis*** **embryos exposed to ethanol displayed altered cardiac morphology and no significant differences in heart rate.** Ethanol treatment of *Xenopus* embryos initiated at stages 8.5, 26, and 33/34 and embryos were exposed either to 20% Steinberg's solution (control) or 1.5% ethanol. Subsequently, whole mount *in situ* hybridization was performed using an antisense mRNA probe against *cardiac troponin I* to outline the myocardium (Panel A). Reductions in ventricular dimensions were observed following exposure to ethanol. Relatively normal cardiac looping was also noted following imaging using HeartMetrics, except following treatment at stage 8.5. Additionally, the effect of ethanol on heart rate was compared (Panel B). Ethanol was not determined to cause statistically significant alterations in heart rate at any of the stages targeted. Heart rate was measured in beats per minute (bpm) and analysis of data involved a two-way ANOVA paired with a Sidak test. The end bars represent ±SEM. n = 16 and 17 for the control and ethanol groups, respectively, for exposure at stage 8.5; n = 15 and 20 for the control and ethanol groups, respectively, for exposure at stage 26; n = 15 and 16 for the control and ethanol groups, respectively, for exposure at stage 33/34

#### 3.3.3.1 Treatment of *Xenopus laevis* embryos at stage 8.5 with ethanol

Embryos were treated at stage 8.5 during the mid-blastula transition and immersed in either Steinberg’s solution, which served as the control group, or 1.5% ethanol (Movie 16) (Nieuwkoop and Faber, 1994). Stage 8.5 represents a time point in development that precedes the induction of cardiac progenitors (Afouda and Hoppler, 2009; Lohr and Yost, 2000).

Functional comparison revealed that ventricular wall thickness at end-diastole was significantly reduced in embryos exposed to ethanol compared to the control (Figure 25A). Cross-sectional area of the ventricular cavity and volume of blood in the ventricular cavity were not significantly affected by ethanol exposure.

Subsequently, embryos were fixed and underwent an *in situ* hybridization to outline the myocardium using an antisense mRNA probe against *cardiac troponin I* mRNA. This permitted the measurement of several ventricular dimensions to elucidate cardiac morphology changes following exposure to ethanol (Figure 25B). There were significant reductions in longitudinal length, transverse length, and perimeter of the ventricle for ethanol-treated embryos. However, ethanol had no effect on the cross-sectional area of the ventricle.

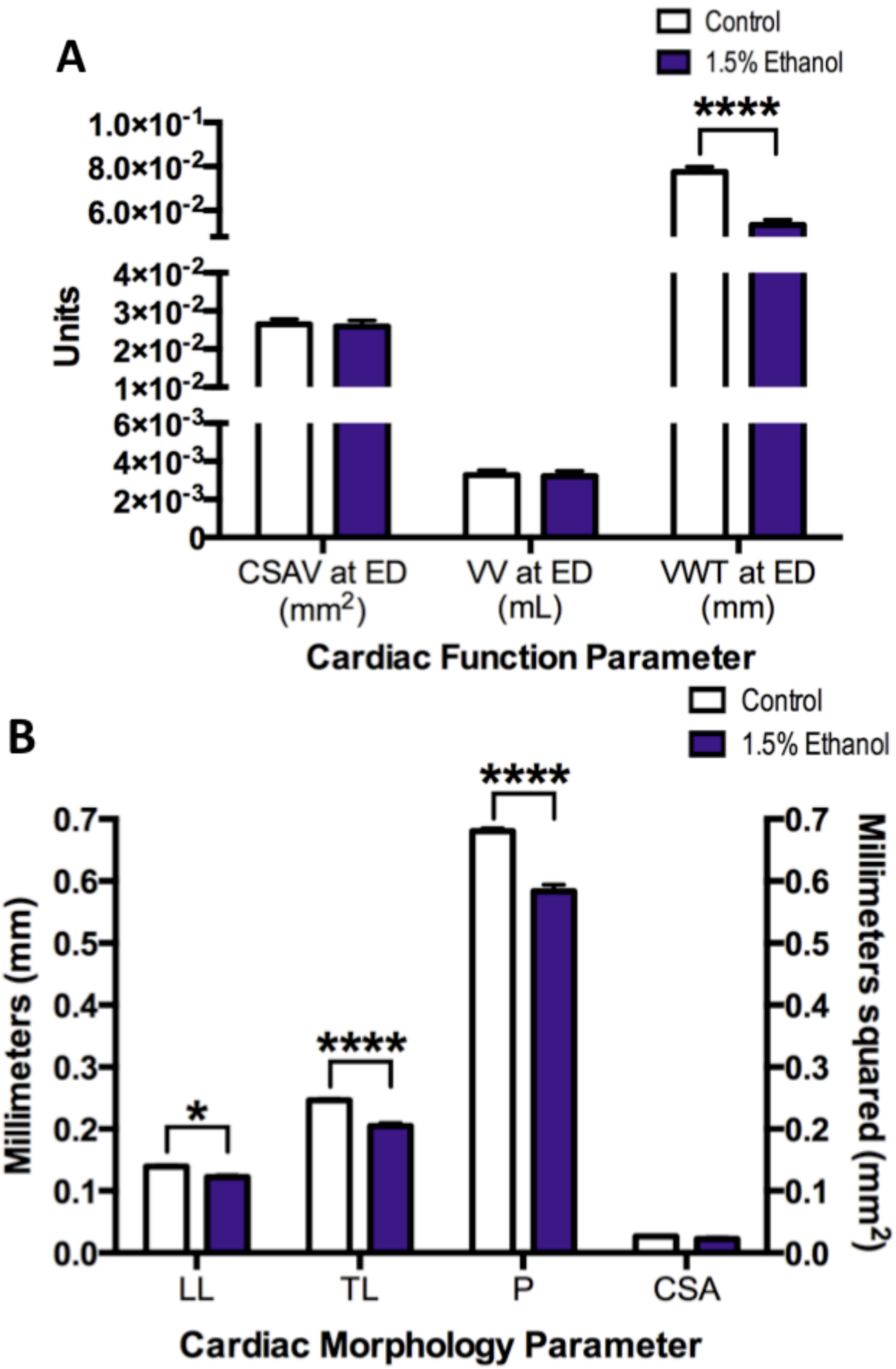
A
Control
1.5% Ethanol
Units
1.0×10⁻¹
8.0×10⁻²
6.0×10⁻²
4×10⁻²
3×10⁻²
2×10⁻²
1×10⁻²
6×10⁻³
4×10⁻³
2×10⁻³
0
****
CSAV at ED (mm²)
VV at ED (mL)
VWT at ED (mm)
Cardiac Function Parameter
B
Control
1.5% Ethanol
Millimeters (mm)
0.7
0.6
0.5
0.4
0.3
0.2
0.1
0.0
*
****
****
LL
TL
P
CSA
Millimeters squared (mm²)
Cardiac Morphology Parameter

**Figure 25. Ethanol exposure at stage 8.5 caused reductions in ventricular morphology and cardiac function.** *Xenopus laevis* embryos were either exposed to 20% Steinberg's solution (control) or 1.5% ethanol commencing at stage 8.5. Cardiac function was analyzed at end-diastole (ED) and a significant reduction in ventricular wall thickness (VWT) was observed in the ethanol-exposed group (Panel A). There were no significant alterations following ethanol exposure for cross-sectional area of the ventricular cavity (CSAV) and volume of blood in the ventricular cavity (VV). *In situ* hybridization images were used to compare cardiac morphology (Panel B). There were significant reductions in the ethanol-treated group for several ventricular parameters including longitudinal length (LL), transverse length (TL), and perimeter (P). Ethanol exposure did not result in a statistically significant difference for cross-sectional area (CSA) of the ventricle. A two-way ANOVA paired with a Sidak test was used to assess the cardiac data. The end bars represent ±SEM. n = 16 and 17 for the control and ethanol-treated groups, respectively, for the functional comparison; n = 83 and 67 for the control and ethanol groups, respectively, for the morphological comparison; $^{**}p \leq 0.01$; $^{****}p \leq 0.0001$

### 3.3.3.2 Treatment of *Xenopus laevis* embryos at stage 26 with ethanol

*Xenopus* embryos were immersed in ethanol initiating at stage 26 in order to evaluate cardiac disruption at a developmental period directly preceding cardiac differentiation and overlapping with closure of the linear heart tube (Kolker et al., 2000; Lohr and Yost, 2000; Mohun et al., 2000). The embryos were divided into two treatment groups, either 20% Steinberg's solution (control) or 1.5% ethanol (Movie 17).

Comparison of cardiac function revealed no statistically significant alterations when comparing cross-sectional area of the ventricular cavity and volume of blood in the ventricular cavity at end-diastole (Figure 26A). A statistically significant reduction in ventricular wall thickness at end-diastole was observed in the ethanol-treated group compared to the control.

Afterwards, the *Xenopus* embryos were fixed in preparation for *in situ* hybridization, which permitted analysis of static ventricular parameters to examine cardiac morphology changes (Figure 26B). Ethanol treatment was associated with significant decreases in transverse length and perimeter. Longitudinal length and cross-sectional area were not significantly different between the two groups.

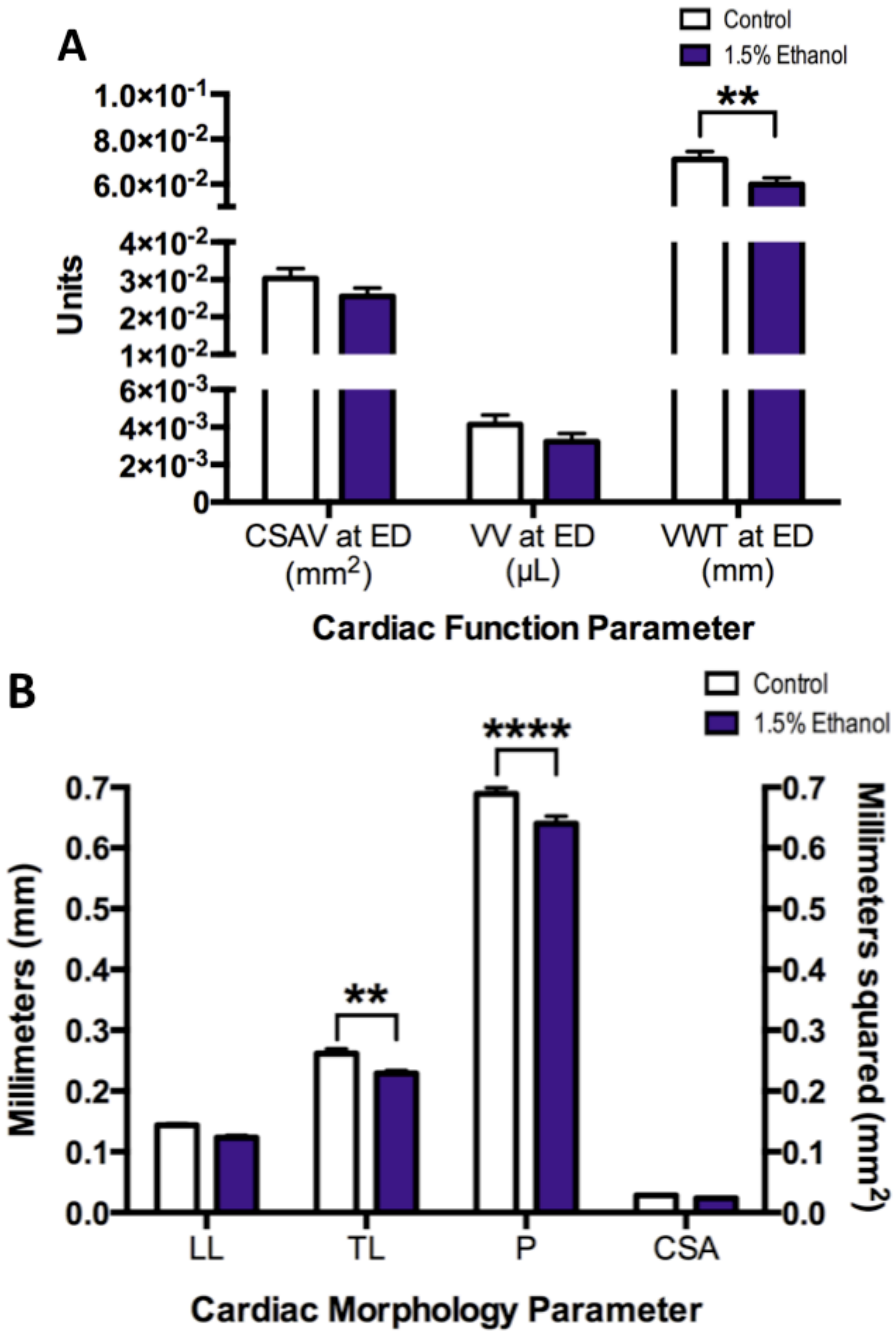
A
Control
1.5% Ethanol
Units
1.0×10⁻¹
8.0×10⁻²
6.0×10⁻²
4×10⁻²
3×10⁻²
2×10⁻²
1×10⁻²
6×10⁻³
4×10⁻³
2×10⁻³
0
**
CSAV at ED (mm²)
VV at ED (µL)
VWT at ED (mm)
Cardiac Function Parameter
B
Control
1.5% Ethanol
Millimeters (mm)
Millimeters squared (mm²)
0.7
0.6
0.5
0.4
0.3
0.2
0.1
0.0
**
****
LL
TL
P
CSA
Cardiac Morphology Parameter

**Figure 26. Reductions in cardiac function and morphology following exposure to ethanol commencing at stage 26.** Initiating at stage 26, *Xenopus* embryos were either exposed to 20% Steinberg's solution (control) or 1.5% ethanol. Panel A displays the comparison of cardiac function for end-diastolic (ED) parameters. A significant reduction in ventricular wall thickness (VWT) was detected following ethanol exposure. There were no significant differences regarding cross-sectional area of the ventricular cavity (CSAV) and volume of blood in the ventricular cavity (VV). Subsequently, embryos underwent an *in situ* hybridization to examine ventricular morphology (Panel B). Statistically significant reductions were observed for transverse length (TL) and perimeter (P) of the ventricle in the ethanol-exposed group. There were no significant differences for longitudinal length (LL) and cross-sectional area (CSA). A two-way ANOVA paired with a Sidak test was used to analyze the cardiac parameters. The end bars represent ±SEM. n = 15 and 20 for the control and ethanol groups, respectively, for the functional analysis; n = 62 and 57 for the control and ethanol-treated groups, respectively, for the morphological analysis; $^{**}p \leq 0.01$; $^{****}p \leq 0.0001$

### 3.3.3.3 Treatment of *Xenopus laevis* embryos at stage 33/34 with ethanol

To elucidate on functional changes following ethanol treatment, *Xenopus* embryos were either exposed to 20% Steinberg's solution (control) or 1.5% ethanol (Movie 18) starting at stage 33/34. This developmental period corresponds to the initiation of cardiac looping following complete closure of the cardiac tube (Afouda and Hoppler, 2009; Bartlett et al., 2010; Kolker et al., 2000; Lohr and Yost, 2000; Mohun et al., 2000).

Analysis of cardiac function showed that ethanol exposure resulted in a significant reduction in ventricular wall thickness at end-diastole compared to the control embryos (Figure 27A). Cross-sectional area of the ventricular cavity and volume of blood in the ventricular cavity were not significantly altered.

Next, embryos underwent an *in situ* hybridization to examine ventricular morphology (Figure 27B). Significant reductions in transverse length and perimeter resulted from ethanol exposure. There were no significant differences between the two groups regarding longitudinal length and cross-sectional area.

### 3.3.3.4 Conclusions

Therefore, our system was able to corroborate the findings published by Yelin et al. that described less mature trabeculae following exposure to 1.5% ethanol at stage 8.5 (Yelin et al., 2007b). This corresponds to the reduction in ventricular wall thickness observed in my experiments. The functional and morphological reductions resulting from ethanol exposure were observed following treatment at each developmental interval targeted.

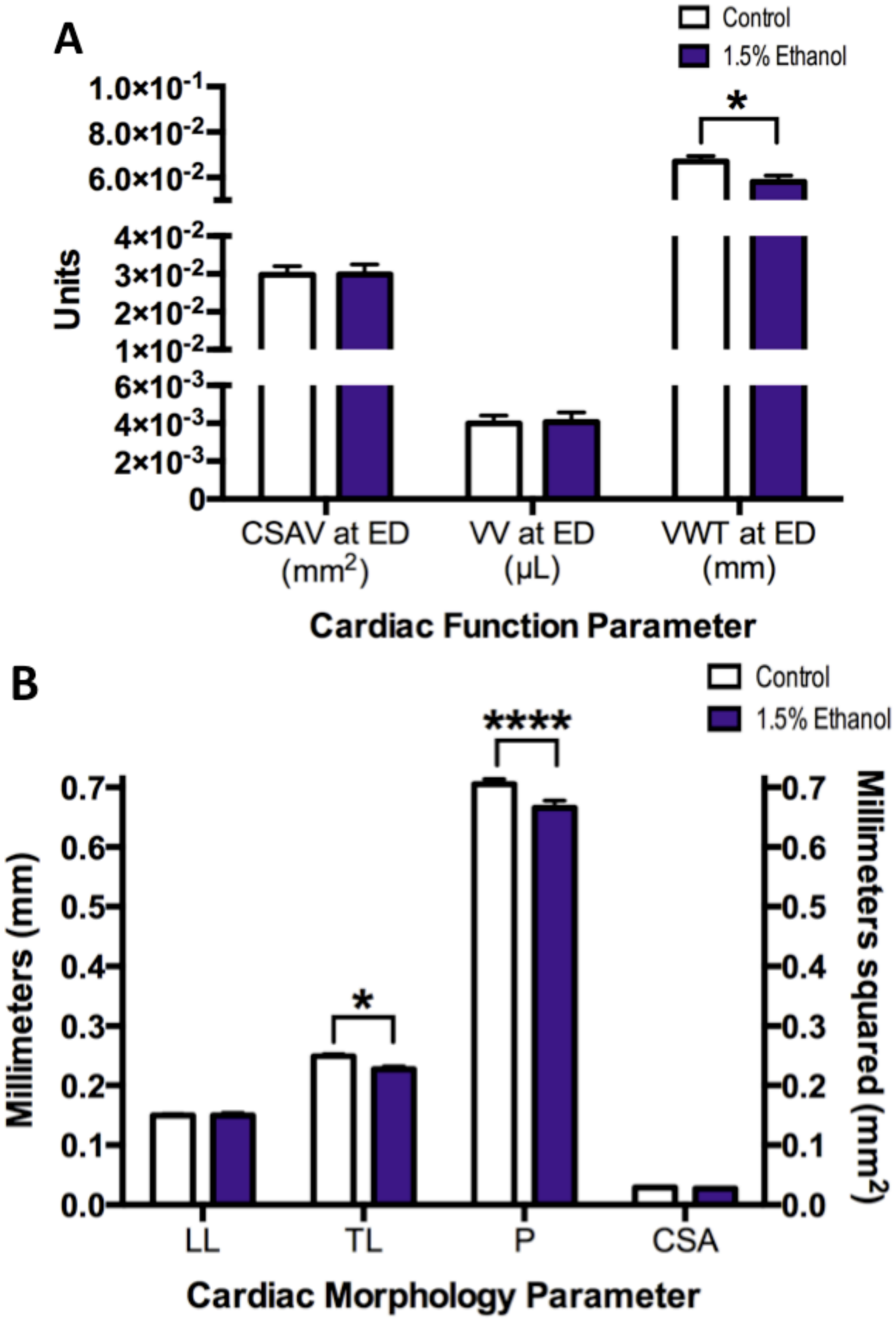
A
☐ Control
■ 1.5% Ethanol
Units
1.0×10^-1
8.0×10^-2
6.0×10^-2
4×10^-2
3×10^-2
2×10^-2
1×10^-2
6×10^-3
4×10^-3
2×10^-3
0
*
CSAV at ED (mm²)
VV at ED (µL)
VWT at ED (mm)
Cardiac Function Parameter
B
☐ Control
■ 1.5% Ethanol
Millimeters (mm)
Millimeters squared (mm²)
0.7
0.6
0.5
0.4
0.3
0.2
0.1
0.0
*
****
LL
TL
P
CSA
Cardiac Morphology Parameter

**Figure 27.** ***Xenopus*** **embryos exposed to ethanol initiating at stage 33/34 displayed reductions in ventricular morphology and function.** Beginning at stage 33/34, *Xenopus laevis* embryos were either exposed to 20% Steinberg's solution (control) or 1.5% ethanol. Cardiac function was compared at end-diastole (ED) and displayed in panel A. Ventricular wall thickness (VWT) was significantly reduced following ethanol exposure. Cross-sectional area of the ventricular cavity (CSAV) and volume of blood in the ventricular cavity (VV) were not significantly altered. Subsequently, *in situ* hybridizations were performed to permit the collection and comparison of ventricular dimensions (Panel B). The ethanol-treated group displayed significant reductions in transverse length (TL) and perimeter (P) compared to the control group. Longitudinal length (LL) and cross-sectional area (CSA) were not significantly changed. Functional and morphological data was analyzed using a two-way ANOVA paired with a Sidak test. The end bars represent ±SEM. n = 15 and 16 for the control and ethanol groups, respectively, for the functional analysis; n = 63 and 54 for the control and ethanol groups, respectively, for the morphological analysis; $^*p \leq 0.05$; $^{****}p \leq 0.0001$

## 3.4 Origin of Cardiac Response

Diverging from the topic of CHDs, we noted that our observations using the modulators of heart rate would suggest that, at the times we tested, the heart was responding to neuromodulation. Although many aspects of development are well characterized in *Xenopus*, knowledge concerning when cardiac innervation is established is not well documented. The origin of cardiac response is marked by alterations in cardiac function following environmental changes, such as the response to chemical stimuli that I documented. Innervation may imply the existence of a functional nervous system that can control the response of autonomic tissues, such as cardiac responses (Armour, 1999).

Therefore, I exposed embryos to a classical modulator at earlier time points to gain insight into the developmental stage when innervation occurs. If the embryo were able to demonstrate the appropriate cardiac response to the drug, then the embryo would be considered innervated by that stage. Nkx2.5-GFP transgenic frogs were utilized for examination of stages 37/38 and 39 in order to potentially improve imaging at the earlier time points. The Nkx2.5-GFP transgenic embryos should express GFP within the myocardium before the heart starts beating (Mohun et al., 2000). Wild type embryos do not image well prior to stage 40 due to optical considerations.

*Xenopus laevis* embryos were exposed to isoproterenol and assessed for an increase in heart rate. An increase in heart rate upon exposure to the drug would indicate innervation had already been established (Cirić and Susić, 1980). There was a consistent, but variable, increase in heart rate after isoproterenol exposure (Figure 28). This response was observed for each stage examined, including stages 37/38 to 45. A value on the y-axis that was greater than zero would indicate an increase in heart rate from baseline.

In conclusion, my data suggests that innervation in *Xenopus laevis* embryos occurs by at least stage 37/38 during embryonic development since the proper cardiac response was observed. Unfortunately, our imaging system was not capable of visualizing and measuring heart rate at earlier stages due to the opacity of the embryos. Nevertheless, these experiments did elucidate on a narrower interval in which this developmental process occurs.

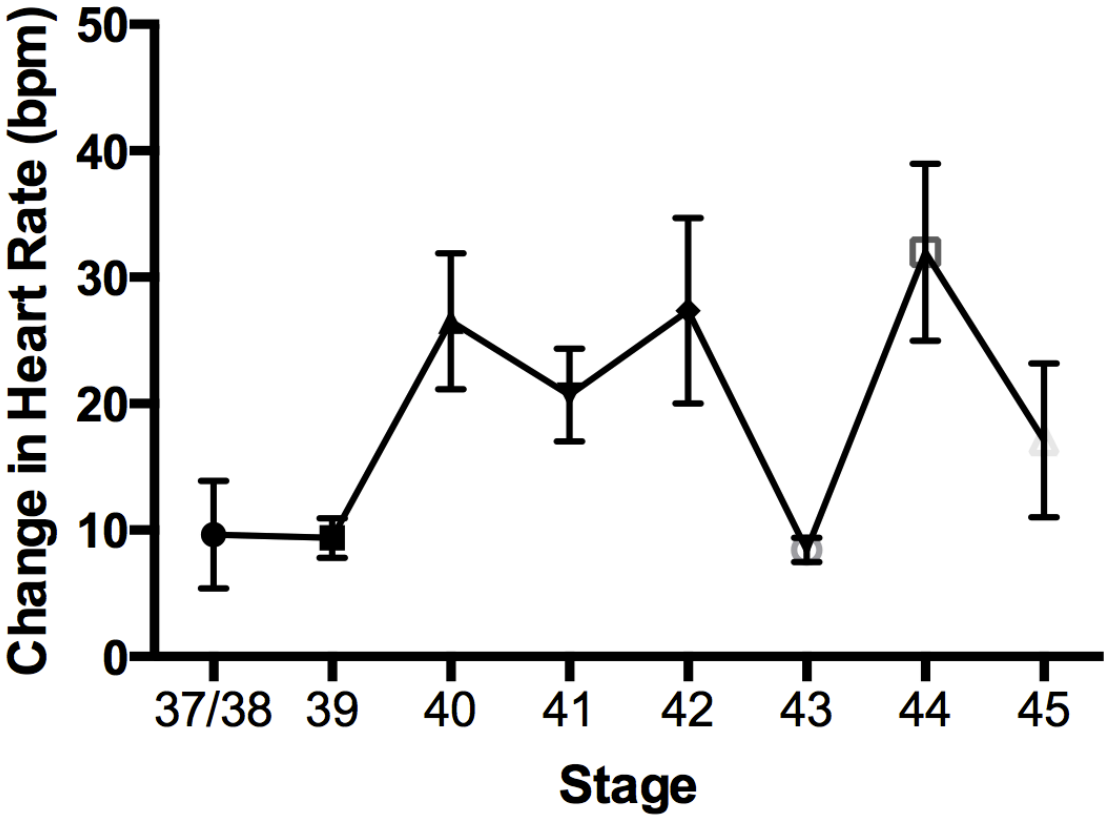

**Figure 28.** ***Xenopus laevis*** **embryos are capable of displaying expected cardiac responses to pharmacological agents by at least stage 37/38.** This experiment involved measuring the baseline heart rate of embryos ranging from stages 37/38 to 45. Subsequently, embryos were exposed to isoproterenol, which is well documented to increase heart rate. Overall, an increase in heart rate was observed indicated by a positive change in heart rate. Hence, this data suggests that embryos are capable of responding to the presence of pharmacological agents by stage 37/38. Furthermore, since autonomic responses, such as a cardiac response, to a classical modulator of heart rate possibly relies on the presence of a functional nervous system, hence it is expected that the *Xenopus laevis* embryo may be innervated by at least stage 37/38. The end bars represent ±SEM. n = 3-4 for each group

# Chapter 4

# 4 Discussion

My primary aim for this project was to develop methods of evaluating heart function in *Xenopus laevis* embryos. To do this, I tailored a video imaging and analysis system that was previously used in chick for use in *Xenopus* and, if successful, this imaging system could serve as a valuable alternative to current imaging modalities at elucidating mechanisms underlying congenital heart defects.

I conclude that this system is capable of accurately measuring cardiac function in *Xenopus laevis* embryos. To support my conclusion, I will discuss the normative sample data and the classical modulators of heart rate.

## 4.1 Measurements of Normal Cardiac Function

General increases in cardiac function were observed within the control embryos. An increase in heart rate was observed upon maturation of the embryo from stages 45 through 48. Similarly, increases in ventricular wall thickness at both end-diastole and end-systole were also detected as embryos developed from stages 45 to 48. This increase in wall thickness was accompanied by an increase in stroke volume and cardiac output.

Furthermore, I noted that flow velocity between embryos displayed large variability. A study conducted in human fetuses using cardiac Doppler tracing estimated the standard error of maximum flow velocity to be 11 to 26 mm/s (Reed et al., 1986). Therefore, the high level of variability for flow velocity observed in human fetuses is consistent with the broad variability seen in my experiments using *Xenopus* embryos.

### 4.1.1 Comparison of our Data to the Previous Measures of Cardiac Function

A simple method for evaluating our video imaging system's measurements is through a comparison to the previous studies using different modalities.

Cardiac function in anesthetized stage 47 *Xenopus laevis* embryos has been analyzed using optical coherence tomography (OCT) (Boppart et al., 1997). This method utilizes the innate ability of biological tissues to reflect light waves. Essentially, light waves are emitted from the equipment towards the biological tissue of interest and subsequently this light is reflected within a range of delay times depending on the tissue composition. This delay time is referred to as the echo delay, which is interpreted to compile cross-sectional images using interferometry. In this study, the heart rate was determined to be approximately 128 beats per minute, which is comparable to the average 139 bpm determined through my experiments. The end-diastolic dimension (EDD) and end-systolic dimension (ESD) were observed to be 666 and 398 microns, respectively. Conversely, I determined the EDD and ESD to be an average of 338 and 246 microns, respectively (see Appendices). Although the raw values are different, my data corroborated with the EDD:ESD ratio of approximately 3:2. Importantly, the end dimension computations by Boppart et al. included both the ventricular cavity as well as the ventricular wall, although a majority of end dimension calculations generally only include the ventricular cavity.

Another publication examined cardiac function using Doppler optical coherence tomography (DOCT), which is similar to OCT except with Doppler extensions (Yang et al., 2003). This technique is more closely analogous to Doppler ultrasound. The DOCT system was capable of obtaining a maximum frame rate of 32 frames per seconds. Using this system, flow velocity in the left and right aortic branches was measured following anesthetization of stage 47 *Xenopus laevis* embryos. The computations indicated at a maximum erythrocyte velocity of 9mm/s. My data suggests that the flow velocity of stage 48 embryos that were not anesthetized was an average of 4mm/s and ranged from 2-8.4mm/s. Therefore, this is comparable to the values that I have observed using our imaging system, which suggests that our system is accurate, although the small differences would require a direct comparison of methodology and staging of embryos.

The ventricular dimensions of fixed, stage 49 embryos have been imaged (Yelin et al., 2007b). In that study, the ventricle was imaged using full-field optical coherence tomography (FFOCT), which uses low-coherence interferometry. The ventricular wall thickness (including the trabeculae) during maximum filling of the ventricle could be approximated to be slightly greater than 100μm. Although I did not examine *Xenopus* embryos at stage 49, at the slightly earlier stage 48, I measured a diastolic ventricular wall thickness of 74μm. Since 7.5 days at room temperature is required to reach stage 48, but an additional 4.5 days is necessary to mature to stage 49, it could be hypothesized that ventricular wall thickness increases considerably during this period. To test this hypothesis, we need to modify our system to optimize imaging at a later stage of development.

My findings are consistent with evidence from a group that studied a very closely related, but smaller species, *Xenopus tropicalis*, that can also be staged using the Nieuwkoop and Faber staging table (Deniz et al., 2012). Analysis of the *tropicalis* embryos determined that the ejection fraction was approximately 100% when assayed using hemoglobin contrast subtraction angiography, which exploits the use of hemoglobin as an endogenous contrast agent. The ventricle is devoid of blood at end-systole represented by the absence of black regions, whereas the ventricle at end-diastole contained a substantial amount of hemoglobin. We confirmed the complete emptying of the ventricle following a cardiac contraction in *Xenopus laevis* using our system (For an example, see Movie 1), which supports the *tropicalis* data (Deniz et al., 2012).

### 4.1.2 Classical Modulators of Heart Rate

Further validation that our video system can clearly measure changes in function used exposure to known modulators of heart rate that have well-established effects. As expected, a dose-dependent increase in heart rate was observed following exposure to atropine, epinephrine, and isoproterenol. Conversely, a concentration-dependent decrease in heart rate was observed following exposure to metoprolol. The imaging system was able to detect alterations in heart rate and thus could potentially be used as an assay for screening of small molecules for cardiac activity in *Xenopus* embryos.

Next, I will discuss the results following disruption of cardiogenesis to further examine how this novel imaging system could be advantageous for the investigation of CHDs.

## 4.2 Novel Assessments of Changes in Function

### 4.2.1 Rationale for Blebbistatin and Rockout

The role of Rho and ROCK in cardiac development has been defined in several species, including chick and zebrafish (Dickover et al., 2014; Sakata et al., 2007). In zebrafish, inhibition of RhoU signaling caused morphological disruptions, such as defects in the formation of the atrioventricular canal and improper cardiac looping (Dickover et al., 2014). RhoU was identified to be a regulator of cell junctions between myocardial cells through a pathway involving Arhgef7b/Pak kinase. Studies in the chick revealed that inhibition of ROCK activity through the small molecule Y27632 resulted in disruption in striated myofibril formation in the heart (Sakata et al., 2007). This inhibition also caused improper formation of the costamere, which is a site for adhesion between the Z-band and sarcolemma. These results suggest a role for ROCK in cell-cell adhesion required for myofibrillogenesis. Therefore, since both blebbistatin and Rockout inhibit ROCK signaling, then both of these small molecules would be predicted to cause morphological defects and possibly functional changes as well.

Blebbistatin was selected for generating defects in cardiogenesis because this small molecule is known to inhibit crucial processes required for the signaling pathway of Shroom3 (Figure 29) (Plageman et al., 2011a). *Shroom3* was first identified for the ability to cause embryonic lethality resulting from exencephaly and *spina bifida* (Hildebrand and Soriano, 1999). The role of Shroom3 is currently being studied by the Drysdale lab and has already been linked to CHDs in mice (Halabi, 2013). Moreover, Shroom3 plays a crucial role in the regulation of cell shape of epithelial cells located in the lens, gut, and neural tube (Chung et al., 2010; Hagens et al., 2006; Haigo et al., 2003; Hildebrand and Soriano, 1999; Lee et al., 2009; Plageman et al., 2010, Plageman et al. 2011a; Suzuki et al., 2012).

Localization of Shroom3 at the adherens junctions allows interaction with β-catenin and F-actin (Suzuki et al., 2012). The ASD2 domain of Shroom3 is responsible for directly interacting with Rho-associated kinases (ROCKI and ROCKII) (Nishimura and Takeichi, 2008). Shroom3's activity requires that the Rho-associated kinases phosphorylate the myosin light chain (MLC) of non-muscle myosin II to activate NM-II. Overall, this signaling cascade ultimately culminates in apical constriction (Nishimura and Takeichi, 2008; Quintin et al., 2008).

Hence, exposure to either a Rho-associated kinase inhibitor, such as Rockout, or a non-muscle myosin II inhibitor, such as blebbistatin, can result in the inability of proper cell shape changes in epithelial cells (Hildebrand, 2005; Kinoshita et al., 2008; Plageman et al., 2011b; Wei et al., 2001).

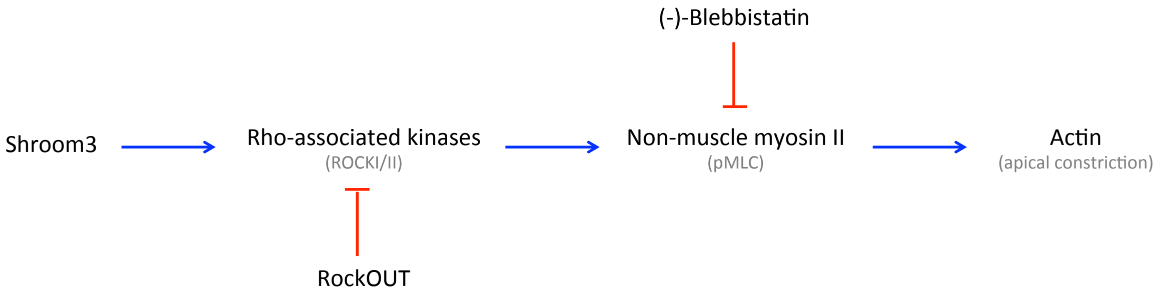
(-)-Blebbistatin
Shroom3
Rho-associated kinases
(ROCKI/II)
Non-muscle myosin II
(pMLC)
Actin
(apical constriction)
RockOUT

**Figure 29. A simplified version of the Shroom3 pathway.** This simplified version of the Shroom3 pathway indicates at some key regulatory proteins required for apical constriction of epithelial cells. Shroom3 physically interacts with Rho-associated kinases (ROCKI and ROCKII) to directly mediate its activity. Subsequently, activation of Rho-associated kinases results in the phosphorylation of the myosin light chain of non-muscle myosin II. Next, this results in the eventual apical constriction of epithelial cells through the role of actin. This diagram illustrates the mechanisms in which two small molecule inhibitors, Rockout and blebbistatin, act on key regulatory proteins to inhibit Shroom3's activity and prevent appropriate apical constriction.

### 4.2.2 Blebbistatin

Significant effects of (-)-blebbistatin were only observed upon exposure at stage 26. There were functional and morphological reductions observed following disruption of ROCK signaling. Conversely, a significant increase in heart rate was observed following exposure to (-)-blebbistatin at stage 26. The absence of significant cardiac alterations following exposure at stage 33/34 may result from the fact that the developmental interval targeted does not disturb cardiac differentiation or the fusion to form a single linear heart tube (Kolker et al., 2000; Lohr and Yost, 2000; Mohun et al., 2000). This stage was targeted to investigate whether inhibition of ROCK signaling, which is necessary for apical constriction, would cause defects in cardiac looping (Colas and Schoenwolf, 2001; Plageman et al., 2011a; Smith and Schoenwolf, 1997). ROCK activation has been shown to be a key regulator in the phosphorylation and subsequent activation of myosin light chain. Therefore, blebbistatin would act to inhibit ROCK-mediated apical constriction (Allingham et al., 2005; Amano et al., 1996; Dou et al., 2007; Swift et al., 2012). As expected, embryos treated with (-)-blebbistatin at both stages demonstrated cardiac looping defects.

Previous work in the lab demonstrated that morpholino knockdown of shroom3 resulted in *Xenopus laevis* embryos that displayed delayed formation of a linear cardiac tube with smaller ventricles and looping defects (Grover, 2009; Halabi, 2013). I observed similar defects following (-)-blebbistatin exposure. The decrease in ventricular size that I observed (refer to Figures 16A and 17A) may be explained by decreased cell thickening in the myocardium resulting from inhibition of ROCK activity. Importantly, using the video imaging, we were able to more clearly measure VWT *in vivo* (refer to Figures 16A and 18A). Although we would predict a reduction in stroke volume and cardiac output, however, we could not show that the changes are functionally relevant as I was not able to measure the endocardial border at end-systole. This will be addressed further in the limitations section.

The gene *Heart and Soul (Has)* encodes for atypical protein kinase C lambda (aPKC lambda), which plays a role in the highly conserved Par-aPKC complex (Horne-Badovinac et al., 2001; Peterson et al., 2001). This complex is localized to the adherens junctions and serves a role in epithelial polarity (Izumi et al., 1998; Kuchinke et al., 1998; Müller and Wieschaus, 1996; Ohno, 2001; Petronczki and Knoblich, 2001; Suzuki et al., 2001; Wodarz et al., 2000). Loss of aPKC lambda in zebrafish was associated with defects in the retina, neural tube, and gut, including abnormalities in gut looping (Horne-Badovinac et al., 2001). Another publication also examining the *has* mutation in zebrafish demonstrated that disruption of aPKC lambda resulted in cardiac chamber misalignment (Peterson et al., 2001). The mutation in *has* was originally identified to cause disruptions in cell-cell interactions and was later determined to also result in a phenotype where the ventricle formed within the atrial zone of the heart tube due to the disturbances in cellular polarity, which is essential for cardiac tube positioning. Furthermore, a study screening numerous genes identified mutations in *heart and soul* to be associated with a small heart and indistinctive chamber formation in zebrafish (Stainier et al., 1996). These cardiac defects are similar to the phenotype that I observed in *Xenopus* following blebbistatin treatment. RhoA has been shown to be required for Shroom3-dependent apical constriction and the function and localization of *has* and *shroom3* are similar (Plageman et al., 2011a). Therefore, the looping and diminished ventricular size abnormalities that are observed in the gut and heart of zebrafish may explain the defects observed following disruption of ROCK signaling using blebbistatin in my *Xenopus* experiments.

### 4.2.3 Rockout

Rockout inhibits ROCK signaling, as is the case with blebbistatin (Morckel et al., 2012; Yarrow et al., 2005). As expected, the Rockout exposure resulted in similar changes as observed for the blebbistatin treatment. Specifically, there were reductions in both functional and morphological cardiac measurements upon exposure at stage 26. Treatment at stage 33/34 did not cause a statistically significant alteration in cardiac function and morphology, except for a significant increase detected in ventricular cross-sectional area. However, the parameter was not associated with any functional changes and this may be due to the stage specific consequences of ROCK inhibition.

In contrast to exposure to blebbistatin, there were no looping malformations identified following Rockout treatment. This absence may be the result of Rockout simply not being fully effective. This could be confirmed through western blot analysis to observe levels of phosphorylated myosin light chain, which should be reduced following exposure to Rockout. The Rockout treatment could be substituted with another small molecule that inhibits ROCK, such as Y-27632, HA1077, and H-89 (Yarrow et al., 2005).

### 4.2.4 Retinoic Acid and Retinoic Acid Receptor Antagonist

The cardiac phenotype resulting from absence of retinoic acid signaling can be explained by research that has demonstrated that retinoic acid is partially responsible for establishing the posterior boundary of the second heart field (Ryckebusch et al., 2008). *Raldh2*$^{-/-}$ murine embryos with a deficiency in the production of retinoic acid demonstrated failure to undergo proper cardiac looping (Ryckebusch et al., 2008; Sirbu et al., 2008). This was proposed to be a consequence of decreased *Hoxa1* expression. In contrast, another publication utilizing *Raldh2*$^{-/-}$ mice demonstrated abnormal positioning of cardiac structures resulting from an expanded Isl-positive population due to increased Fgf8 signaling (Sirbu et al., 2008). An additional study identified the essential role for retinoic acid signaling in the differentiation and renewal of the progenitor population during addition of cells from the secondary heart field to the outflow tract (Li et al., 2010). Mice with aberrant retinoic acid receptors demonstrated misalignment of the outflow tract. This publication identified a retinoic acid deficiency phenotype including improper looping and absence of adequate trabeculation (Niederreither et al., 2001). Therefore, these findings corroborate with the looping defects and diminished ventricular size that were demonstrated following RAA-exposure in my experiments.

Next, I will attempt to explain factors contributing to the cardiac defects observed following exposure to physiologically excessive levels of retinoic acid. In a study that used zebrafish as a developmental model, exogenous RA exposure resulted in a dose-dependent reduction in dimension and subsequent disappearance of cardiac tissue (Stainier and Fishman, 1992). From this publication, the assumption would be that higher than physiological levels of retinoic acid result in small ventricles, which was observed following RA-treatment in my project. The addition of excess retinoic acid has been associated with a plethora of cardiac defects, which also corroborates with some of my observations (Collop et al., 2006).

Therefore, my experiments demonstrated that disruption of retinoic acid signaling resulted in predictable reductions in ventricular morphology in *Xenopus laevis* embryos and these were correlated with expected reductions in cardiac function. As well, I observed reductions in heart rate following both RA and RAA exposure during neurulation, which is corroborated by previous work in the lab (Collop et al., 2006).

I observed that the RA- and RAA-exposed groups had similar phenotypes. However, since these treatments represent opposites, then opposing phenotypes may be expected. The extent of my project hinders my capability to fully explain the mechanism underlying my findings. A possible explanation may be that the retinoic acid was not fully effective since cardiac structures should be absent at high doses when treated at earlier stages, which was not observed in my data (Collop et al., 2006). Alternatives for inhibiting retinoic acid signaling could be used, such as *raldh2*$^{-/-}$ embryos, morpholinos targeting *raldh2* mRNA, or an anti-retinoic acid monoclonal antibody (Twal et al., 1995). These reductions in ventricular dimension and wall thickness may be indicative of decreased stroke volume and cardiac output, which may ultimately result in pathological consequences.

### 4.2.5 Ethanol

Ethanol exposure caused statistically significant reductions in both functional and morphological parameters following treatment at each developmental interval that was targeted. The decrease in ventricular wall thickness that was noted in my experiments is similar to findings using static imaging in *Xenopus* (Yelin et al., 2007b). Furthermore, a study demonstrated maximal sensitivity to ethanol during late blastula and early gastrulation (Yelin et al., 2005). The reduction in ventricular wall thickness observed in my experiments was most prominent when exposure overlapped with the mid-blastula transition and this parameter may signify reductions in stroke volume and cardiac output.

Several hypotheses have emerged to explain the symptoms associated with ethanol exposure during embryonic development. For instance, damage resulting from increased free-radical generation could be the mechanism underlying the teratogenic effects (Kotch et al., 1995). Following exposure to ethanol *in utero*, mice demonstrated increased levels of superoxide anions, lipid peroxidation, and cell death and an increased occurrence of mice with disrupted morphogenesis such as failure of neural tube closure. Rescue experiments using superoxide dismutase (SOD), which acts as an antioxidant, aided in decreasing the teratogenic effects observed. Another proposed mechanism for ethanol teratogenesis includes increased apoptosis, demonstrated through changes in caspase-3 activation, resulting in neurodegeneration in mice (Olney et al., 2002a; Olney et al., 2002b). Similarly, experiments performed in the chick observed increased incidence of apoptosis in neural crest cells upon exposure to ethanol (Cartwright and Smith, 1995a). Alteration of gene expression of specific proteins such as insulin-like growth factors (IGF) (Singh et al., 1996b) or GLUT1 (Singh et al., 1996a) has also been noted. Another research group noted reduced epidermal growth factor (EGF)-dependent cell replication following hepatic exposure to ethanol in fetal rats (Henderson et al., 1989).

One explanation proposed to elucidate the mechanisms underlying the cardiac defects was the competition of ethanol for metabolism, thereby antagonizing the synthesis of retinoic acid (Deltour et al., 1996; Duester, 1991; Pullarkat, 1991; Van Thiel et al., 1974; Yelin et al., 2005; Yelin et al., 2007a). Vitamin A, otherwise referred to as retinol, must be oxidized by endogenous enzymes to synthesize retinoic acid, that is required for proper cardiac development (Collop et al., 2006; Drysdale and Crawford, 1994; Jiang et al., 1999; Keegan et al., 2005; Smith et al., 1997; Twal et al., 1995; Xavier-Neto et al., 2000). The enzymes alcohol dehydrogenase (ADH) and aldehyde dehydrogenase (ALDH), in this situation Raldh2, are necessary for the synthesis of RA from retinol (Boleda et al., 1993; Connor and Smit, 1987; Yang et al., 1994). However, this may be competitively inhibited by the presence of ethanol, which requires these enzymes for detoxification (Duester, 1991; Mezey and Holt, 1971; Van Thiel et al., 1974). Therefore, the presence of ethanol could result in an overall decrease in RA levels.

This hypothesis is supported by the recapitulation in phenotype resulting from both RA deficiency and ethanol-induced teratogenesis (Cartwright and Smith, 1995b; Dickman et al., 1997; Gale et al., 1996; Johnson et al., 1996; Maden et al., 1996; Yelin et al., 2005; Yelin et al., 2007a). Exogenous retinoic acid administration resulted in *Xenopus* embryos with the opposite gene expression profile to embryos exposed to ethanol, such as differential expression of *hoxA2, hoxB4, hoxB9*, *gsc, otx2,* and *chordin* (Yelin et al., 2005). This proposition was further supported by over expression of cyp26*,* which is an enzyme that degrades RA. Cyp26 over expression resulted in a similar phenotype to FAS in *Xenopus* embryos. Furthermore, co-exposure with retinoic acid and ethanol resulted in a phenotypic rescue in both *Xenopus* and quail embryos (Twal et al., 1997; Yelin et al., 2005).

These defects did not result from an increased metabolism of retinoic acid as a contrasting reduction in cyp26 expression was observed following ethanol administration (Yelin et al., 2005). Although cyp2E1 is another enzyme involved in ethanol metabolism and free radical synthesis, this gene is not activated at a relevant developmental interval (Deltour et al., 1996). Following analysis of my data, I also noticed that both the RAA and ethanol treatment caused similar reductions in ventricular morphology and function, which supports the hypothesis that the teratogenic consequences induced by ethanol exposure could be caused by a reduction in retinoic acid levels.

## 4.3 Origin of Cardiac Response

I pursued to answer a distinct and unique question not related to CHDs, although this experiment still served the purpose of establishing this novel imaging system's usefulness. I sought to determine the time at which cardiac response originates, which possibly initiates upon the completion of innervation. *Xenopus* has historically served as a valuable model for studying developmental biology, however, the timing of initiating the cardiac response has not, to our knowledge, been established.

Future experiments should investigate developmental intervals preceding stage 37/38. A caveat of this technique is that the heartbeat must be present to examine innervation. Since coordinated myocardial contractions commence in the primitive heart at approximately stage 35, when cardiac looping is finishing, then innervation cannot be studied prior to this stage using this method (Lohr and Yost, 2000; Warkman and Krieg, 2007). A developmental window that is worth investigating would be stages 35 and 36. Imaging at this stage may be possible through manipulation of the embryo by physically removing the ectodermal layers that are positioned ventral to the heart, which would resolve optical constraints that I encountered in my experiments.

I acutely exposed embryos to classical modulators of heart rate to attempt to narrow down the developmental window that corresponds to the initiation of innervation. The rationale follows that if embryos are responsive to a drug at a certain stage, then innervation has probably occurred allowing the embryo to display the appropriate cardiac response in the presence of the pharmacological agent.

Due to limitations of this system, I was not able to precisely identify the origin of cardiac response. Nevertheless, I was capable of narrowing the developmental window by identifying that innervation originates by at least stage 37/38, which is following the completion of cardiac differentiation and looping (Kolker et al., 2000; Lohr and Yost, 2000; Mohun et al., 2000).

## 4.4 Advantages

I will now review the video imaging system as a method of analyzing cardiac function, including both the advantages and limitations.

Firstly, there are numerous advantages of the techniques and system that I have used in studying the early heart and it can be a particularly useful alternative to current imaging modalities. Two important advantages of using *Xenopus* are the ability to view the embryo from the ventral side without manipulation and the ability of the embryo to survive without a properly functioning heart until later tadpole stages (Kaltenbrun et al., 2011; Mohun et al., 2000).

There are several advantages of the mounting protocol that I used (Kieserman et al., 2010). Some of the highlights include the ability to re-use an embryo for acute drug exposure studies or for longitudinal studies examining maturation. This procedure is non-invasive, therefore should not affect cardiac function and anesthetization is unnecessary. Furthermore, modifications to this mounting protocol allows for relatively long-term live imaging without embryo desiccation.

This novel imaging system offers several advantages compared to current imaging modalities. For instance, the cost of the software and the video camera is far less expensive compared to other equipment, such as magnetic resonance imaging or confocal microscopy. The level of expertise required to use the software and equipment is much less extensive than that expected of other modalities such as MRI, ultrasound, echocardiography, optical coherence tomography, and intrathoracic cardiac recording. Certain imaging modalities require further expertise since the images are more subjective and difficult to interpret compared to the higher resolution images that are obtained using our video imaging system. However, the relatively high-resolution images do not require a low frame-rate, which is very useful for studying a rapidly beating heart. The ability to analyze real-time videos is also useful compared to modalities that require embryo fixation, such as scanning electron microscopy and 3D reconstructions using histological sections. Simple normal light optics is used to visualize the heart since the camera uses endogenous hemoglobin to create contrast. This is less invasive compared to other imaging modalities that require the use of exogenously labeled dyes to create sufficient contrast to obtain an image.

Our video imaging system offers significant advantages compared to current imaging modalities. However, this imaging system is not without caveats, which will be addressed in the next section.

## 4.5 Limitations

As noted previously, only four stages of embryonic development for the normative sample were ideal for functional examination using this system. These stages included the later stages of development once cardiac morphology is relatively established (Mohun et al., 2000). These limitations arise due to optical considerations, since this system does not manipulate the embryo and uses normal light optics.

Development before stage 45 is difficult to measure due to ectodermal pigmentation and general opacity on the ventral side surrounding the heart. Although beating hearts could be seen, there was difficulty in establishing a clear outline of the epicardial and endocardial borders. As well, decreased presence of blood and blood flow creates difficulty in tracing the endocardial border since hemoglobin was important for creating contrast (Movie 19). Subsequently, during development in later stage 48 and onwards, the myocardium has substantially thickened and the working distance from the ventral surface to the heart increased causing the cardiac borders to again be difficult to distinguish accurately (Movie 20) (Wessels and Sedmera, 2003).

Limitations were also present for the experiments examining the origin of cardiac response, however, distinct endocardial and epicardial borders were not as rigorously required for investigation of only heart rate. This was nevertheless challenging due to the presence of the pigmentation and opacity on the ventral and lateral ectoderm surrounding the heart, that resulted in measurement difficulty prior to stage 40. By exploiting the Nkx2.5-GFP transgenic line, I could visualize the heart at earlier stages (stages 37-39) using a fluorescent stereomicroscope. These stages were not imaged using the Flare camera and HeartMetrics software as this system required an abundance of light for visualization, which prohibited the use of fluorescence. Even so, earlier measurements are still challenging due to the ectodermal covering.

Embryos that were chronically exposed to various treatments were challenging to examine and limited the parameters that could be studied. The dorsal side became curved causing difficulty in viewing the ventral side without embryo manipulation. Furthermore, the pericardial edema located on the ventral side that is normally associated with these treatments caused an increased working distance as the heart became located more dorsally, making ventral imaging more difficult. Therefore, cardiac function was examined exclusively at end-diastole following exposure to small molecules, resulting in the omission of key parameters, such as stroke volume and cardiac output.

## 4.6 Significance

The video imaging system that I used can measure cardiac function even following exposure to small molecules that disrupt cardiogenesis, therefore, this system may be a useful alternative to current imaging modalities. Using this system, understanding the contribution of functional changes due to or causing CHDs may be easier to examine. As well, the association between normal morphogenesis and function may be simpler to assess.

A future aspiration would be to create a fully automated high-throughput system that is capable of using this system to quickly analyze hundreds of compounds for cardiac activity. This may provide the ability to screen for novel compounds that are capable of causing disruptions in cardiogenesis or alterations in cardiac function.

# References

Abel, E. L. (1990). Fetal alcohol syndrome. Oradell, New Jersey: Medical Economics Books.

Abu-Issa, R., Smyth, G., Smoak, I., Yamamura, K. and Meyers, E. N. (2002). Fgf8 is required for pharyngeal arch and cardiovascular development in the mouse. *Development*. **129**: 4613-25.

Afouda, B. A. and Hoppler, S. (2009). *Xenopus* Explants as an Experimental Model System for Studying Heart Development. *Trends Cardiovasc Med*. **19**: 200-26.

Agarwal, C., Chandraratna, R. A., Johnson, A. T., Rorke, E. A. and Eckert, R. L. (1996). AGN193109 is a highly effective antagonist of retinoid action in human ectocervical epithelial cells. *J Biol Chem.* **271**: 12209-12.

Al Naieb, S. A., Happel, C. M. and Yelbuz, T. M. (2013). A detailed atlas of chick heart development in vivo. *Ann Anat*. **195**: 324-41.

Allingham, J.S., Smith, R. and Rayment, I. (2005). The structural basis of blebbistatin inhibition and specificity for myosin II. *Nat Struct Mol Biol*. **12**: 378-9.

Alsan, B. H. and Schultheiss, T. M. (2002). Regulation of avian cardiogenesis by Fgf8 signaling. *Development*. **129**: 1935-43.

Amano, M., Ito, M., Kimura, K., Fukata, Y., Chihara, K., Nakano, T., Matsuura, Y. and Kaibuchi, K. (1996). Phosphorylation and activation of myosin by Rho-associated kinase (Rho-kinase). *J Biol Chem*. **271**: 20246-9.

Amaya, E., Stein, P. A., Musci, T. J. and Kirschner, M. W. (1993). FGF signalling in the early specification of mesoderm in *Xenopus*. *Development*. **118**: 477-87.

Armour, J. A. (1999). Myocardial ischaemia and the cardiac nervous system. *Cardiovasc Res*. **41**: 41-54.

Auman, H. J., Coleman, H., Riley, H. E., Olale, F., Tsai, H. J., and Yelon, D. (2007). Functional modulation of cardiac form through regionally confined cell shape changes. *PLoS Biol.* **5**: E53

Bartlett, H. L., Escalera, R. B., Patel, S. S., Wedemeyer, E. W., Volk, K. A., Lohr, J. L. and Reinking, B. E. (2010). Echocardiographic Assessment of Cardiac Morphology and Function in *Xenopus*. *Comp Med*. **60**: 107-13.

Bartlett, H. L., Scholz, T. D., Lamb, F. S. and Weeks, D. L. (2004). Characterization of embryonic cardiac pacemaker and atrioventricular conduction physiology in *Xenopus laevis* using noninvasive imaging. *Am J Physiol Heart Circ Physiol.* **286**: H2035-41.

Bartlett, H. L., Sutherland, L., Kolker, S. J., Welp, C., Tajchman, U., Desmarais, V. and Weeks, D. L. (2007). Transient early embryonic expression of *Nkx2.5* mutations linked to congenital heart defects in human causes heart defects in *Xenopus laevis*. *Dev Dyn*. **236**: 2475-84.

Bartman, T., Walsh, E. C., Wen, K. K., McKane, M., Ren, J., Alexander, J., Rubenstein, P. A., and Stainier, D. Y. (2004). Early myocardial function affects endocardial cushion development in zebrafish. *PLoS Biol.* **2**: E129.

Bodmer, R. (1993). The gene *tinman* is required for specification of the heart and visceral muscles in *Drosophila*. *Development*. **118**: 719-29.

Bodmer, R. and Venkatesh, T. V. (1998). Heart development in *Drosophila* and vertebrates: conservation of molecular mechanisms. *Dev Genet.* **22**: 181-6.

Boleda, M. D., Saubi, N., Farrés, J. and Parés, X. (1993). Physiological substrates for rat alcohol dehydrogenase classes: aldehydes of lipid peroxidation, omega-hydroxyfatty acids, and retinoids. *Arch Biochem Biophys*. **307**: 85-90.

Boppart, S. A., Tearney, G. J., Bouma, B. E., Southern, J. F., Brezinski, M. E. and Fujimoto, J. G. (1997). Noninvasive assessment of the developing *Xenopus* cardiovascular system using optical coherence tomography. *Proc Natl Acad Sci U S A*. **94**: 4256-61.

Boskovski, M. T., Yuan, S., Pedersen, N. B., Goth, C. K., Makova, S., Clausen, H., Brueckner, M. and Khokha, M. K. (2013). The heterotaxy gene *GALNT11* glycosylates Notch to orchestrate cilia type and laterality. *Nature*. **504**: 456-9.

Bosman, A., Letourneau, A., Sartiani, L., Del Lungo, M., Ronzoni, F., Kuziakiv, R., Tohonen, V., Zucchelli, M., Santoni, F., Guipponi, M., Dumevska, B., Hovatta, O., Antonarakis, S. E. and Jaconi, M. E. (2015). Perturbations of heart development and function in cardiomyocytes from human embryonic stem cells with trisomy 21. *Stem Cells*. **33**: 1434-46.

Brade, T., Gessert, S., Kühl, M. and Pandur, P. (2007). The amphibian second heart field: *Xenopus islet-1* is required for cardiovascular development. *Dev Biol*. **311**: 297-310.

Breckenridge, R. A., Mohun, T. J. and Amaya, E. (2001). A role for BMP signaling in heart looping morphogenesis in *Xenopus*. *Dev Biol*. **232**: 191-203.

Cai, C. L., Liang, X., Shi, Y., Chu, P. H., Pfaff, S. L., Chen, J. and Evans, S. (2003). Isl-1 identifies a cardiac progenitor population that proliferates prior to differentiation and contributes a majority of cells to the heart. *Dev Cell*. **5**: 877-89.

Callaway, C. W. (2013). Epinephrine for cardiac arrest. *Curr Opin Cardiol*. **28**: 36-42.

Cartwright, M. M. and Smith S. M. (1995). Increased cell death and reduced neural crest cell numbers in ethanol-exposed embryos: partial basis for fetal alcohol syndrome phenotype. *Alcohol Clin Exp Res*. **19**: 378-86.

Cartwright, M. M. and Smith, S. M. (1995). Stage-dependent effects of ethanol on cranial neural crest cell development: partial basis for the phenotypic variations observed in fetal alcohol syndrome. *Alcohol Clin Exp Res.* **19**: 1454-62.

Chung, M. I., Nascone-Yoder, N. M., Grover, S. A., Drysdale, T. A., and Wallingford, J. B. (2010). Direct activation of Shroom3 transcription by Pitx proteins drives epithelial morphogenesis in the developing gut. *Development*. **137**: 1339-49.

Cirić, O. and Susić, D. (1980). Effect of isoproterenol on blood pressure and heart rate in different phases of the oestrous cycle. *Endokrinologie*. **76**: 274-8.

Cohen, E. D., Wang, Z., Lepore, J. J., Lu, M. M., Taketo, M. M., Epstein, D. J. and Morrisey, E. E. (2007). Wnt/beta-catenin signaling promotes expansion of Isl-1 positive cardiac progenitor cells through regulation of FGF signaling. *J Clin Invest*. **117**: 1794-804.

Colas, J. F. and Schoenwolf, G. C. (2001). Towards a cellular and molecular understanding of neurulation. *Dev Dyn*. **221**: 117-45.

Collop, A. H., Broomfield, J. A. S., Chandraratna, R. A. S., Yong, Z., Diemling, S. J., Kolker, S. J., Weeks, D. L. and Drysdale, T. A. (2006). Retinoic acid signaling is essential for formation of the heart tube in *Xenopus*. *Dev Biol*. **291**: 96-109.

Connor, M. J. and Smit, M. H. (1987). Terminal-group oxidation of retinol by mouse epidermis: inhibition *in vitro* and *in vivo*. *Biochem J.* **244**: 489-92.

Deimling, S. J. and Drysdale, T. A. (2011). Fgf is required to regulate anterior-posterior patterning in the *Xenopus* lateral plate mesoderm. *Mech Dev*. **128**: 327-41.

Deimling, S. J. and Drysdale, T. A. (2009). Retinoic acid regulates anterior-posterior patterning within the lateral plate mesoderm of *Xenopus*. *Mech Dev*. **126**: 913-23.

Deimling, S. J., Halabi, R. R., Grover, S. A., Wang, J. H. and Drysdale, T. A. (2015). Understanding early organogenesis using a simplified *in situ* hybridization protocol in *Xenopus*. *J Vis Exp*. **e51526.** DOI: 10.3791/51526.

Deltour, L., Ang, H. L. and Duester, G. (1996). Ethanol inhibition of retinoic acid synthesis as a potential mechanism for fetal alcohol syndrome. *FASEB J*. **10**: 1050-7.

Deniz, E., Jonas, S., Khokha, M. and Choma, M. A. (2012). Endogenous contrast blood flow imaging in embryonic hearts using hemoglobin contrast subtraction angiography. *Opt Lett*. **37**: 2979-81.

Dickman, E. D., Thaller, C., and Smith, S. M. (1997). Temporally-regulated retinoic acid depletion produces specific neural crest, ocular and nervous system defects. *Development*. **124**: 3111-21.

Dickover, M., Hegarty, J. M., Ly, K., Lopez, D., Yang, H., Zhang, R., Tedeschi, N., Hsiai, T. K. and Chi, N. C. (2014). The atypical Rho GTPase, RhoU, regulates cell-adhesion molecules during cardiac morphogenesis. *Dev Biol*. **389**: 182-91.

Dietzel, S., Pircher, J., Nekolla, A. K., Gull, M., Brändi, A. W., Pohl, U. and Rehberg, M. (2014). Label-free determination of hemodynamic parameters in the microcirculation with third harmonic generation microscopy. *PLoS One.* **9**: e99615. doi: 10.1371/journal.pone.0099615

Dou, Y., Arlock, P. and Arner, A. (2007). Blebbistatin specifically inhibits actin-myosin interaction in mouse cardiac muscle. *Am J Physiol Cell Physiol*. **293**: C1148-53.

Drysdale, T. A. and Crawford, M. J. (1994). Effects of localized application of retinoic acid on *Xenopus laevis* development. *Dev Biol*. **162**: 394-401.

Drysdale, T. A., Tonissen, K. F., Patterson, K. D., Crawford, M. J. and Krieg, P. A. (1994). Cardiac Troponin I is a Heart-Specific Marker in the *Xenopus* Embryo: Expression during Abnormal Heart Morphogenesis. *Dev Biol*. **165**: 432-41.

Duester, G. (1991). A hypothetical mechanism for fetal alcohol syndrome involving ethanol inhibition of retinoic acid synthesis at the alcohol dehydrogenase step. *Alcohol Clin Exp Res*. **15**: 568-72.

Dyer, L. A. and Kirby, M. L. (2009). Sonic hedgehog maintains proliferation in secondary heart field progenitors and is required for normal arterial pole formation. *Dev Biol*. **330**: 305-17.

Dyer, L. A. and Kirby, M. L. (2009). The role of secondary heart field in cardiac development. *Dev Biol.* **336**: 137-44.

Fakhro, K. A., Choi, M., Ware, S. M., Belmont, J. W., Towbin, J. A., Lifton, R. P., Khokha, M. K. and Bruekner, M. (2011). Rare copy number variations in congenital heart disease patients identify unique genes in left-right patterning. *Proc Natl Acad Sci U S A.* **108**: 2915-20.

Foley, A. C. and Mercola, M. (2005). Heart induction by Wnt antagonists depends on the homeodomain transcription factor Hex. *Genes Dev*. **19**: 387-96.

Fu, J. D., Stone, N. R., Liu, L., Spencer, C. I., Qian, L., Hayashi, Y., Delgado-Olguin, P., Ding, S., Bruneau, B. G. and Srivastava, D. (2013). Direct reprogramming of human fibroblasts toward a cardiomyocyte-like state. *Stem Cell Reports.* **1**: 235-47.

Fujito, K., Takayanagi, R., Kimura, K., Yokoyama, H. and Yamada, Y. (2014). Evaluation of clinical bradycardiac effect and respiratory adverse effect of β-blocking agents in coronary computed tomography angiography based on theoretical analysis. *Eur J Drug Metab Pharmacokinet*. DOI 10.1007/s13318-014-0244-3.

Gale, E., Prince, V., Lumsden, A., Clarke, J., Holder, N. and Maden, M. (1996). Late effects of retinoic acid on neural crest and aspects of rhombomere. *Development*. **122**: 783-93.

Galvin, K. M., Donovan, M. J., Lynch, C. A., Meyer, R. I., Paul, R. J., Lorenz, J. N., Fairchild-Huntress V., Dixon, K. L., Dunmore, J. H., Gimbrone, M. A. Jr., Falb, D. and Huszar, D. (2000). A role for Smad6 in development and homeostasis of the cardiovascular system. *Nat Genet*. **24**: 171-4.

Gao, J., Lyon, J. A., Szeto, D. P. and Chen, J. (2012). *In vivo* imaging and quantitative analysis of zebrafish embryos by digital holographic microscopy. *Biomed Opt Express*. **3**: 2623-35.

Glass, C. K. and Rosenfeld, M. G. (2000). The coregulator exchange in transcriptional functions of nuclear receptors. *Genes Dev*. **14**: 121-41.

Goddeeris, M. M., Schwartz, R., Klingensmith, J. and Meyers, E. N. (2007). Independent requirements for hedgehog signaling by both the anterior heart field and neural crest cells for outflow tract development. *Development*. **134**: 1593-604.

Grover, S. (2009). *The role for shroom3 in the cellular and molecular mechanisms of linear heart tube formation*. (Master's thesis). Western University. London, Ontario Canada.

Hagens, O., Ballabio, A., Kalscheuer, V., Kraehenbuhl, J. P., Schiaffino, M. V., Smith, P., Staub, O., Hildebrand, J. and Wallingford, J. B. (2006). A new standard nomenclature for proteins related to Apx and Shroom. *BMC Cell Biol.* **7**: 18.

Haigo, S. L., Hildebrand, J. D., Harland, R. M. and Wallingford, J. B. (2003). Shroom induces apical constriction and is required for hingepoint formation during neural tube closure. *Curr Biol.* **13**: 2125-37.

Halabi, R. R. (2013). *Shroom3 deficient mice show congenital heart defects*. (Master's thesis). Western University. London, Ontario Canada.

Harland, R. M. (1991). *In situ* hybridization: an improved whole-mount method for *Xenopus* embryos. *Methods Cell Biol.* **36**: 685-95.

Haselbeck, R. J., Hoffman, I. and Duester, G. (1999). Distinct functions for Aldh1 and Raldh2 in the control of ligand production for embryonic retinoid signaling pathways. *Dev Genet*. **25**: 353-64.

Haworth, K. E., Kotecha, S., Mohun, T. J. and Latinkic, B. V. (2008). *GATA4* and *GATA5* are essential for heart and liver development in *Xenopus* embryos. *BMC Dev Biol*. **8**: 74. DOI: 10.1186/1471-213X-8-74.

Henderson, G. I., Baskin, G. S., Horbach, J., Porter, P., and Schenker, S. (1989). Arrest of epidermal growth factor-dependent growth in fetal hepatocytes after ethanol exposure. *J Clin Invest*. **84**: 1287-94.

High, F. A., Jain, R., Stoller, J. Z., Antonucci, N. B., Lu, M. M., Loomes, K. M., Kaestner, K. H., Pear, W. S. and Epstein, J. A. (2009). Murine Jagged1/Notch signaling in the second heart field orchestrates Fgf8 expression and tissue-tissue interactions during outflow tract development. *J Clin Invest*. **119**: 1986-96.

Hildebrand, J. D. (2005). Shroom regulates epithelial cell shape via the apical positioning of an actomyosin network. *J Cell Sci*. **118**: 5191-203.

Hildebrand, J. D. and Soriano, P. (1999). Shroom, a PDZ domain-containing actin binding protein, is required for neural tube morphogenesis in mice. *Cell*. **99**: 485-97.

Hochgreb, T., Linhares, V. L., Menezes, D. C., Sampaio, A. C., Yan, C. Y., Cardoso, W. V., Rosenthal, N. and Xavier-Neto, J. (2003). A caudorostral wave of RALDH2 conveys anteroposterior information to the cardiac field. *Development*. **130**: 5363-74.

Hoffman, J. I. and Kaplan, S. (2002). The incidence of congenital heart disease. *J Am Coll Cardiol*. **12**: 1890-900.

Hollemann, T., Chen Y., Grunz, H. and Pieler, T. (1998). Regionalized metabolic activity establishes boundaries of retinoic acid signaling. *EMBO J*. **17**: 1761-72.

Horne-Badovinac, S., Lin, D., Waldron, S., Schwarz, M., Mbamalu, G., Pawson, T., Jan, Y., Stainier, D. Y. and Abdelilah-Seyfried, S. (2001). Positional cloning of heart and soul reveals multiple roles for PKC lambda in zebrafish organogenesis. *Curr Biol.* **11**: 1492-502.

Hove, J. R., Köster, R. W., Forouhar, A. S., Acevedo-Bolton, G., Fraser, S. E. and Gharib, M. (2003). Intracardiac fluid forces are an essential epigenetic factor for embryonic cardiogenesis. *Nature*. **421**: 172-7.

Izumi, Y., Hirose, T., Tamai, Y., Hirai, S., Nagashima, Y., Fujimoto, T., Tabuse, Y., Kemphues, K. J. and Ohno, S. (1998). An atypical PKC directly associates and colocalizes at the epithelial tight junction with ASIP, a mammalian homologue of *Caenorhabditis elegans* polarity protein PAR-3. *J Cell Biol*. **143**: 95-106.

Jahr, M. and Männer, J. (2011). Development of the venous pole of the heart in the frog *Xenopus laevis*: a morphological study with special focus on the development of the venoatrial connections. *Dev Dyn*. **240**: 1518-27.

Jahr, M., Schlueter, J., Brand, T. and Männer, J. (2008). Development of the proepicardium in *Xenopus laevis*. *Dev Dyn*. **237**: 3088-96.

Jiang, Y., Drysdale, T. A. and Evans, T. (1999). A role for GATA-4/5/6 in the regulation of Nkx2.5 expression with implications for patterning of the precardiac field. *Dev Biol*. **216**: 57-71.

Johnson, V. P., Swayze, V. W. II, Sato, Y. and Andreasen, N. C. (1996). Fetal alcohol syndrome: craniofacial and central nervous system manifestations. *Am J Med Genet*. **61**: 329-39.

Jones, K. L. and Smith, D. W. (1973). Recognition of the fetal alcohol syndrome in early infancy. *Lancet*. **302**: 999-1001.

Kaltenbrun, E., Tandon, P., Amin, N. M., Waldron, L., Showell, C. and Conlon, F. L. (2011). *Xenopus*: An Emerging Model for Studying Congenital Heart Disease. *Birth Defects Res A Clin Mol Teratol*. **91**: 495-510.

Keegan, B. R., Feldman, J. L., Begemann, G., Ingham, P. W. and Yelon, D. (2005). Retinoic acid signaling restricts the cardiac progenitor pool. *Science*. **307**: 247-9.

Kenny, A. P., Rankin, S. A., Allbee, A. W., Prewitt, A R., Zhang, Z., Tabangin, M. E., Shifley, E. T., Louza, M. P. and Zorn, A. M. (2012). Sizzled-tolloid interactions maintain foregut progenitors by regulating fibronectin-dependent BMP signaling. *Dev Cell*. **23**: 292-304.

Khoshnood, B., Lelong, N., Houyel, L., Thieulin, A. C., Jouannic, J. M., Magnier, S., Delezoide, A. L., Magny, J. F., Rambaud, C., Bonnet, D., Goffinet, F. and EPICARD Study Group. (2012). Prevalence, timing of diagnosis and mortality of newborns with congenital heart defects: a population based study. *Heart*. **98**: 1667-73.

Kieserman E. K., Lee, C., Gray, R. S., Park, T. J. and Wallingford, J. B. (2010). Highmagnification *in vivo* imaging of *Xenopus* embryos for cell and developmental biology. *Cold Spring Harb Protoc*. **2010**: pdb.prot5427. doi: 10.1101/pdb.prot5427.

Kinoshita, N., Sasai, N., Misaki, K. and Yonemura, S. (2008). Apical accumulation of Rho in the neural plate is important for neural plate cell shape change and neural tube formation. *Mol Biol Cell*. **19**: 2289-99.

Kolker, S. J., Tajchman, U. and Weeks, D. L. (2000). Confocal Imaging of Early Heart Development in *Xenopus laevis*. *Dev Biol*. **218**: 64-73.

Komuro, I. and Izumo, S. (1993). *Csx*: A murine homeobox-containing gene specifically expressed in the developing heart. *Proc Natl Acad Sci U S A*. **90**: 8145-9.

Kotch, L. E., Chen, S. Y. and Sulik, K. K. (1995). Ethanol-induced teratogenesis: free radical damage as a possible mechanim. *Teratology*. **52**: 128-36.

Kuchinke, U., Grawe, F. and Knust, E. (1998). Control of spindle orientation in *Drosophila* by the Par-3-related PDZ-domain protein Bazooka. *Curr Biol.* **8**: 1357-65.

Kwon, S. M., Alev, C. and Asahara, T. (2009). The role of notch signaling in endothelial progenitor cell biology. *Trends Cardiovasc Med*. **19**: 170-3.

Lee, C., Le, M. P. and Wallingford, J. B. (2009). The shroom family proteins play broad roles in the morphogenesis of thickened epithelial sheets. *Dev Dyn*. **238**: 1480-91.

Li, P., Pashmforoush, M. and Sucov, H. M. (2010). Retinoic acid regulates differentiation of the secondary heart field and TGFbeta-mediated outflow tract septation. *Dev Cell*. **18**: 480-5.

Li, P., Yin, X., Rugonyi, S. and Wang, R. K. (2012). *In vivo* functional imaging of blood flow and wall strain rate in outflow tract of embryonic chick heart using ultrafast spectral domain optical coherence tomography. *J Biomed Opt*. **17**: 96006-1. DOI: 10.1117/1.JBO.17.9.096006.

Lienkamp, S. S., Liu, K., Karner, C. M., Carroll, T. J., Ronneberger, O., Wallingford, J. B. and Walz, G. (2012). Vertebrate kidney tubules elongate using a planar cell polarity-dependent, rosette-based mechanism of convergent extension. *Nat Genet*. **44**: 1382-7.

Lohr, J. L. and Yost, H. J. (2000). Vertebrate Model Systems in the Study of Early Heart Development: *Xenopus* and Zebrafish. *Am J Med Genet*. **97**: 248-57.

Lyons, I., Parsons, L. M., Hartley, L., Li, R., Andrews, J. E., Robb, L. and Harvey, R. P.

(1995). Myogenic and morphogenetic defects in the heart tubes of murine embryos lacking the homeo box gene *Nkx2.5*. *Genes Dev.* **9**: 1654-66.

Maden, M., Gale, E., Kostetskii, I. and Zile, M. (1996). Vitamin-A deficient quail embryos have half a hindbrain and other neural defects. *Curr Biol*. **6**: 417-26.

Mariampillai, A., Standish, B. A., Munce, N. R., Randall, C., Liu, G., Jiang, J. Y., Cable, A. E., Vitkin, I. A. and Yang, V. X. (2007). Doppler optical cardiogram gated 2D color flow imaging at 1000 fps and 4D *in vivo* visualization of embryonic heart at 45 fps on a swept source OCT system. *Opt Express*. **15**: 1627-38.

Marvin, M. J., Di Rocco, G., Gardiner, A., Bush, S. M. and Lassar, A. B. (2001). Inhibition of Wnt activity induces heart formation from posterior mesoderm. *Genes Dev*. **15**: 316-27.

McCright, B., Gao, X., Shen, L., Lozier, J., Lan, Y., Maguire, M., Herzlinger, D., Weinmaster, G., Jiang, R. and Gridley, T. (2001). Defects in development of the kidney, heart, and eye vasculature in mice homozygous for a hypomorphic *Notch2* mutation. *Development*. **128**: 491-502.

Meilhac, S., Kelly, R., Rocancourt, D. and Buckingham, M. (2003). The mouse as a model of heart morphogenesis in mammals: origin and lineage of myocytes. *J Soc Biol*. **197**: 179-86.

Meyers, E. N. and Martin, G. R. (1999). Differences in left-right axis pathways in mouse and chick: functions of FGF8 and SHH. *Science*. **285**: 403-6.

Mezey, E. and Holt, P. R. (1971). The inhibitory effect of ethanol on retinol oxidation by human liver and cattle retina. *Exp Mol Pathol*. **15**: 148-56.

Mohun, T. J., Leong, L. M., Weninger, W. J. and Sparrow, D. B. (2000). The Morphology of Heart Development in *Xenopus laevis*. *Dev Biol*. **218**: 74-88.

Monzen, K., Shiojima, I., Hiroi, Y., Kudoh, S., Oka, T., Takimoto, E., Hayashi, D., Hosoda, T., Habara-Ohkubo, A., Nakaoka, T., Fujita, T., Yazaki, Y. and Komuro, I. (1999). Bone morphogenetic proteins induce cardiomyocyte differentiation through the mitogen-activated protein kinase kinase kinase TAK1 and cardiac transcription factors Csx/Nkx2.5 and GATA-4. *Mol Cell Biol*. **19**: 7096-105.

Moosmann, J., Ershov, A., Altapova, V., Baumbach, T., Prasad, M. S., LaBonne, C., Xiao, X., Kashef, J. and Hofmann, R. (2013). X-ray phase-contrast *in vivo* microtomography probes new aspects of *Xenopus* gastrulation. *Nature*. **497**: 374-7.

Morckel, A. R., Lusic, H., Farzana, L., Yoder, J. A., Deiters, A. and Nascone-Yoder, N.

M. (2012). A photoactivatable small-molecule inhibitor for light-controlled spatiotemporal regulation of Rho kinase in live embryos. *Development*. **139**: 437-42.

Müller, H. A. and Wieschaus, E. (1996). armadillo, bazooka, and stardust are critical for early stages in formation of the zonula adherens and maintenance of the polarized blastoderm epithelium in *Drosophila*. *J Cell Biol.* **134**: 149-63.

Nascone, N. and Mercola, M. (1995). An inductive role for the endoderm in *Xenopus* cardiogenesis. *Development*. **121**: 515-23.

Niederreither, K., Vermot, J., Messaddeq, N., Schuhbaur, B., Chambon, P. and Dollé, P. (2001). Embryonic retinoic acid synthesis is essential for heart morphogenesis in the mouse. *Development*. **128**: 1019-31.

Nieuwkoop, P. D. and Faber, J. (1994). Normal Table of *Xenopus laevis* (Daudin): A Systematical and Chonological Survey of the Development from the Fertilized Egg Till the End of Metamorphosis. Garland Pub, New York.

Nishimura, T. and Takeichi, M. (2008). Shroom3-mediated recruitment of Rho kinases to the apical cell junctions regulates epithelial and neuroepithelial planar remodeling. *Development*. **135**: 1493-502.

Ohno, S. (2001). Intercellular junctions and cellular polarity: the Par-aPKC complex, a conserved core cassette playing fundamental roles in cell polarity. *Curr Opin Cell Biol*. **13**: 641-8.

Olney, J. W., Tenkova, T., Dikranian, K., Muglia, L. J., Jermakowicz, W. J., D'Sa, C. and Roth, K. A. (2002). Ethanol-induced caspase-3 activation in the *in vivo* developing mouse brain. *Neurobiol Dis*. **9**: 205-19.

Olney, J. W., Tenkova, T., Dikranian, K., Qin, Y. Q., Labruyere, J. and Ikonomidou, C. (2002). Ethanol-induced apoptotic neurodegeneration in the developing C57BL/6 mouse brain. *Brain Res Dev Brain Res*. **133**: 115-26.

Orhan, G., Baron, S., Norozi, K., Männer, J., Hornung, O., Blume, H., Misske, J., Heimann, B., Wessel, A. and Yelbuz, T. M. (2007). Construction and establishment of a new environmental chamber to study real-time cardiac development. *Microsc Microanal*. **13**: 204-10.

Pandur, P., Läsche, M., Eisenberg, L. M. and Kühl, M. (2002). Wnt-11 activation of a non-canonical Wnt signaling pathway is required for cardiogenesis. *Nature*. **418**: 636-41.

Park, E. J., Watanabe, Y., Smyth, G., Miyagawa-Tomita, S., Meyer, E., Klingensmith, J., Camenisch, T., Buckingham, M. and Moon, A. M. (2008). An FGF autocrine loop initiated in second heart field mesoderm regulates morphogenesis at the arterial pole of the heart. *Development*. **135**: 3599-610.

Peterson, R. T., Mably, J. D., Chen, J. N. and Fishman, M. C. (2001). Convergence of distinct pathways to heart patterning revealed by the small molecule concentramide and the mutation *heart-and-soul*. *Curr Biol*. **11**: 1481-91.

Petronczki, M. and Knoblich, J. A. (2001). DmPAR-6 directs epithelial polarity and asymmetric cell division of neuroblasts in *Drosophila*. *Nat Cell Biol.* **3**: 43-9.

Plageman, T. F. Jr., Chauhan, B. K., Yang, C., Jaudon, F., Shang, X., Zheng, Y., Lou, M., Debant, A., Hildebrand, J. D. and Lang, R. A. (2011). A Trio-RhoA-Shroom3 pathway is required for apical constriction and epithelial invagination. *Development*. **138**: 5177-88.

Plageman, T. F. Jr., Chung, M. I., Lou, M., Smith, A. N., Hildebrand, J. D., Wallingford, J. B. and Lang, R. A. (2010). Pax6-dependent Shroom3 expression regulates apical constriction during lens placode invagination. *Development*. **137**: 405-15.

Plageman, T. F. Jr., Zacharias, A. L., Gage, P. J. and Lang R. A. (2011). Shroom3 and a Pitx2-N-cadherin pathway function cooperatively to generate asymmetric cell shape changes during gut morphogenesis. *Dev Biol*. **357**: 227-34.

Prall, O. W., Menon, M. K., Solloway, M. J., Watanabe, Y., Zaffran, S., Bajolle, F., Biben, C., McBridge, J. J., Robertson, B. R., Chaulet, H., Stennard, F. A., Wise, N., Schaft, D., Wolstein, O., Furtado, M. B., Shiratori, H., Chien, K. R., Hamada, H., Black, B. L., Saga, Y., Robertson, E. J., Buckingham, M. E. and Harvey, R. P. (2007). An Nkx2-5/Bmp2/Smad1 negative feedback loop controls heart progenitor specification and proliferation. *Cell*. **128**: 947-59.

Pullarkat, R. K. (1991). Hypothesis: prenatal ethanol-induced birth defects and retinoic acid. *Alcohol Clin Exp Res.* **15**: 565-7.

Quintin, S., Gally, C. and Labouesse, M. (2008). Epithelial morphogenesis in embryos: asymmetries, motors, and brakes. *Trends Genet*. **24**: 221-30.

Reed, K. L., Meijboom, E. J., Sahn, D. J., Scagnelli, S. A., Valdes-Cruz, L. M. and Shenker, L. (1986). Cardiac Doppler flow velocities in human fetuses. *Circulation*. **73**: 41-6.

Rones, M. S., McLaughlin, K. A., Raffin, M. and Mercola, M. (2000). Serrate and Notch specify cell fates in the heart field by suppressing cardiomyogenesis. *Development*. **127**: 3865-76.

Ross, A. C., Zolfaghari, R. and Weisz, J. (2001). Vitamin A: recent advances in the biotransformation, transport, and metabolism of retinoids. *Curr Opin*

*Gastroenterol*. **17**: 184-92.

Ryckebusch, L., Wang, Z., Bertrand, N., Lin, S. C., Chi, X., Schwartz, R., Zaffran, S. and Niederreither, K. (2008). Retinoic acid deficiency alters second heart field formation. *Proc Natl Acad Sci U S A*. **105**: 2913-8.

Sadler, T. W. (1990). Langman's Medical Embryology. Williams & Wilkens, Baltimore.

Sakata, H., Sakabe, M., Matsui, H., Kawada, N., Nakatani, K., Ikeda, K., Yamagishi, T. and Nakajima, Y. (2007). Rho kinase inhibitor Y27632 affects initial heart myofibrillogenesis in cultured chick blastoderm. *Dev Dyn*. **236**: 461-72.

Sater, A. K. and Jacobson, A. G. (1990). The role of the dorsal lip in the induction of heart mesoderm in *Xenopus laevis*. *Development*. **108**: 461-70.

Schilling, H. F., Concordet, J. P. and Ingham, P. W. (1999). Regulation of left-right asymmetries in the Zebrafish by Shh and BMP4. *Dev Biol*. **210**: 277-87.

Schneider, V. A. and Mercola, M. (1999). Spatially distinct head and heart inducers within the *Xenopus* organizer region. *Curr Biol*. **9**: 800-9.

Schneider, V. A. and Mercola, M. (2001). Wnt antagonism initiates cardiogenesis in *Xenopus laevis*. *Genes Dev*. **15**: 304-15.

Schott, J. J., Benson, D. W., Basson, C. T., Pease, W., Silberbach, G. M., Moak, G. P., Maron, B. J., Seidman, C. E. and Seidman, J. G. (1998). Congenital heart disease caused by mutations in transcription factors NKX2.5. *Science*. **281**: 108-11.

Schultheiss, T. M., Burch, J. B. and Lassar, A. B. (1997). A role for bone morphogenetic protein in the induction of cardiac myogenesis. *Genes Dev*. **11**: 451-62.

Shi, Y., Katsev, S., Cai, C. and Evans, S. (2000). BMP signaling is required for heart formation in vertebrates. *Dev Biol*. **224**: 226-37.

Shutt, L. E. and Bowes, J. B. (1979). Atropine and hyoscine. *Anaesthesia*. **34**: 476-90.

Singh, L. D., Singh, S. P., Handa, R. K., Ehmann, S. and Snyder, A. K. (1996). Effects of ethanol on GLUT1 protein and gene expression in rat astrocytes. *Metab Brain Dis*. **11**: 343-57.

Singh, S. P., Ehmann, S. and Snyder, A. K. (1996). Ethanol-induced changes in insulin like growth factors and IGF gene expression in the fetal brain. *Proc Soc Exp Biol Med*. **212**: 349-54.

Sirbu, I. O., Zhao, X. and Duester, G. (2008). Retinoic acid controls heart anteroposterior patterning by downregulating Isl1 through the Fgf8 pathway. *Dev Dyn*. **237**: 1627-35.

Smith, J. L. and Schoenwolf, G. C. (1997). Neurulation: coming to closure. *Trends Neurosci*. **20**: 510-7.

Smith, S. M., Dickman, E. D., Thompson, R. P., Sinning, A. R., Wunsch, A. M. and Markwald, R. R. (1997). Retinoic acid directs cardiac laterality and the expression of early markers of precardiac asymmetry. *Dev Biol.* **182**: 162-71.

Stainier, D. Y. and Fishman, M. C. (1992). Patterning the zebrafish heart tube: acquisition of anteroposterior polarity. *Dev Biol*. **153**: 91-101.

Stainier, D. Y., Fouquet, B., Chen, J. N., Warren, K. S., Weinstein, B. M., Meiler, S. E., Mohideen, M. A., Neuhauss, S. C., Solnica-Krezel, L., Schier, A. F., Zwartkruis, F., Stemple, D. L., Malicki, J., Driever, W. and Fishman, M. C. (1996). Mutations affecting the formation and function of the cardiovascular system in the zebrafish embryo. *Development*. **123**: 285-92.

Sun, Y., Liang, X., Najafi, N., Cass, M., Lin, L., Cai, C. L., Chen, J. and Evans, S. M. (2007). Islet 1 is expressed in distinct cardiovascular lineages, including pacemaker and coronary vascular cells. *Dev Biol*. **304**: 286-96.

Suzuki, A., Yamanaka, T., Hirose, T., Manabe, N., Mizuno, K., Shimizu, M., Akimoto, K., Izumi, Y., Ohnishi, T. and Ohno, S. (2001). Atypical protein kinase C is involved in the evolutionarily conserved par protein complex and plays a critical role for establishing epithelia-specific junctional structures. *J Cell Biol*. **152**: 1183-96.

Suzuki, M., Morita, H. and Ueno, N. (2012). Molecular mechanisms of cell shape changes that contribute to vertebrate neural tube closure. *Dev Growth Differ*. **54**: 266-76.

Swift, L. M., Asfour, H., Posnack, N. G., Arutunyan, A., Kay, M. W. and Sarvazyan, N. (2012). Properties of blebbistatin for cardiac optical mapping and other imaging applications. *Eur J Physiol*. **464**: 503-12.

Szigeti, K., Máthé, D. and Osváth, S. (2014). Motion-based X-ray imaging modality. *IEEE Trans Med Imaging*. **33**: 2031-8.

Tripathi, O. N., Ravens, U. and Sanguinetti, M. C. (2011). Heart Rate and Rhythm: Molecular Basis, Pharmacological Manipulation and Clinical Implications. *Springer*. Chapter 1: Unit 1.1.

Tullio, A. N., Accili, D., Ferrans, V. J., Yu, Z., Takeda, K., Grinberg, A., Westphal, H., Preston, Y. A. and Adelstein, R. S. (1997). *Proc Natl Acad Sci USA*. **94**: 12407-12.

Twal, W., Roze, L. and Zile, M. H. (1995). Anti-retinoic acid monoclonal antibody localizes all-trans retinoic acid in target cells and blocks normal development in early quail embryo. *Dev Biol.* **168**: 225-34.

Twal, W. O. and Zile, M. H. (1997). Retinoic acid reverses ethanol-induced cardiovascular abnormalities in quail embryos. *Alcohol Clin Exp Res.* **21**: 1137-43.

Van Thiel, D. H., Gavaler, J. and Lester, R. (1974). Ethanol inhibition of vitamin A metabolism in the testes: possible mechanism for sterility in alcoholics. *Science*. **186**: 941-2.

Vicente-Manzanares, M., Ma, X. Adelstein, R. S. and Horwitz, A. R. (2009). Non-muscle myosin II takes centre stage in cell adhesion and migration. *Nat Rev Mol Cell Biol.* **10**: 778-90.

Ward, C., Stadt, H., Hutson, M. and Kirby, M. L. (2005). Ablation of the secondary heart field leads to tetralogy of Fallot and pulmonary atresia. *Dev Biol*. **284**: 72-83.

Warkman, A. S. and Krieg, P. A. (2007). *Xenopus* as a model system for vertebrate heart development. *Semin Cell Dev Biol*. **18**: 46-53.

Washington Smaok, I., Byrd, N. A., Abu-Issa, R., Goddeeris, M. M., Anderson, R., Morris, J., Yamamura, K., Klingensmith, J. and Meyers, E. N. (2005). Sonic hedgehog is required for cardiac outflow tract and neural crest cell development. *Dev Biol*. **283**: 357-72.

Wei, L., Imanaka-Yoshida, K., Wang, L., Zhan, S., Schneider, M. D., DeMayo, F. J. and Schwartz, R. J. (2002). Inhibition of Rho family GTPases by Rho GDP dissociation inhibitor disrupts cardiac morphogenesis and inhibits cardiomyocyte proliferation. *Development*. **129**: 1705-14.

Wei, L., Roberts, W., Wang, L., Yamada, M., Zhang, S., Zhao, Z., Rivkees, S. A., Schwartz, R. J. and Imanaka-Yoshida, K. (2001). Rho kinases play an obligatory role in vertebrate embryonic organogenesis. *Development*. **128**: 2953-62.

Wessels, A. and Sedmera, D. (2003). Developmental anatomy of the heart: a tale of mice and man. *Physiol Genomics.* **15**: 165-76.

Wodarz, A. and Nusse, R. (1998). Mechanisms of Wnt signaling in development. *Annu Rev Cell Dev Biol*. **14**: 59-88.

Wodarz, A., Ramrath, A., Grimm, A. and Knust, E. (2000). *Drosophila* atypical protein kinase associates with Bazooka and controls polarity of epithelia and neuroblasts. *J Cell Biol*. **150**: 1361-74.

Woolner, S. and Papalopulu N. (2012). Spindle position in symmetric cell divisions during epiboly is controlled by opposing and dynamic apicobasal forces. *Dev Cell*. **22**: 775-87.

Xavier-Neto, J., Neville, C. M., Shapiro, M. D., Houghton, L., Wang, G. F., Nikovits, W. Jr, Stockdale, F. E. and Rosenthal, N. (1999). A retinoic acid-inducible transgenic marker of sinoatrial development in the mouse heart. *Development*. **126**: 1677-87.

Xavier-Neto, J., Shapiro, M. D., Houghton, L. and Rosenthal, N. (2000). Sequential programs of retinoic acid synthesis in the myocardial and epicardial layers of the developing avian heart. *Dev Biol*. **219**: 129-41.

Yang, V. X. Gordon, M., Seng-Yue, E., Lo, S., Qi, B., Pekar, J., Mok, A., Wilson, B. and Vitkin, I. (2003). High speed, wide velocity dynamic range Doppler optical coherence tomography (part II): Imaging *in vivo* cardiac dynamics of *Xenopus laevis*. *Opt Express*. **11**: 1650-8.

Yang, Z. N., Davis, G. J., Hurley, T. D., Stone, C. L., Li, T. K. and Bosron, W. F. (1994). Catalytic efficiency of human alcohol dehydrogenases for retinol oxidation and retinal reduction. *Alcohol Clin Exp Res*. **18**: 587-91.

Yarrow, J. C., Totsukawa, G., Charras, G. T. and Mitchison, T. J. (2005). Screening for Cell Migration Inhibitors via Automated Microscopy Reveals a Rho-Kinase Inhibitor. *Chem Biol*. **12**: 385-95.

Yazdanfar, S., Kulkarni, M. and Izatt, J. (1997). High resolution imaging of *in vivo* cardiac dynamics using color Doppler optical coherence tomography. *Opt Express*. **1**: 424-31.

Yelbuz, T. M., Leatherbury, L., Wolfe, R. R., Loewy, R. and Kirby, M. L. (2002). Images in cardiovascular medicine: Time-lapse study with high speed video camera in the early embryonic chick heart to visualize a time window of normal and abnormal heart development. *Circulation*. **106**: e44-5.

Yelbuz, T. M., Waldo, K. L., Kumiski, D. H., Stadt, H. A., Wolfe, R. R., Leatherbury, L. and Kirby, M. L. (2002). Shortened outflow tract leads to altered cardiac looping after neural crest ablation. *Circulation*. **106**: 504-10.

Yelin, R., Kot, H., Yelin, D. and Fainsod, A. (2007). Early molecular effects of ethanol during vertebrate embryogenesis. *Differentiation*. **75**: 393-403.

Yelin, R., Schyr, R. B., Kot, H., Zins, S., Frumkin, A., Pillemer, G. and Fainsod, A.

(2005). Ethanol exposure affects gene expression in the embryonic organizer and reduces retinoic acid levels. *Dev Biol*. **279**: 193-204.

Yelin, R., Yelin, D., Oh, W. Y., Yun, S. H., Boudoux, C., Vakoc, B. J., Bouma, B. E. and Tearney, G. J. (2007). Multimodality optical imaging of embryonic heart microstructure. *J Biomed Opt*. **12**: 064021. doi: 10.1117/1.2822904.

Zaffran, S. and Kelly, R. G. (2012). New developments in the second heart field. *Differentiation*. **84**: 17-24.

Zhang, J., Burridge, K. A. and Friedman, M. H. (2008). *In vivo* differences between endothelial transcription profiles of coronary and iliac arteries revealed by microarray analysis. *Am J Physiol Heart Circ Physiol*. **295**: H1556-61.

Zile, M. H. (2001). Function of vitamin A in vertebrate embryonic development. *J Nutr*. **131**: 705-8.

# Appendix

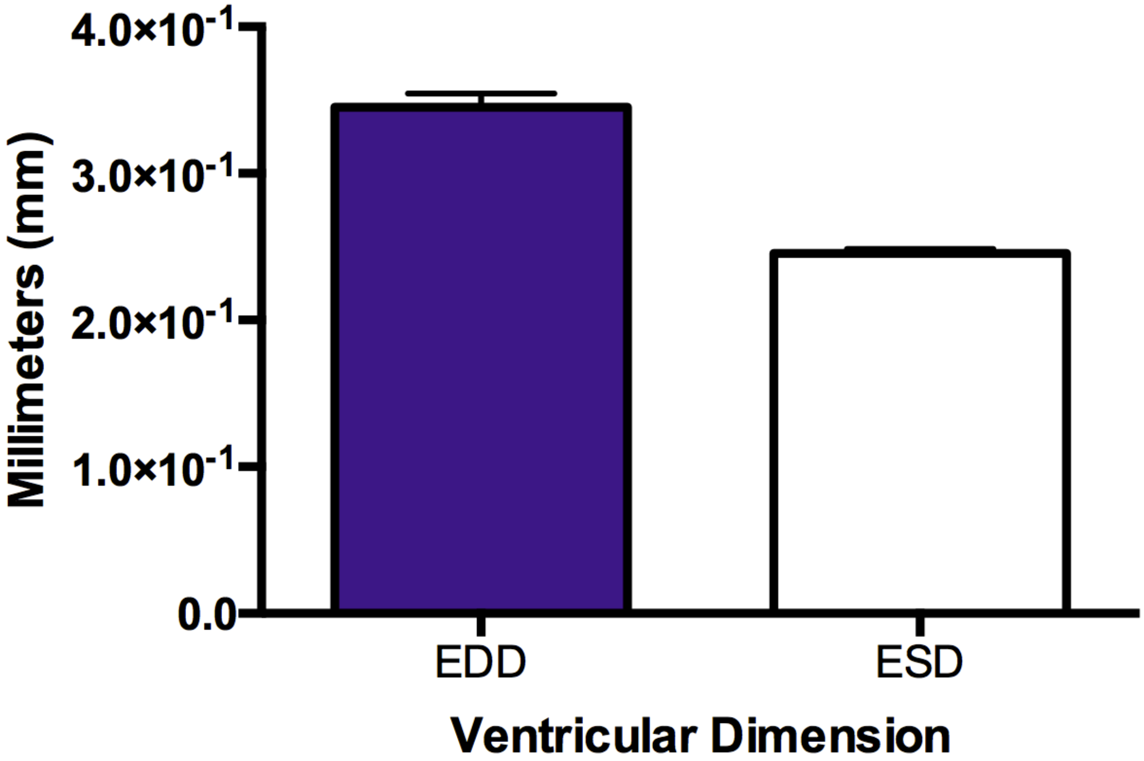

**Figure A1. Examination of end-diastolic dimension and end-systolic dimension for *Xenopus laevis* embryos at stage 47.** The end-diastolic dimension (EDD) and end-systolic dimension (ESD) were examined for stage 47 *Xenopus laevis* embryos. These ventricular dimensions included the measurement of both the ventricular cavity and the ventricular wall. n = 50

# Curriculum Vitae

| | |
|---|---|
| **Name:** | Judith Sull |
| **Post-secondary Education and Degrees:** | University of Western Ontario<br>London, Ontario, Canada<br>2008-2012 BMSc |
| | The University of Western Ontario<br>London, Ontario, Canada<br>2013-2015 M.Sc |
| **Honours and Awards:** | Western Graduate Research Scholarship (WGRS)<br>01/2013 – 12/2014 |
| | Department of Pediatrics Graduate Studentship<br>09/2013 – 04/2014 |
| | Ontario Graduate Scholarship (OGS)<br>05/2014 – 04/2015 |
| **Related Work Experience** | Teaching Assistant<br>The University of Western Ontario<br>09/2013 – 04/2014 |

**Poster Presentations:**

Physiology and Pharmacology Research Day. London, Ontario. “Cardiac Imaging in *Xenopus* Embryos Using a Novel Imaging System” **Sull, J.**, Norozi, K., and Drysdale, T. Poster Presentation (10/2014).

Annual Developmental Biology Day. London, Ontario. “Cardiac Imaging in *Xenopus* Embryos Using a Novel Imaging System” **Sull, J.**, Norozi, K., and Drysdale, T. Poster Presentation (5/2014).

CHRI Paediatric Research Day. London, Ontario. “Cardiac Imaging in *Xenopus* Embryos Using a Novel Imaging System” **Sull, J.**, Norozi, K., and Drysdale, T. Poster Presentation (5/2014).

Canadian Developmental Biology Conference. Mont Tremblant, Quebec. “Cardiac Imaging in *Xenopus* Embryos Using a Novel Imaging System” **Sull, J.**, Norozi, K., and Drysdale, T. Poster Presentation (03/2014).

Physiology and Pharmacology Research Day. London, Ontario. “Cardiac Imaging in *Xenopus* Embryos Using a Novel Imaging System” **Sull, J.**, Norozi, K., and Drysdale, T. Poster Presentation (10/2013).

Annual Developmental Biology Day. London, Ontario. “Cardiac Imaging in *Xenopus* Embryos Using a Novel Imaging System” **Sull, J.**, Norozi, K., and Drysdale, T. Poster Presentation (5/2013).